AD

USAAML TECHNICAL REPORT 65-20

CURVED JET FLOWS

VOLUME II

May 1965

U.S. ARMY AVIATION MATERIEL LABORATORIES
FORT EUSTIS, VIRGINIA

CONTRACT DA 44-177-AMC-238(T)
PETER R. PAYNE, INC.

Cont from Vol I AD 616 395

In this section the shape integral is calculated for a number of idealized asymmetric distributions when, from Equation (195)

$$\lambda = \frac{\int_0^{t'} (3\xi)\, \Delta P_j\, \alpha(3\xi)}{\int_0^{t'} \Delta P_j\, \alpha(3\xi)} - \frac{1}{2}.$$

It is obvious from Equation (196) that (as long as viscous effects are unimportant) maximum cushion pressure will be obtained when λ is maximum. This implies that the maximum pressure peak must be on the cushion side of the jet centerline, as indicated in Figure 66.

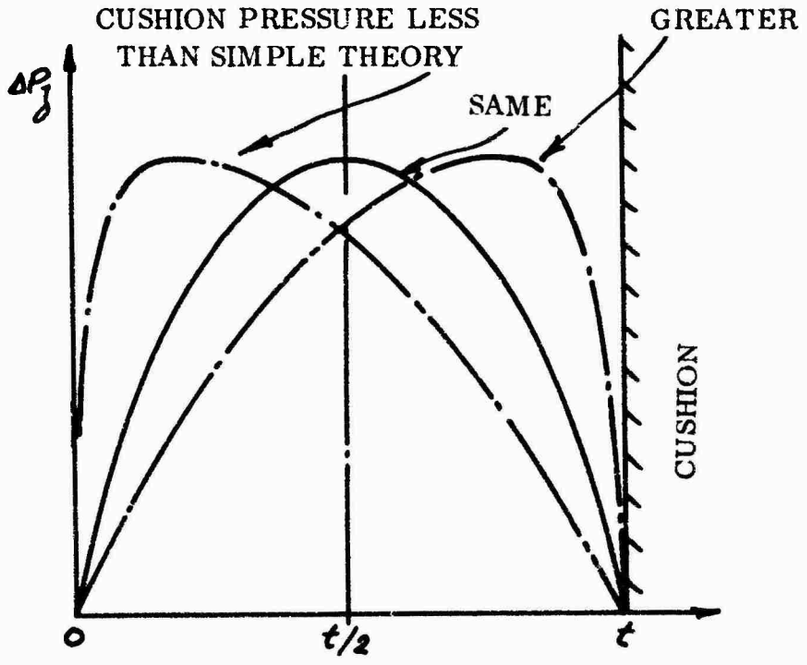

Figure 66. Symmetric and Asymmetric Jet Total Head Profiles.

It should be remembered that the ratio

$$\frac{\Delta p_c}{\Delta P}_{\text{mean}}$$

is entirely artificial; that is to say, it is not a true parameter, since it will change with the shape integral (λ). This leads to a number of anomalies,

and indeed, the only reason for presenting the following results is the widespread use of the ratio $\Delta p_c / \Delta P_{MEAN}$ as a means of reporting experimental measurements.

The Jet Thickness Anomaly

Suppose now that a test nozzle has the geometry of Figure 67 and that an insert has been placed in the nozzle, unknown to the experimenter. Thus a traverse across the (original) nozzle width (t) gives the total head distribution indicated in the figure. As a result, the unobservant experimenter computes the mean total pressure as

$$\Delta P_{mean} = \Delta P_{max} \cdot \frac{t}{T}$$

and the cushion pressure ratio as

$$\frac{\Delta p_c}{\Delta P_{mean}} = \frac{\Delta p_c}{\Delta P_{max}} \cdot \frac{T}{t} .$$

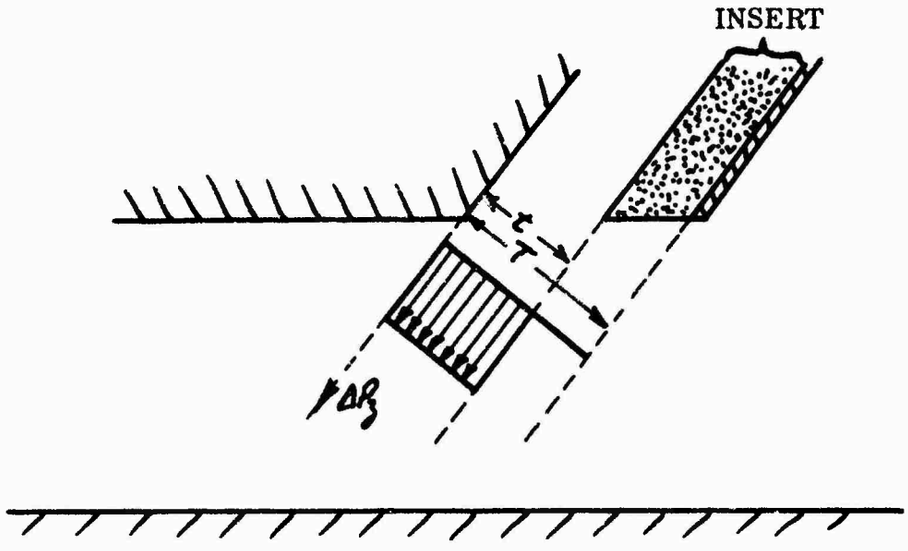

Figure 67. Geometry for the Jet Thickness Anomaly.

The simple theory equation for Δp_c gives him

$$\frac{\Delta p_c}{\Delta P_{mean}} = 2(T/R) - (T/R)^2 = \left(\frac{T}{t}\right)\frac{\Delta p_c}{\Delta P_{max}}$$

The correct equation is

$$\frac{\Delta p_c}{\Delta P_{mean}} = 2(t/R) - (t/R)^2 .$$

Thus the apparent ratio between experiment and theoretical results is

$$\frac{\text{Experiment}}{\text{Theory}} = \frac{2(t/R) - (t/R)^2}{[2(T/R) - (T/R)^2]\frac{t}{T}} = \frac{2 - t/R}{2 - T/R} .$$

Thus, the unobservant experimenter would conclude that his measured ratio $\Delta p_c/\Delta P$-mean exceeds the "theoretical" value. His belief would be illusory, however, and in the same way the limit cases of the total head distributions discussed below will show the misleading result that a jet should have all its energy concentrated at the inner boundary. While this conclusion is perfectly correct so far as obtaining the maximum value of the ratio ($\Delta p_c/\Delta P$ mean) is concerned, minimizing the mean total pressure has no physical importance; it does not correspond to minimum jet power, for example.

Rectangular Total Head Distributions

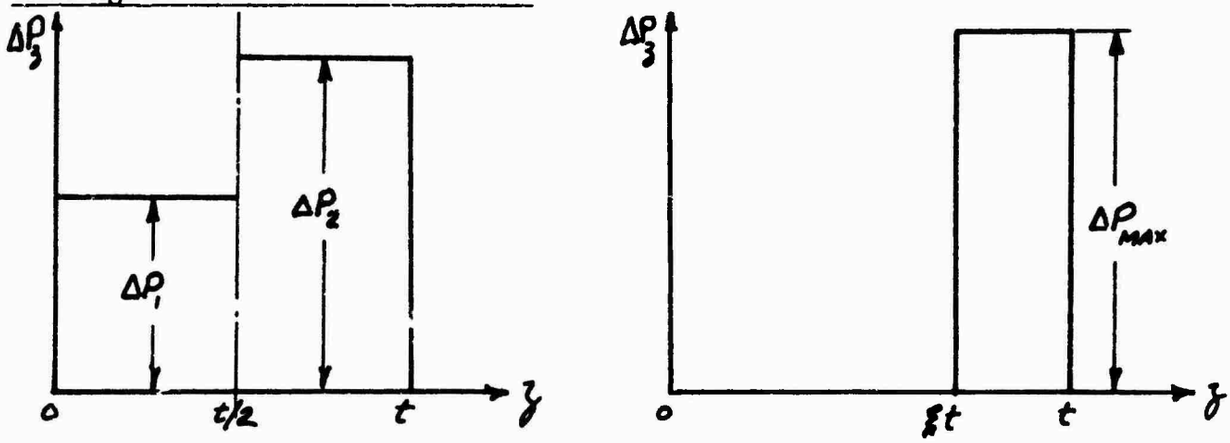

$$\int_0^1 \Delta P_j \, d(y/t) = \frac{\Delta P_1 + \Delta P_2}{2} \qquad = (1 - \xi)\Delta P_{MAX}$$

$$\int (y/t)\Delta P_j \, d(y/t) = \tfrac{1}{8}\Delta P_1 + \tfrac{3}{8}\Delta P_2 \qquad = \tfrac{1}{2}(1 - \xi^2)\Delta P_{MAX}$$

$$\lambda \quad (-\tfrac{1}{4} < \lambda < +\tfrac{1}{4}) = \frac{\tfrac{1}{4}\left[1 - \Delta P_1/\Delta P_2\right]}{\left[1 + \Delta P_1/\Delta P_2\right]} \qquad = \tfrac{1}{2}\xi \quad (0 < \lambda < \tfrac{1}{2})$$

Figure 68. Two Rectangular Total Head Distributions.

For the first of the two distributions sketched in Figure 68, it can be seen that as ΔP_2 diminishes we encounter the physical limitation of reverse flow, which requires $\Delta p_3 < \Delta P_3$. Since the jet static pressure gradient $dp/dz > 0$, this condition must occur at either $z = t$ or $z = \frac{1}{2}t$. For the first position,

$$\Delta P_c \geq \Delta p_c .$$

But $$\Delta P_1 + \Delta P_2 = 2\Delta P_{mean} ;$$

$$\therefore \quad \frac{\Delta p_c}{\Delta P_{mean}} \leq 2 - \frac{\Delta P_1}{\Delta P_{mean}}$$

$$\leq \frac{2}{1 + \Delta P_1/\Delta P_2} .$$

For $z = t/2$,

$$\Delta p_{t/2} = \frac{(1 - t/R)\cdot t/R}{(1 - t/R + \frac{1}{2}t/R)^2}\left[\Delta P_1 + \frac{t/R}{4(1 - t/R)}\Delta P_1\right]$$

$$\frac{\Delta p_{t/2}}{\Delta P_1} = \frac{(t/R)(1 - \frac{3}{4}t/R)}{(1 - \frac{1}{2}t/R)^2} .$$

Thus at $t/2$, the limiting condition is

$$\frac{\Delta p_{t/2}}{\Delta P_1} = \frac{(t/R)(1 - \frac{3}{4}t/R)}{(1 - \frac{1}{2}t/R)^2} \leq \frac{\Delta P_2}{\Delta P_1} .$$

This limit is plotted in Figure 69, and the curves of cushion pressure ratio for the stepped distribution are plotted in Figure 70.

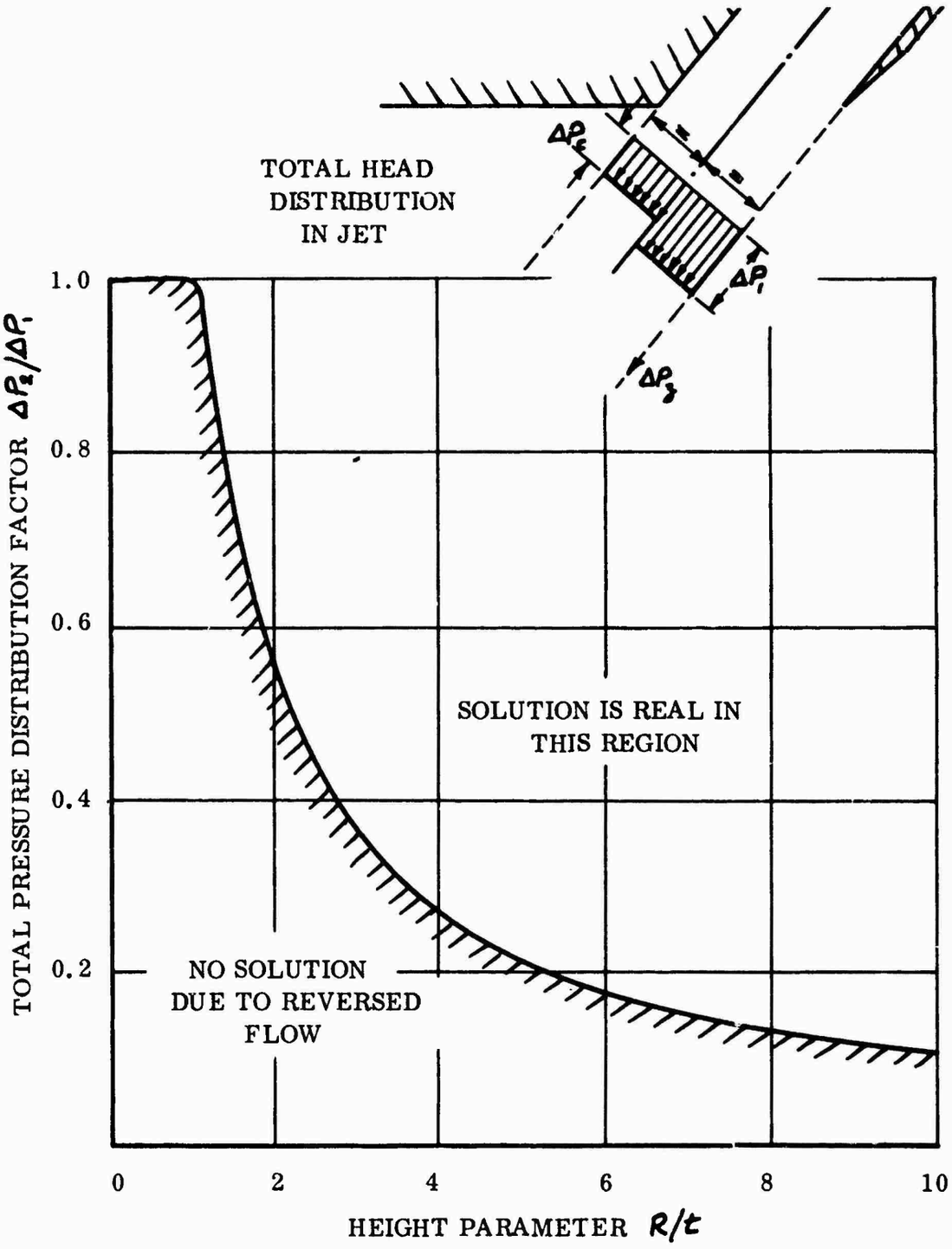

Figure 69. Solution Limits for the Rectangular Total Pressure Distribution.

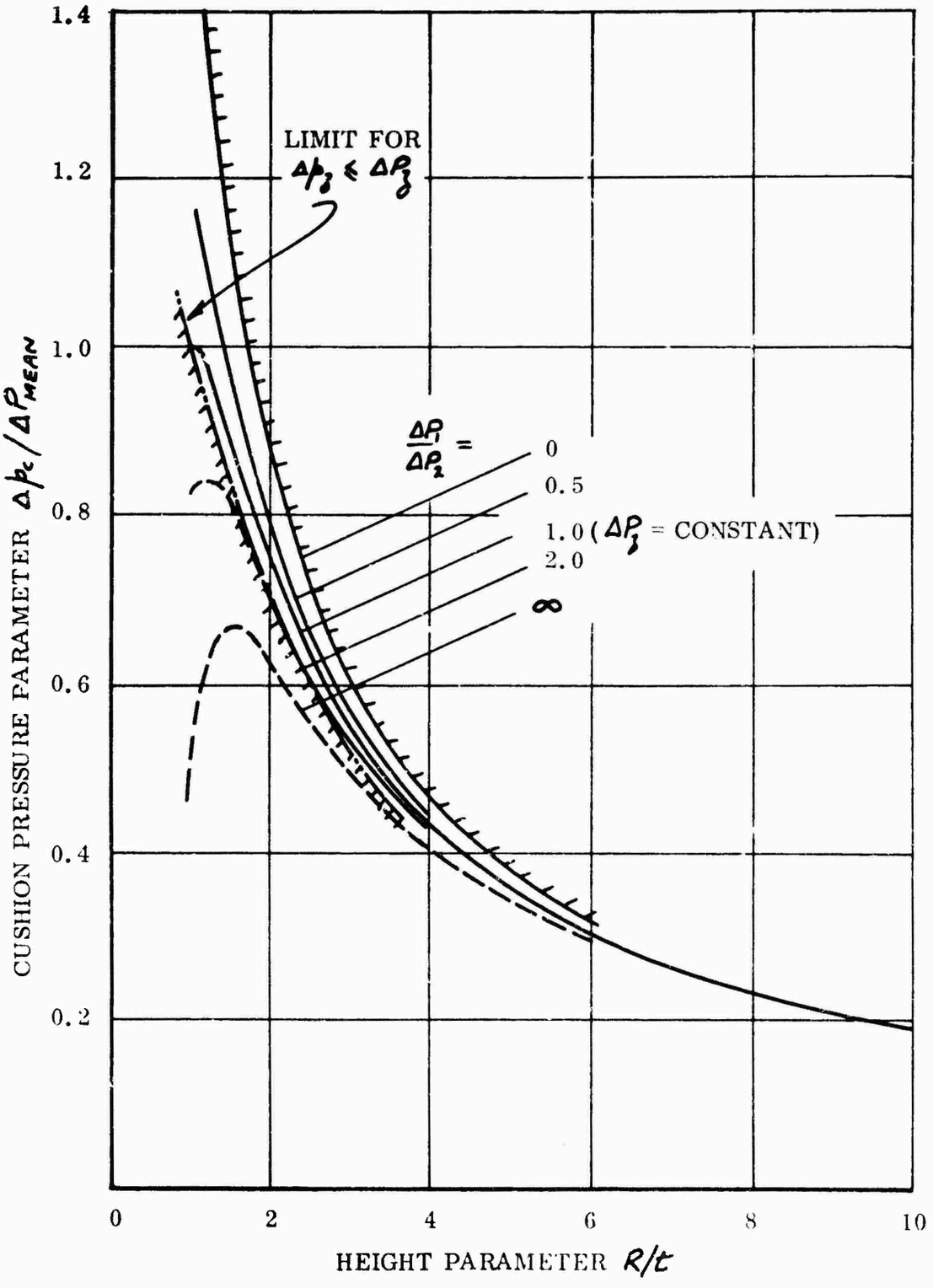

Figure 70. Effect of a Stepped Rectangular Jet Total Head Distribution Upon Cushion Pressure.

A General Linear Variation

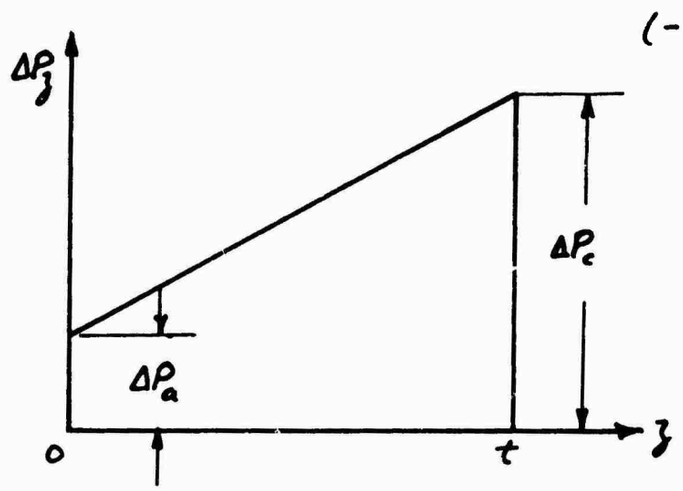

$$\int_0^t \Delta P_z \, d(z/t) = \frac{\Delta P_a + \Delta P_c}{2} \qquad \int_0^t (z/t) \Delta P_z \, d(z/t) = \frac{1}{c} \Delta P_a + \frac{1}{3} \Delta P_c$$

$$\lambda = \frac{\frac{1}{c}\{1 - \Delta P_a/\Delta P_c\}}{\{1 + \Delta P_a/\Delta P_c\}}$$

Figure 71. General Linear Variation.

This case was first solved in Reference 13, from which Figure 72 was abstracted.

The reverse flow limitation can in this case be simplified to

$$\Delta P_c \geq \Delta p_c .$$

But

$$\Delta P_c + \Delta P_a = 2\Delta P_{MEAN} ;$$

$$\frac{\Delta p_c}{\Delta P_{MEAN}} \leq 2 - \frac{\Delta P_a}{\Delta P_{MEAN}}$$

$$\leq 2/(1 + \Delta P_a/\Delta P_c) .$$

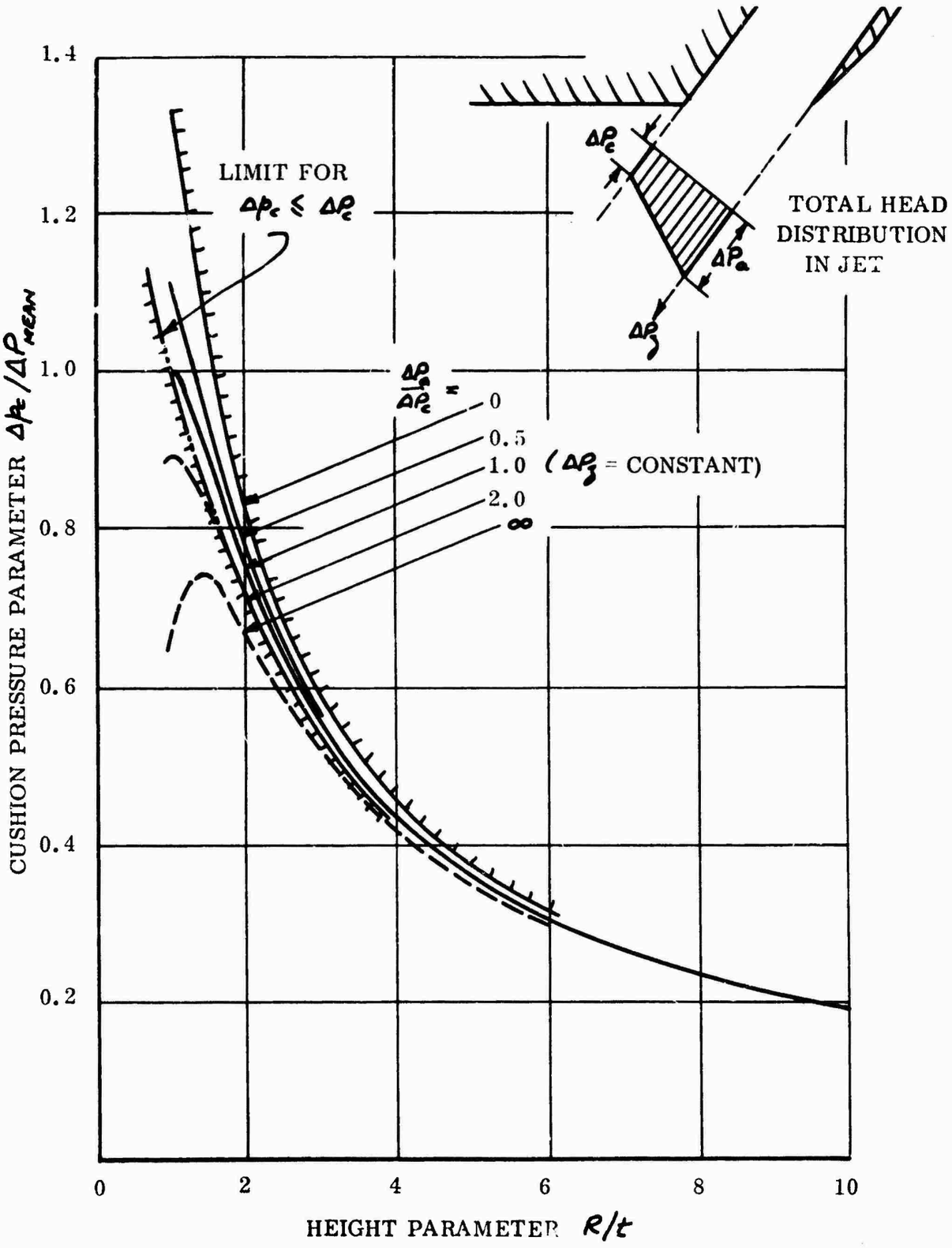

Figure 72. Effect of a Linearly Varying Jet Total Head Distribution Upon Cushion Pressure.

This limit is superimposed on Figure 72 and is seen to confine the attainable cushion pressures to a fairly narrow band. However, a value of ($\Delta h_c/\Delta P$ mean) equal to 4/3 times the (uniform ΔP_z) theory value is seen to be attainable at the limit $h/R \rightarrow 1.0$.

A General Power Law Variation

This case includes that of Figure 71, when ΔP_a or ΔP_c = 0 and also the constant total head case ($n \rightarrow \infty$). It is based on the relationship

$$\Delta P_z = K(z/t)^n,$$

although the actual value of K does not influence the results.

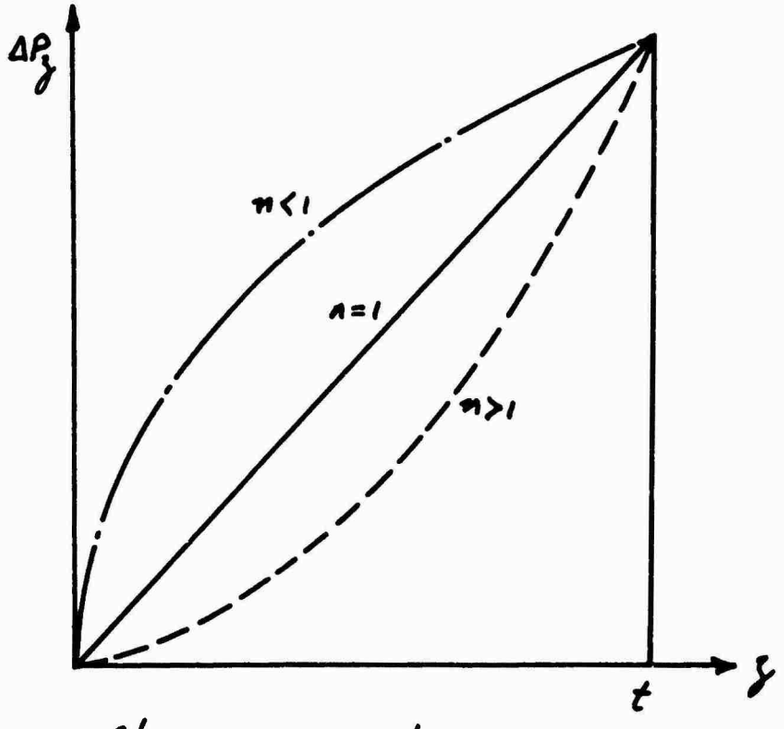

$$\int_0^1 \Delta P_z \, d(z/t) = \frac{k}{n+1}$$

$$\int_0^1 (z/t)\,\Delta P_z \, d(z/t) = \frac{k}{n+2}$$

$$\lambda = \frac{n+1}{n+2} - \frac{1}{2} \qquad (0 < \lambda < \tfrac{1}{2})$$

Figure 73. General Power Law Distribution.

It is obvious that the maximum cushion pressure (at $t/R = 1.0$) will be twice the simple theory value, in the limit $n \to \infty$.

CUSHION PRESSURE AS A RATIO OF MEAN TOTAL PRESSURE WITH A LINEAR VARIATION IN TOTAL PRESSURE ACROSS THE JET (EXPONENTIAL THEORY)

In this section the problem will be simplified by considering only a linear variation of total pressure across the jet.

From Equation (164) cushion pressure is given by

$$\Delta p_c = \frac{2}{R} e^{-2t/R} \int_0^t e^{2z/R} \Delta P_z \, dz \tag{197}$$

and the mean total pressure by

$$\Delta P_m = \frac{1}{t} \int_0^t \Delta P_z \, dz . \tag{198}$$

For a linear variation in ΔP_z across the jet

$$\Delta P_z = \Delta P_a (1 + b z/t)$$

where

$$b = \frac{\Delta P_c}{\Delta P_a} - 1 .$$

Substituting in Equation (197),

$$\Delta p_c = \frac{2 P_a}{R} \cdot e^{-2t/R} \int_0^t e^{2z/R} (1 + b z/t) \, dz$$

$$= P_a \left[\left(1 - \frac{Rb}{2t}\right)\left(1 - e^{-2t/R}\right) + b \right] .$$

From Equation (198),

$$\Delta p_m = \frac{p_a}{t}\int_0^t (1 + b z/t)\,dz = p_a(1 + b/2) = p_c\frac{1 + b/2}{1 + b} \qquad (199)$$

$$\Delta p_c/\Delta p_m = \left[\left(1 - \frac{Rb}{2t}\right)\left(1 - e^{-2t/R}\right) + b\right](1 + b/2)^{-1}. \qquad (200)$$

This expression is evaluated for various pressure ratios,

$p_c/p_a = 0, \frac{1}{2}, 1, 2, \infty$, over the height range $0 < R/t < 10$

and is plotted in Figure 74.

For $b = 0$, $p_c/p_a = 1$, the expression reduces to $1 - e^{-2t/R}$.

For $b \to \infty$, $p_a/p_c \to 0$, the expression becomes

$$\Delta p_c/\Delta p_m = 2 - \frac{R}{t}\left(1 - e^{-2t/R}\right).$$

At values of the pressure ratio less than unity, that is to say, when

$$\Delta p_c < \Delta p_m,$$

the solution is limited by the condition

$$\Delta p_c > \Delta p_c;$$

otherwise, there would be a reversal of flow in the jet next to the cushion. The existence of this limit was noted in the previous section.

$$\frac{\Delta p_c}{\Delta p_c} = \frac{\Delta p_c}{\Delta p_m}\cdot\frac{1 + b/2}{1 + b}$$

$$= \left[\left(1 - \frac{Rb}{2t}\right)\left(1 - e^{-2t/R}\right) + b\right](1 + b)^{-1}.$$

That is,

$$1 > \left(1 - \frac{Rb}{2t}\right)\left(1 - e^{-2t/R}\right)$$

for real values.

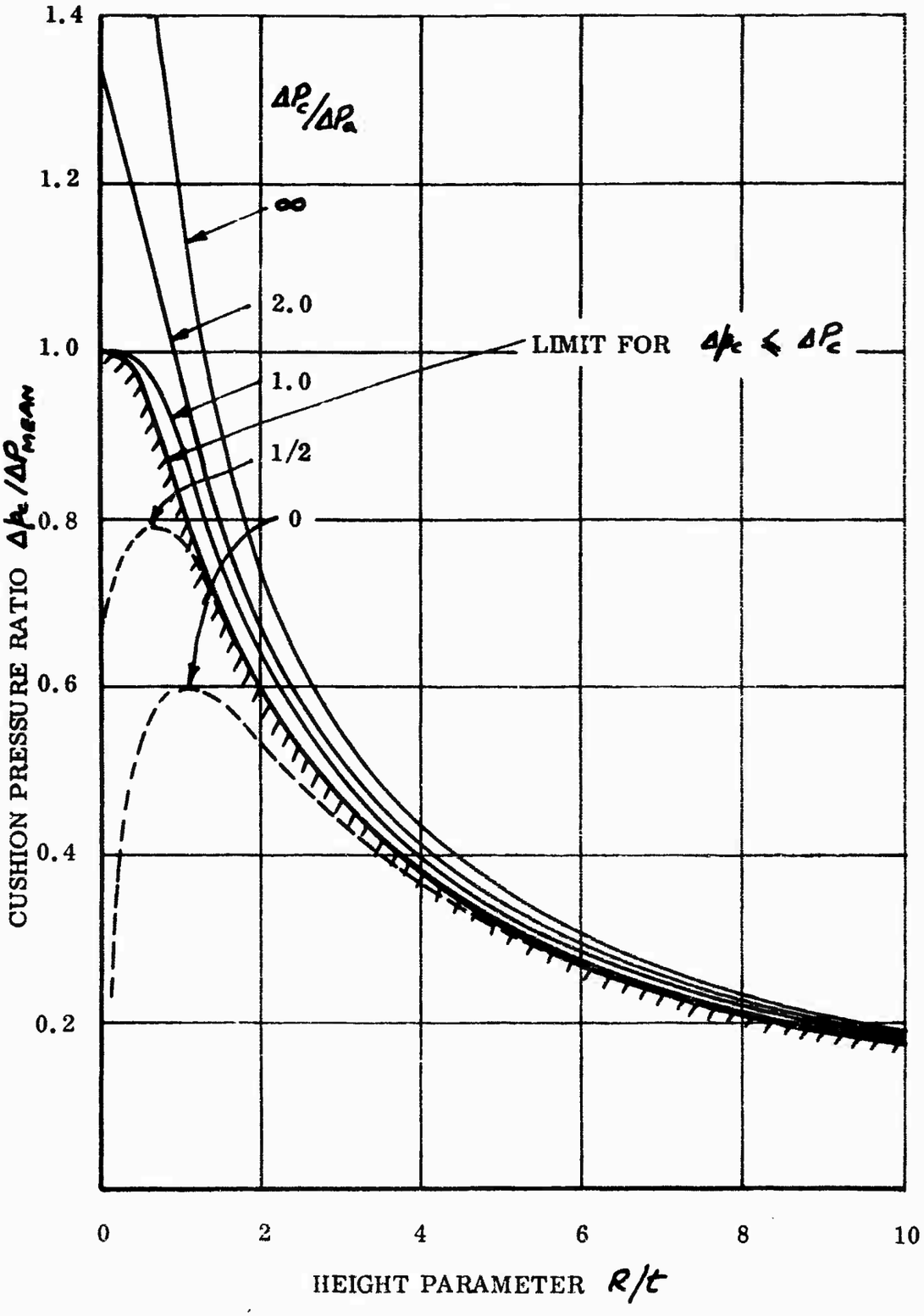

Figure 74. Cushion Pressure as Affected by a Linear Distribution of Total Head Pressure in the Jet (Exponential Flow).

When the limit is reached,

$$1 - \frac{Rb}{2t} = \left(1 - e^{-2b/R}\right)^{-1}$$

$$b = \frac{2t}{R}\left[1 - \left(1 - e^{-2b/R}\right)^{-1}\right]$$

and

$$\frac{\Delta p_c}{\Delta P_m} = \left(1 + b\right)\left(1 + b/2\right)^{-1}$$

$$= f''(t/R).$$

This is computed and plotted in Figure 74. It will be seen that the limit is asymptotic to the curve for $p_c/p_a = 0$ at great heights and reaches the value 1 when $p_c/p_a = 1$ at zero heights.

The results are replotted in Figure 75 for fixed heights with pressure ratio as abscissa.

THE EFFECT OF A LINEAR TOTAL HEAD VARIATION OF THE CUSHION PRESSURE PARAMETER $\Delta\bar{p}_c$

Because of the large variation of $\Delta p_c/\Delta P_m$ with jet total pressure gradient, we are forced to conclude that the cushion pressure parameter $\Delta\bar{p}_c$ defined in Equation (142) is a more meaningful measure of an annular jet's effectiveness.

Therefore, it is of interest to see how the cushion pressure parameter is affected by nonuniformity of total pressure distribution in the jet. Since this parameter is the measure of the pressure obtained in the cushion in relation to the energy supplied to the jet, the presence of a well-defined optimum would indicate the choice of jet structure to give the best operating performance.

For simplicity in computation we considered a distribution which gives a linear variation of total pressure across the jet. This may be defined by a pressure ratio $\Delta P_c/\Delta P_a$ where the total pressure ΔP_z varies from ΔP_a at the outside of the jet to ΔP_c on the cushion side.

Then

$$\Delta P_z = \Delta P_a\left(1 + b \cdot z/t\right) \qquad (201)$$

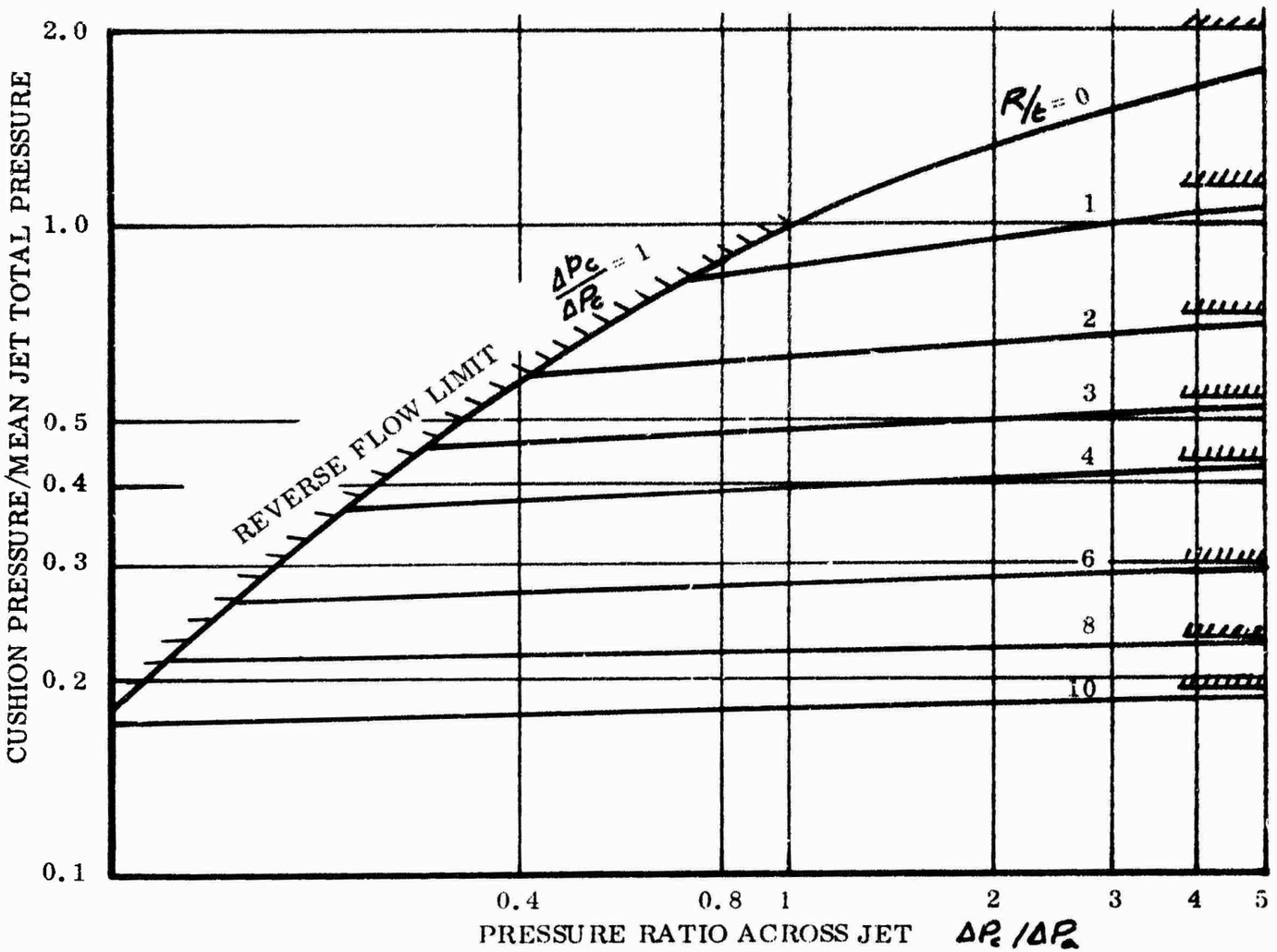

Figure 75. Cushion Pressure as Affected by a Linear Distribution of Total Head Pressure in the Jet (Exponential Theory).

where $\beta = \Delta P_c / \Delta P_a - 1.$

Substituting for ΔP_z in the expression for cushion pressure, Equation (145) results in

$$\frac{t}{h}\cdot\Delta\bar{p}_c = \frac{(r_0+\eta t)^{-3/\eta}\left[2\int_0^t (r_0+\eta z)^{2/\eta-1}(1+\beta z/t)\,dz\right]^{3/2}}{\int_0^t (1+\beta z/t)\left[1+\beta z/t-(r_0+\eta z)^{-2/\eta}\left[2\int_0^z (r_0+\eta z)^{2/\eta-1}(1+\beta z/t)\,dz\right]^{1/2}\right]dt} \quad (202)$$

We should then evaluate this expression over a range of values of the pressure ratio parameter β and the height parameter R/t.

This is an excessively laborious computation which may properly be deferred until the value of the result is more clearly apparent. However, it is likely that the result will be intermediate between the two simpler cases in which $\eta = 0$ (exponential flow) and $\eta = 1$ (free-vortex flow).

Accordingly, these two cases were computed over the ranges

$$1/5 < P_c/P_a < 5$$

and

$$1/4 < R/t < 10.$$

Variation in Cushion Pressure Parameter According to Exponential Flow Theory With a Linear Gradient of Total Pressure Across the Jet

The cushion pressure parameter is given by

$$\frac{t}{h}\cdot\Delta\bar{p}_c = \frac{\left[2t/R\cdot e^{-2z/R}\cdot\frac{1}{t}\int_0^t e^{2z/R}\Delta P_z\,dz\right]^{3/2}}{1/t\int_0^t \Delta P_z\left[\Delta P_z - 2t/R\,e^{-2z/R}\cdot\frac{1}{t}\int_0^z e^{2z/R}\Delta P_z\,dz\right]^{1/2}dz} \quad (203)$$

Substituting

$$\Delta P_z = \Delta P_a(1+\beta z/t),$$

$$\frac{t}{h}\Delta\bar{p}_c = \frac{\left[2t/R\cdot e^{-2z/R}\cdot\frac{1}{t}\int_0^t e^{2z/R}(1+\beta z/t)\,dz\right]^{3/2}}{\frac{1}{t}\int_0^t (1+\beta z/t)\left[1+\beta z/t-2t/R\cdot e^{-2z/R}\cdot\frac{1}{t}\int_0^z e^{2z/R}(1+\beta z/t)\,dz\right]^{1/2}dz}.$$

Writing $R/2t = A$ and $z/t = x$,

$$\frac{t}{\rho}\Delta\bar{p}_c = \frac{\left[\frac{1}{A}e^{-\frac{1}{A}}\int_0^1 e^{\frac{x}{A}}(1+bx)\,dx\right]^{3/2}}{\int_0^1 (1+bx)\left[1+bx-\frac{1}{A}e^{-x/A}\int_0^x e^{x/A}(1+bx)\,dx\right]^{\frac{1}{2}}dx}$$

$$= \frac{\left[B_1 + b(1-AB_1)\right]^{3/2}}{\int_0^1 (1+bx)\left[1-B_x+bAB_x\right]^{\frac{1}{2}}dx} \qquad (204)$$

where

$$B_x = 1 - e^{-x/A}$$

$$A = R/2t$$

$$b = p_c/p_a - 1.$$

Note: Numerator is unreal when $b < -B_1/(1-AB_1)$.

Denominator is unreal when $b < (1-B_1)/-AB_1$.

Since b is essentially <0 at both these limits, the denominator limit is effective because

$$\left|\frac{1-B_1}{AB_1}\right| \not> \left|\frac{B_1}{1-AB_1}\right|.$$

Details of the actual computation are omitted from this report. It should be remarked that the expression in this form requires a numerical integration of the denominator for each point evaluated. Since this appears to be a monotonic type of function of x, a sufficient accuracy may be obtained from a fairly small number of stations $0 < x < 1$.

The computed values are presented in Table 3. These are plotted in Figure 76 as the broken lines, together with the results (full lines) from a similar computation for free-vortex flow described in the next section.

Variation in Cushion Pressure Parameter According to Free-Vortex Flow with a Linear Gradient of Total Pressure Across the Jet

In free-vortex flow $\eta = 1$, and we have for the cushion pressure parameter, from Equation (145),

$$\frac{t}{h}\Delta\bar{p}_c = \frac{\left[2\int_0^1 \left(\frac{r_0}{t}+\frac{z}{t}\right)\Delta p_z \, d\left(\frac{z}{t}\right)\right]^{3/2}}{\left(1+\frac{r_0}{t}\right)^3 \int_0^1 \Delta p_z \left[\Delta p_z - \left(\frac{r_0}{t}+\frac{z}{t}\right)^{-2} 2\int_0^{z/t}\left(\frac{r_0}{t}+\frac{z}{t}\right)\Delta p_z \, d\left(\frac{z}{t}\right)\right]^{1/2} d\left(\frac{z}{t}\right)} \quad (205)$$

The simple case when Δp_z = constant was given by Equation (149).

Putting $z/t = x$ and writing $r_0/t = a$, we have $R = r_0 + t$ so that

$$R/t = a + 1.$$

Then,

$$\frac{t}{h}\Delta\bar{p}_c = \frac{\left[2\int_0^1 (a+x)(1+bx)\,dx\right]^{3/2}}{(1+a)^3 \int_0^1 (1+bx)\left[1+bx-(a+x)^{-2}\,2\int_0^x (a+x)(1+bx)\,dx\right]dx}$$

$$= \frac{\left[2a+1+ab+2b/3\right]^{3/2}}{(1+a)^3 \int_0^1 \left[a^2+bx\left(a^2+ax+\frac{x^2}{3}\right)\right]^{1/2} \frac{1+bx}{a+x}\,dx} \quad (206)$$

The expression is evaluated over the ranges

$$-0.902 < b < +2.0$$

and

$$1 < a < 4.$$

TABLE 3

COMPUTED VALUES OF $t/R \cdot \Delta\bar{p}_c$ FOR A LINEAR GRADIENT OF TOTAL PRESSURE ACROSS THE NOZZLE - EXPONENTIAL THEORY

Pc/Pa	R/t = 0.25	0.5	1.0	2.0	4.0	10.0
5	4.35	2.67	1.43	0.675	0.283	0.0795
3	4.12					
2	4.02	2.47	1.38	0.667	0.283	0.082
1.5	3.81	2.30				
1.25	3.70					
1.00	4.075 x	2.26	1.27	0.639	0.279	0.081
0.95		2.21				
0.925		2.48 x				
0.800			1.25	0.630	0.276	0.0803
0.687			1.22 x			
0.600				0.613	0.268	0.0807
0.418				0.602 x		
0.400					0.263	0.0792
0.228					0.249 x	
0.200						0.0760
0.095						0.0700 x

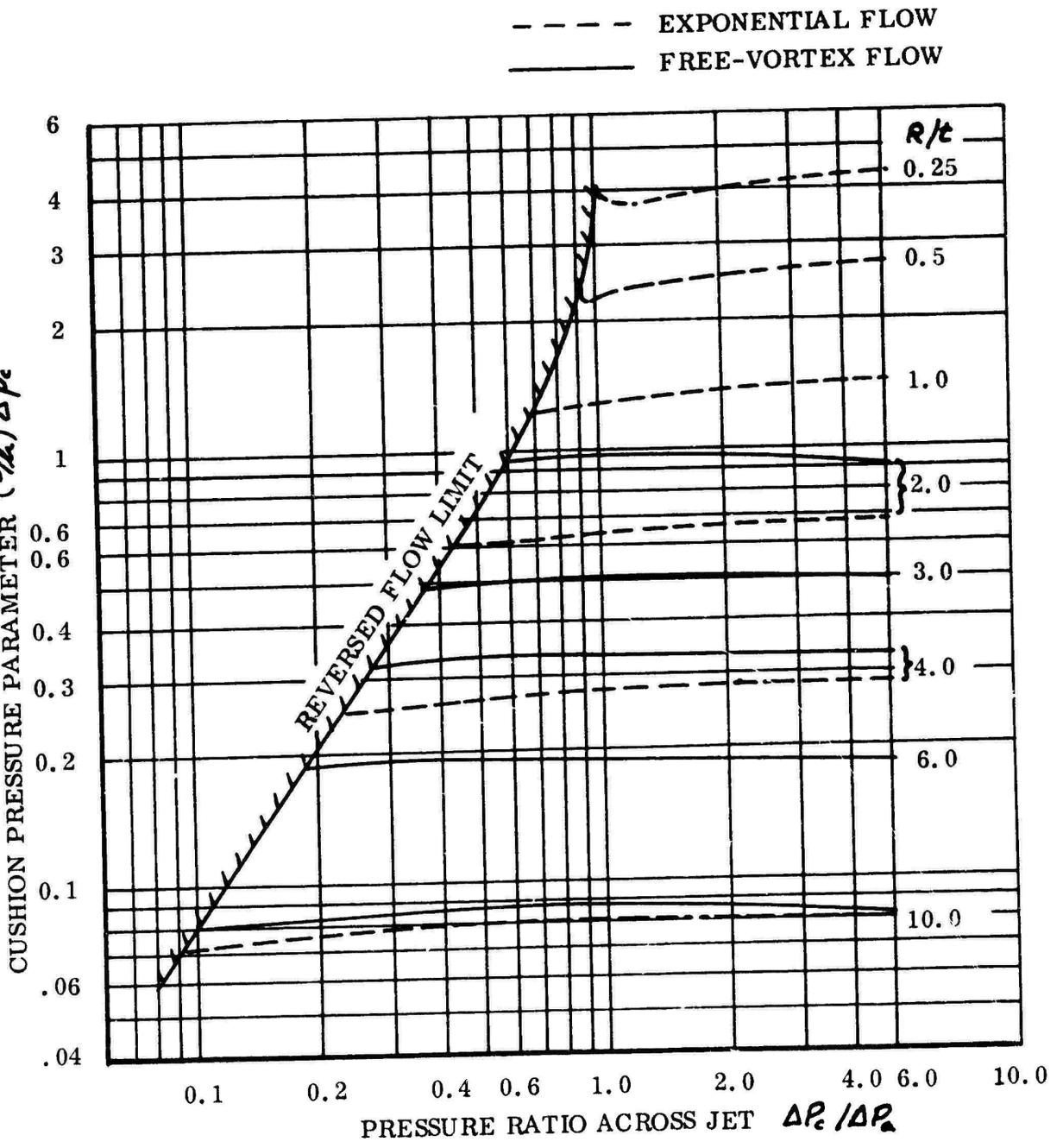

Figure 76. Cushion Pressure Parameter With Linear Gradient of Total Pressure Across Jet - Free-Vortex and Exponential Flow.

As in the preceding case we omit details of the computation and give the resulting values in Table 4. These are plotted in Figure 76 in conjunction with those from the exponential flow method. As before, we observe that the curves are bounded to the left by the condition that the denominator shall be wholly real.

Discussion of the Results

It is remarkable that the limit for real values seems to be the same for both cases. There is no very obvious reason why this should be so. The physical meaning, of course, is that the flow pattern near the inner (cushion side) boundary of the jet can not be maintained when the total head pressure Δp_3 is reduced to the local static pressure $\Delta \phi_3$. Therefore, the limit appears when $\Delta p_c = \Delta \phi_c$, assuming an absence of other disturbance to the flow locally. However, the two methods give differing values of $\Delta \phi_c$ at the same operating height and pressure ratio, and, if the limits do really coincide, the value of the cushion pressure parameter at the limit is a function only of the pressure ratio. It therefore depends upon other factors which are common to both methods. Further, it can be hopefully said that the same limit will apply to the Payne theory, intermediate between the two computed cases.

Considering first the curves for exponential flow, it is seen that a high value of the pressure ratio is favorable, though only slightly so. The effect is most marked at low height ratios, and there appears to be a minimum close to the reverse flow limit for heights below $R/t = 1$. Here, too, the reverse flow limit is approaching asymptotically $p_c/p_a = 1$, and since the exponential flow method is more valid at these low heights, this is clearly indicative of the advantage of having p_c/p_a much greater than unity for heavily loaded, low-flying GEMs.

At the other end of the scale, at $R/t = 10$, the exponential method loses validity. This curve has been plotted chiefly for comparison with the free-vortex result. This shows a gentle maximum at $p_c/p_a = 1$, which means simply that a uniform total pressure across the jet is more efficient than any linear variation of pressure. Even so, the effect is slight and becomes less marked at lower operating height ratios.

Therefore, the conclusion is that pressure gradient in the jet makes very little difference when R/t is greater than 2, let us say.

These results suggest that it may not be worthwhile to work out the cases using the more precise model of the flow developed in this report, having regard to the computational difficulty using ordinary methods. This is a job for an electronic computer, and, for the sake of completeness, it would be pleasant to see the result. However, it is fairly evident what this will be. Over the inter-

TABLE 4

COMPUTED VALUES OF $\bar{t}/R \cdot \Delta\bar{p}_c$ FOR A LINEAR GRADIENT OF TOTAL PRESSURE ACROSS THE NOZZLE - FREE-VORTEX FLOW ($\gamma = 1$)

Pc/Pa	R/t = 2	3	4	6	10
5	0.905	0.492	0.330	0.186	0.0823
2	0.957	0.503	0.333	0.1885	0.0855
1	0.971	0.507	0.333	0.1870	0.875
0.8	0.960	0.508	0.335	0.1900	0.870
0.6	0.960	0.494	0.335	0.1885	0.868
0.57	0.960 x				
0.40		0.492	0.332	0.1920	0.862
0.37		0.490 x			
0.27			0.319 x		
0.20				0.1935	0.833
0.176				0.1750 x	
0.098 (limit for R/t = 9)					0.794 x

mediate range of height, the Payne model moves from approximation to the free-vortex result at the high end ($R/t = 10$) toward the exponential result at the low end. In the middle it will be between them, and, from the appearance of the curves, it will probably show only slight effects of pressure gradient with some advantage in having the pressure high on the cushion side. However, the effect will be slight, and one should not expect a gain of more than 10 percent or so from a pressure ratio 5:1, compared with a uniform pressure design.

In an earlier section, the effect of a total pressure gradient in the jet was examined for free-vortex flow in terms of the parameter $\Delta p_c/\Delta P_{MEAN}$, the cushion pressure ratio to the linear mean total pressure in the jet. This showed a larger effect than the present analysis; for instance, at $R/t = 2$.

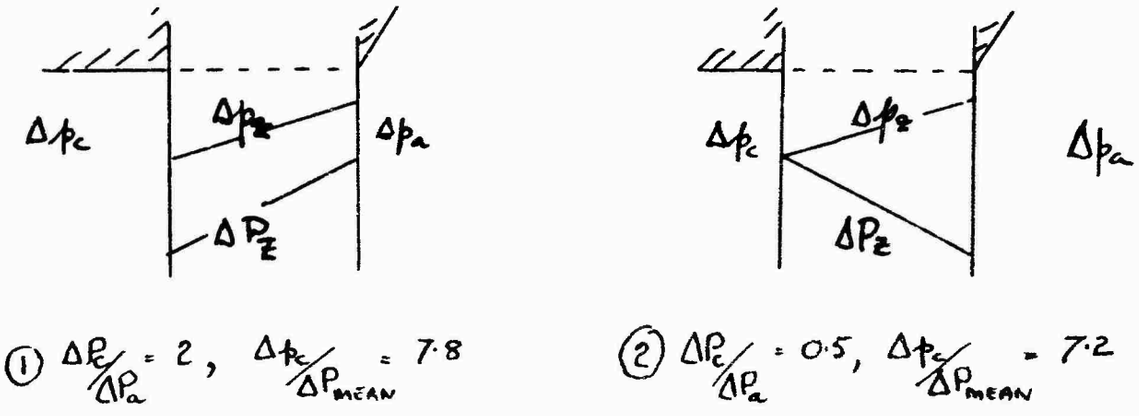

Figure 77. Pressure Distributions in Jets.

Although these jets look the same, they are absorbing different amounts of power.

$$\text{Power} \propto \int_0^t P_z (P_z - p_z)^{\frac{1}{2}} dz,$$

and this is greater when the higher total pressure is on the same side as the higher static (= cushion) pressure. Not surprisingly, the more powerful jet produces greater cushion pressure, which accounts for most, if not all, of the difference in $\Delta p_c/\Delta P_{mean}$.

This example serves to illustrate the superiority of the cushion pressure parameter as a criterion of cushion pressure achieved in proportion to power expended in the jet.

Chapter Six

VISCOUS MIXING EFFECTS IN THE ANNULAR JET

The first known treatment of the problem of viscous mixing effects in the annular jet is due to Chaplin[20], who used a simple analysis to show that mixing always causes a reduction in performance, relative to the idealized inviscid flow case.

It is doubtful whether real precision in the calculation of mixing effects can ever be achieved, because of the complexity of the induced flow fields. Nor can these effects be measured until a better understanding of annular jet flow mechanisms has been achieved, since it is impossible to say what portion of the observed loss is due to viscosity and what is due to nozzle diffusion and local flow distortions. The position is rather analogous to trying to measure the viscous drag of wings before the publication of Lanchester and Prandtl's lifting line theories, when the effects of aspect ratio on lift-curve slope and induced drag were unknown.

Reviewing the possible sources of loss which have to be separated from the viscous losses, if experimental data are to be obtained on the latter, we see that there are really only five:

1. Loss of cushion pressure due to nonuniformity of total head.

2. Loss of cushion pressure due to a local flow distortion, where the flow angle is not the same as the geometrical nozzle angle.

3. Total pressure loss due to diffusion or separation in the nozzle.

4. Fundamental reduction in cushion pressure associated with a curved planform.

5. Experimental error; the latter may be

   (a) simple errors in instrumentation or calibration,

   (b) measurements at the wrong location (measuring "cushion pressure" near the jet, for example), or

(c) rig leakage, such as a two-dimensional jet rig which has a low energy jet near the boundaries.

There are evidently enough hazards to render the unquestioning acceptance of published measurements quite impracticable, at least without a detailed analysis of the investigator's test procedures and equipment. And the problem of eliminating all but the viscous losses is correspondingly more difficult.

Figure 78 presents measurements of the cushion pressure ratio $\Delta p_c/\Delta P_{mean}$ made in three different investigations. There is obviously a significant difference between the NASA[16] model, which has a circular planform, and the two-dimensional rig results, and we might be tempted to assume that the difference in planform is the cause. The three-dimensional correction of Equation (114) indicates that this effect is small, however. Reference 16 also gives two measurements of the total head distribution across the nozzle of the Kuhn and Carter nozzle showing considerable distortion from the uniform condition. If we take a linear approximation to this distortion, we can extrapolate as shown in Figure 79. Using the theory of the previous chapter we can use this to obtain the change in cushion pressure, as shown in Figure 80. Note that although the Figure 79 extrapolation becomes progressively less reliable as we move above $h/t = 3.0$, the importance of flow distortion becomes progressively less great, so that this inaccuracy is relatively unimportant.

Making these corrections to the data in Figure 78 gives the plot shown in Figure 81.

There is evidently still a significant difference between the two sets of points, and this is presumably due to either a diffusion loss in the Reference 16 model nozzle, and/or to its jet not emerging at the nominal nozzle angle of $\theta = 0^o$. What is clearly evident is that even the two-dimensional test rig results are well below the inviscid flow theory line, and most of this deficiency is presumably attributable to viscous mixing and nozzle diffusion loss effects. Certainly a negligible amount is due to the vertical flow angle diverging from the geometric angle, as shown by the very careful streamline plotting carried out in Reference 21, from which Figure 82 is abstracted.

We can approach the viscous mixing problem in at least two ways. The most elementary regards the passage of one stream of air over another as a "skin friction" problem which is exactly analogous to the passage of air over a solid surface. Unfortunately this approach gives numerical results only for the limit solution of stationary cushion air.

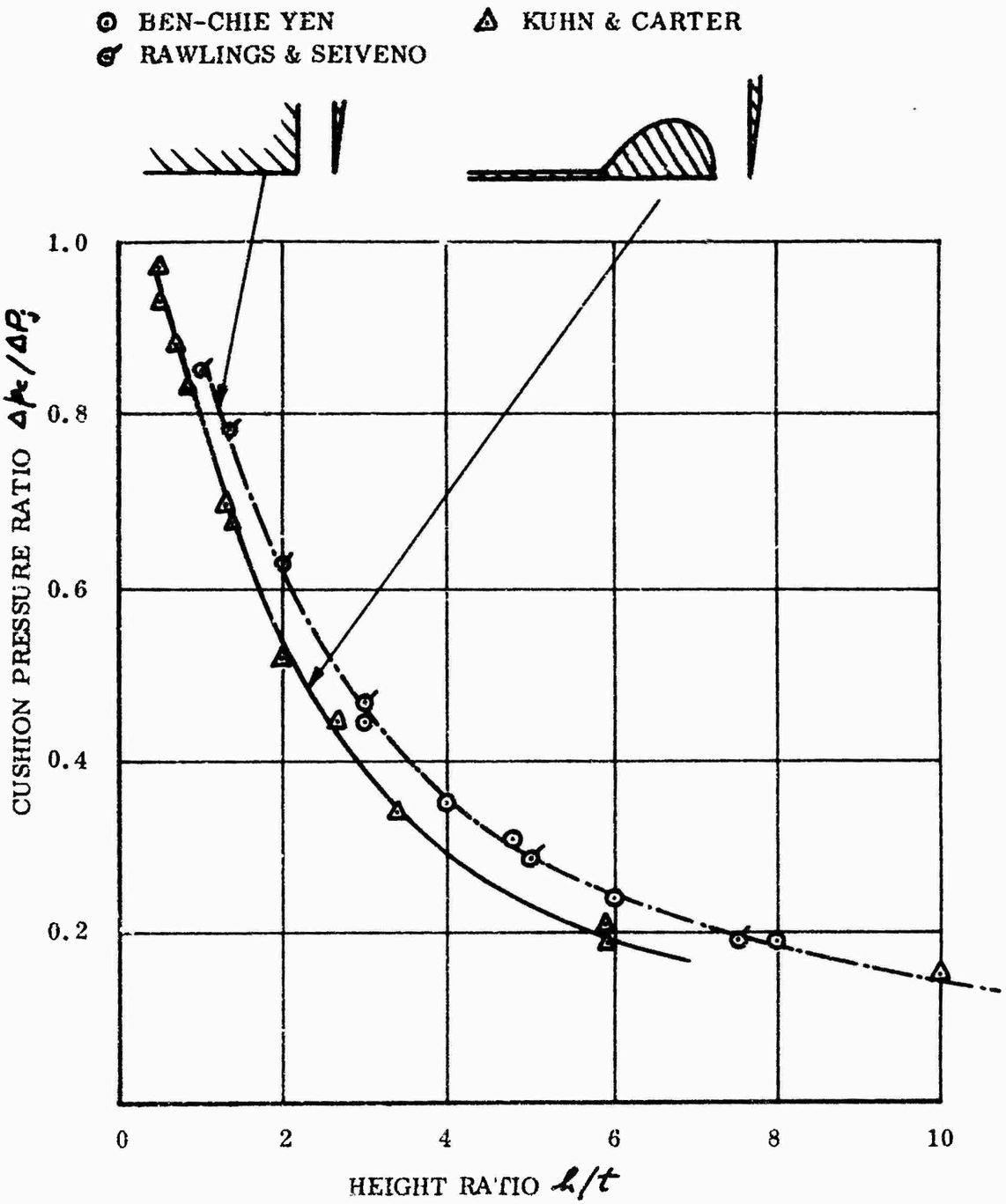

Figure 78. Some Experimental Measurements of the Cushion Pressure Parameter at $\theta = 0^{o}$.

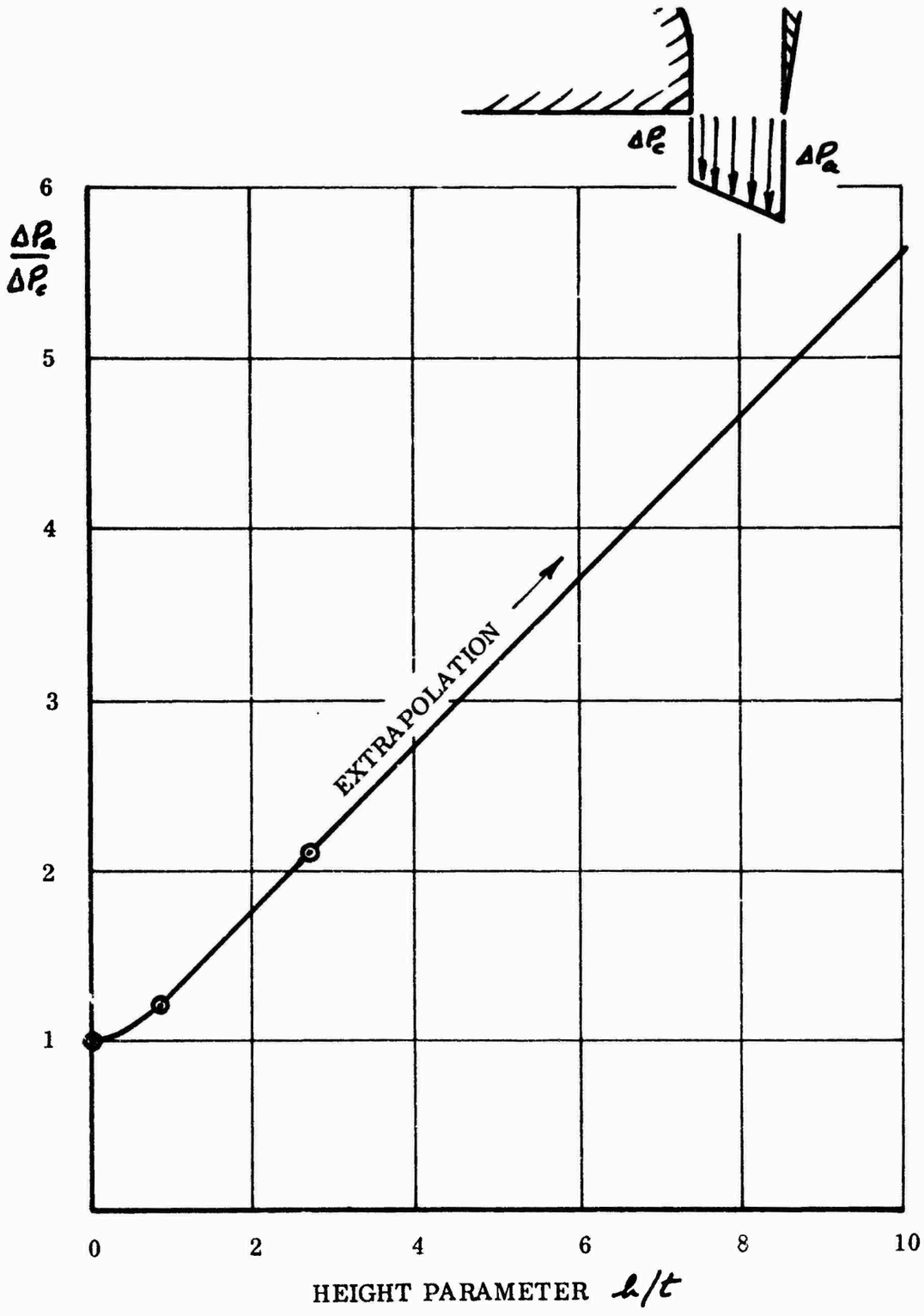

Figure 79. Assumed Equivalent Linear Total Head Distribution Across the Kuhn and Carter Model Jet.

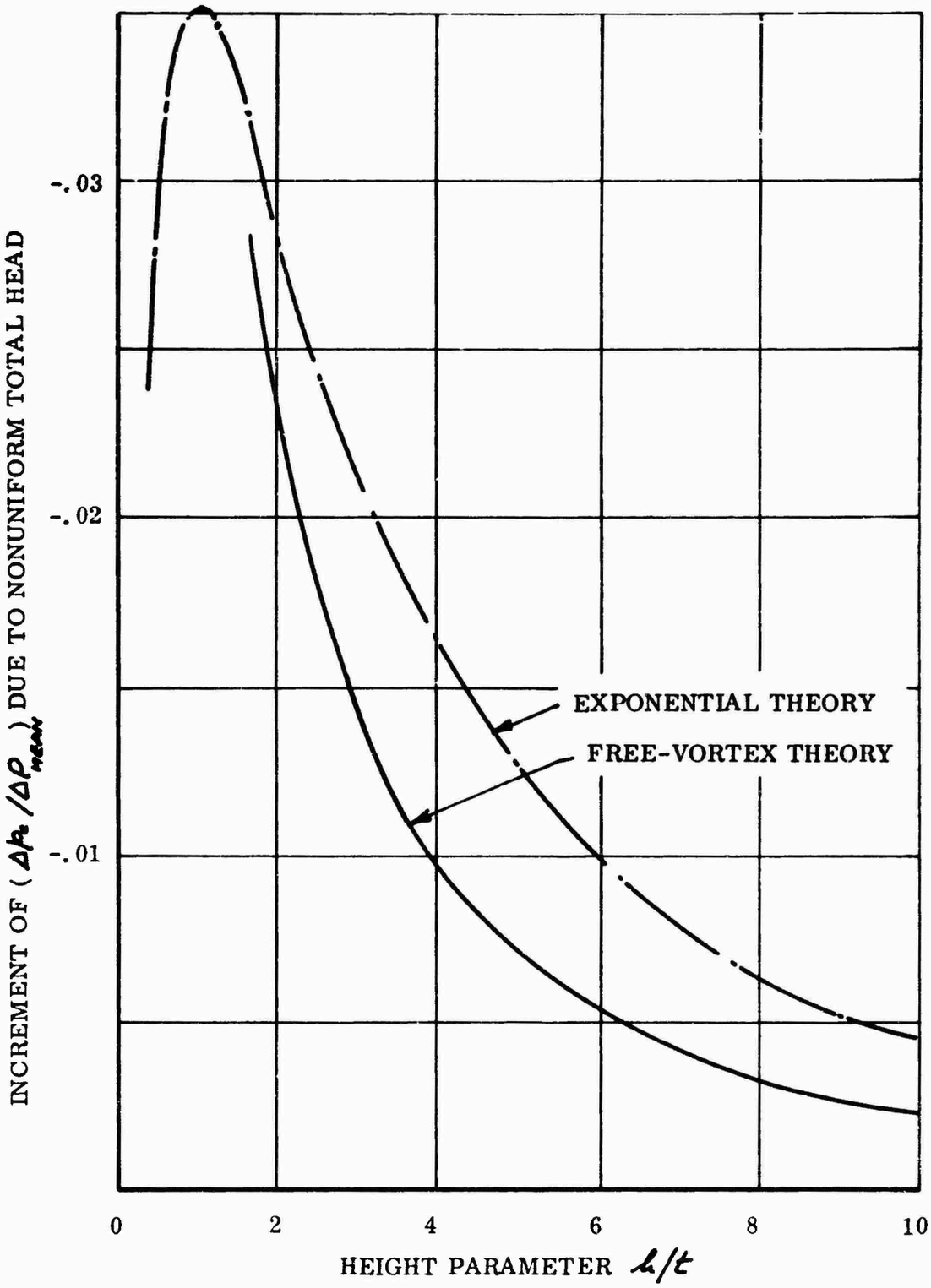

Figure 80. Increment of the Cushion Pressure Ratio Due to Total Head Distortion in the Kuhn and Carter Model.

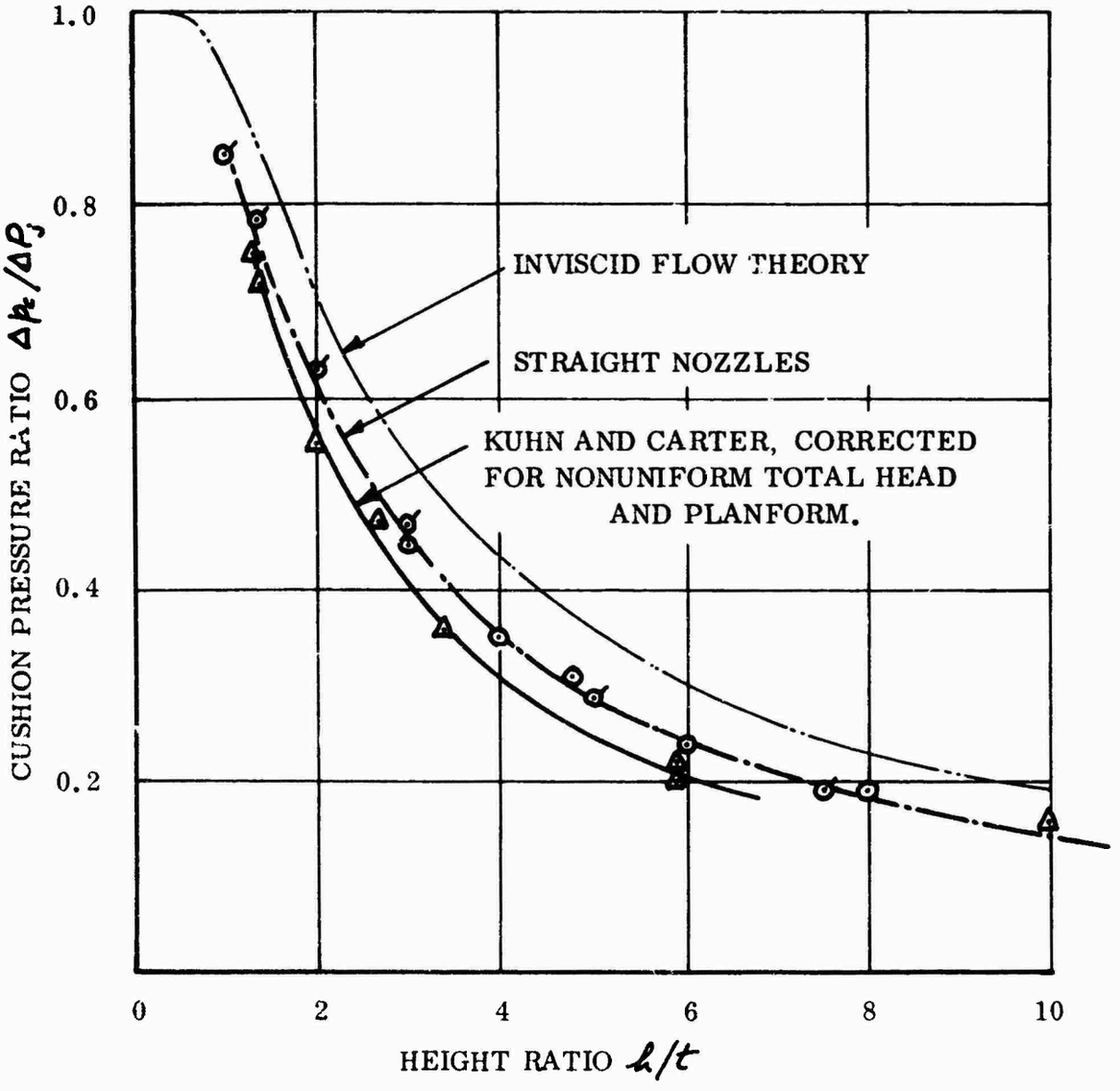

Figure 81. Data of Figure 78 With the Kuhn and Carter Results Corrected to Two-Dimensional Flow With Uniform Total Head.

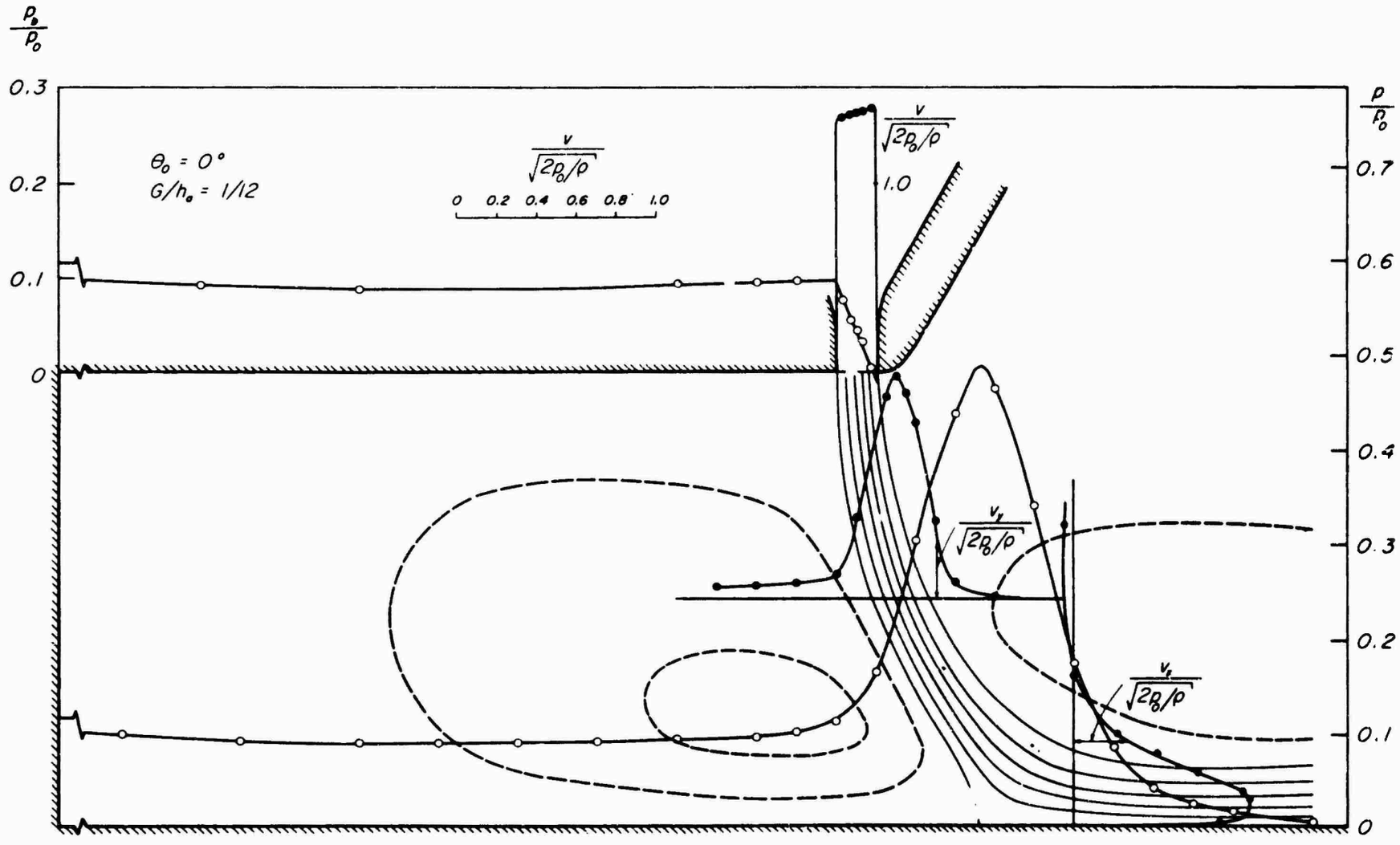

Figure 82. Curved Jet Flow Field in Ground Proximity (From Reference 21).

Alternatively, we can use a more detailed flow picture which accounts for the details of the flow entrainment process inside the cushion. At the present time there seems little point in investigating the finer details of the ambient air entrainment, since this takes place at (approximately) ambient static pressure, and should not greatly influence the cushion pressure, therefore.

THE "AIR FRICTION" CONCEPT

In Reference 3 it is shown that the "effective skin friction loss " of a jet of velocity (v_j) flowing over another stream of air (with velocity v_i) is given approximately by a skin friction coefficient,

$$C_{fa} = \frac{2\frac{\partial n}{\partial(x/t)}\left(1-\frac{v_i}{v_j}\right)}{1+\frac{x}{t}\frac{\partial n}{\partial(x/t)}} \simeq 0.16\left(1-v_i/v_j\right), \tag{207}$$

from the $\partial n/\partial(x/t)$ measurements of Reference 22.

If the length of the jet surface in contact with the cushion air is S_c , the "friction force" is

$$F_f = \tfrac{1}{2}\rho v_{NC}^2 C S_c C_f = J_N - J_j = \Delta J. \tag{208}$$

If ΔP_c is the nozzle total head on the cushion side

$$\tfrac{1}{2}\rho v_{NC}^2 = \Delta P_c - \Delta p_c ;$$

$$\therefore \quad \frac{\Delta J_j}{\Delta P_c} = C S_c C_f \left(1-\frac{\Delta p_c}{\Delta P_c}\right). \tag{209}$$

From Equation (32), for conservation of total head

$$J_a = (J_j - \Delta J_j)\left(1+\Delta p_j/\tfrac{1}{2}\rho v_j^2\right)^{1/2}$$

$$= J_a\Big|_{\text{inviscid}} - \Delta J_j\left(1+\Delta p_j/\tfrac{1}{2}\rho v_j^2\right)^{1/2}. \tag{210}$$

For thick jets, the mixing occurs in the region where the local static pressure is approximately equal to the cushion value.

$$\therefore \quad \left(1 + \Delta p_j / \tfrac{1}{2}\rho v_j^2\right)^{\frac{1}{2}} = \left(1 + \frac{\Delta p_c}{\Delta P_c - \Delta p_c}\right)^{\frac{1}{2}}$$

$$= \left(1 - \Delta p_c / \Delta P_c\right)^{-\frac{1}{2}}. \tag{211}$$

$$\therefore \quad \Delta J_a / \Delta P_c = C S_c C_f \left(1 - \Delta p_c / \Delta P_c\right)^{\frac{1}{2}}. \tag{212}$$

From Equation (101),

$$\Delta p_c = J_a / R_c = \frac{1}{R_c}\left[J_a\right]_{\text{INVISCID}} - \Delta J_{a_{\text{MIXING}}}$$

$$\frac{\Delta p_c}{\Delta P_N} = \left.\frac{\Delta p_c}{\Delta P_N}\right|_{\text{INVISCID}} - \frac{\Delta P_c}{\Delta P_N} \cdot \frac{S_c}{R} \cdot C_f \left(1 - \Delta p_c / \Delta P_c\right)^{\frac{1}{2}}, \tag{213}$$

and for uniform nozzle total head

$$\frac{\Delta p_c}{\Delta P_N} = \left.\frac{\Delta p_c}{\Delta P_N}\right|_{\text{INVISCID}} - \frac{S_c}{R} \cdot C_f \left(1 - \Delta p_c / \Delta P_c\right)^{\frac{1}{2}}. \tag{214}$$

The accuracy of the assumptions is such that we may as well use the inviscid value for $\Delta p_c / \Delta P_N$ inside the square root sign, when the jet is thick; that is, when $h/t < 1.0$ say, so that

$$\frac{\Delta p_c}{\Delta p_{c\,\text{INVISCID}}} = 1 - C_f \frac{S_c}{R} \frac{\left(1 - \Delta p_c / \Delta P_{N,\text{INVISCID}}\right)^{\frac{1}{2}}}{\Delta p_c / \Delta P_{N\,\text{INVISCID}}}. \tag{215}$$

Note from the geometry of Figure 41 that

$$S_c = 2\pi R \cdot \frac{\pi/2 + \theta}{2\pi} = \left(\frac{\pi}{2} + \theta\right) R. \tag{216}$$

When viscosity causes an appreciable reduction in Δp_c, we must solve Equation (214) exactly. By squaring we have

$$\left(\frac{\Delta p_c}{\Delta P_{N\,INV.}}\right)^2 - 2\left(\frac{\Delta p_c}{\Delta P_{N\,INV.}}\right)\left(\frac{\Delta p_c}{\Delta P_N}\right) + \left(\frac{\Delta p_c}{\Delta P_N}\right)^2 = \left(\frac{S_c C_f}{R}\right)^2\left(1 - \Delta p_c/\Delta P_N\right)$$

$$\left(\frac{\Delta p_c}{\Delta P_{N\,INV}}\right)^2 - \frac{\Delta p_c}{\Delta P_N}\left[2\frac{\Delta p_c}{\Delta P_{N\,INV}} - \left(\frac{S_c C_f}{R}\right)^2\right] + \left(\frac{\Delta p_c}{\Delta P_{N\,INV}}\right)^2 - \left(\frac{S_c C_f}{R}\right)^2 = 0. \quad (217)$$

In the quadratic solution to (217)

$$\text{"}b^2 - 4ac\text{"} = \left(\frac{S_c C_f}{R}\right)^4\left[1 + \frac{4\left(1 - \Delta p_c/\Delta P_{N\,INV.}\right)}{\left(\frac{S_c C_f}{R}\right)^2}\right]; \quad (218)$$

$$\therefore \frac{\Delta p_c}{\Delta P_N} = \frac{\Delta p_c}{\Delta P_{N\,INV}} - \frac{1}{2}\left(\frac{S_c C_f}{R}\right)^2\left[1 \mp \left\{1 + \frac{4\left(1 - \Delta p_c/\Delta P_{N,INV}\right)}{\left(\frac{S_c C_f}{R}\right)^2}\right\}^{\frac{1}{2}}\right]. \quad (219)$$

The minus root is the correct solution. As can be seen from Figure 83, the difference between Equations (215) and (219) is quite small.

This particular analysis cannot be extended into the "thin jet" regime because the concept of "skin friction" between two fluid streams, both of which are thicker than the mixing zone between them, is then invalidated.

The theoretical limit is of course $S_c/t = 5.2$

$$S_c = \left(\frac{\pi}{2} + \theta\right)R = 5.2\,t$$

$$\left(\frac{R}{t}\right)_{LIMIT} = \frac{5.2}{\pi/2 + \theta} = 3.31 \text{ for } \theta = 0.$$

As shown in Figure 83, this approach appears to give fair agreement with experiment for $R/t < 1.5$, when we take the limit case of still cushion air

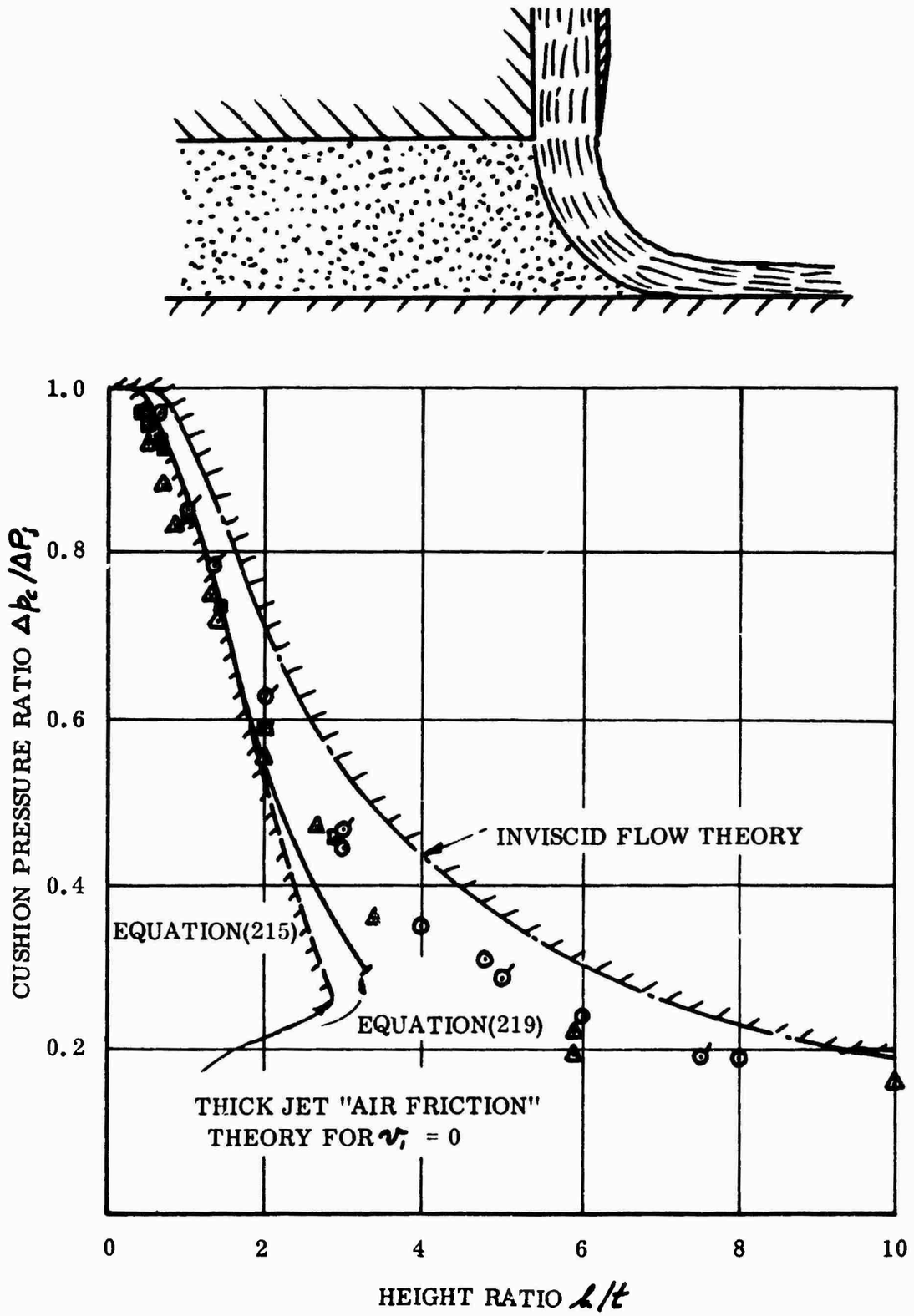

Figure 83. The "Air Friction" Theory of Viscous Losses in a Thick Jet Compared With Inviscid Flow Theory for $\theta = 0^{o}$.

($\eta_1 = 0$), although the Kuhn and Carter points still fall below the line. Presumably the true value of η_1 is somewhere between zero and unity, so that all points would fall above it in the range $0 < h/t < 1.5$, and presumably the deficiency would then represent nozzle losses.

The air friction theory should show a loss in cushion pressure as the length of jet in contact with the cushion is increased. Some experimental work at Aeronutronic[23], involving the use of rigid nozzle extensions, enables us to make a rough check on this hypothesis.

Some raw data from Reference 23 are displayed in Figure 84, in comparison with results obtained from conventional two-dimensional test rigs. The cushion pressure is shown to fall significantly when an extension is fitted, which does not agree with the Payne tests reported in a previous chapter. We presume this is due to some instrumentation error on the Aeronutronic rig.

When the inner extension is shortened or removed, more of the jet will be in contact with the cushion. Thus relative to the extended nozzle results of Figure 84, the cushion pressure should be less than even the reduced values obtained with symmetrical extensions. As shown in Figure 85, this is in fact so, although the results can hardly be regarded as indicating a consistent trend.

Now from Equation (214) we can express the reduction in cushion pressure by the equation

$$\frac{\Delta p_c}{\Delta P_j} = \left(\frac{\Delta p_c}{\Delta P_N}\right)_{\substack{\text{ACTUAL,} \\ \text{FULL NOZZLE} \\ \text{EXTENSIONS}}} - \frac{\Delta S_c C_f}{R}\left(1 - \Delta p_c/\Delta P_{N\ \text{ACTUAL}}\right)^{1/2} \qquad (220)$$

or

$$\Delta\left(\frac{\Delta p_c}{\Delta P_j}\right) = -\frac{\Delta S_c}{\ell} \cdot C_f \frac{\left(1 - \Delta p_c/\Delta P_{N\ \text{ACTUAL}}\right)^{1/2}}{h/t} \qquad (221)$$

when $\theta = 0^\circ$, so that $R = \ell$.

For the geometry of Figure 85,

$$\Delta S_c/t = (c_o - \ell_i)/t,$$

of course.

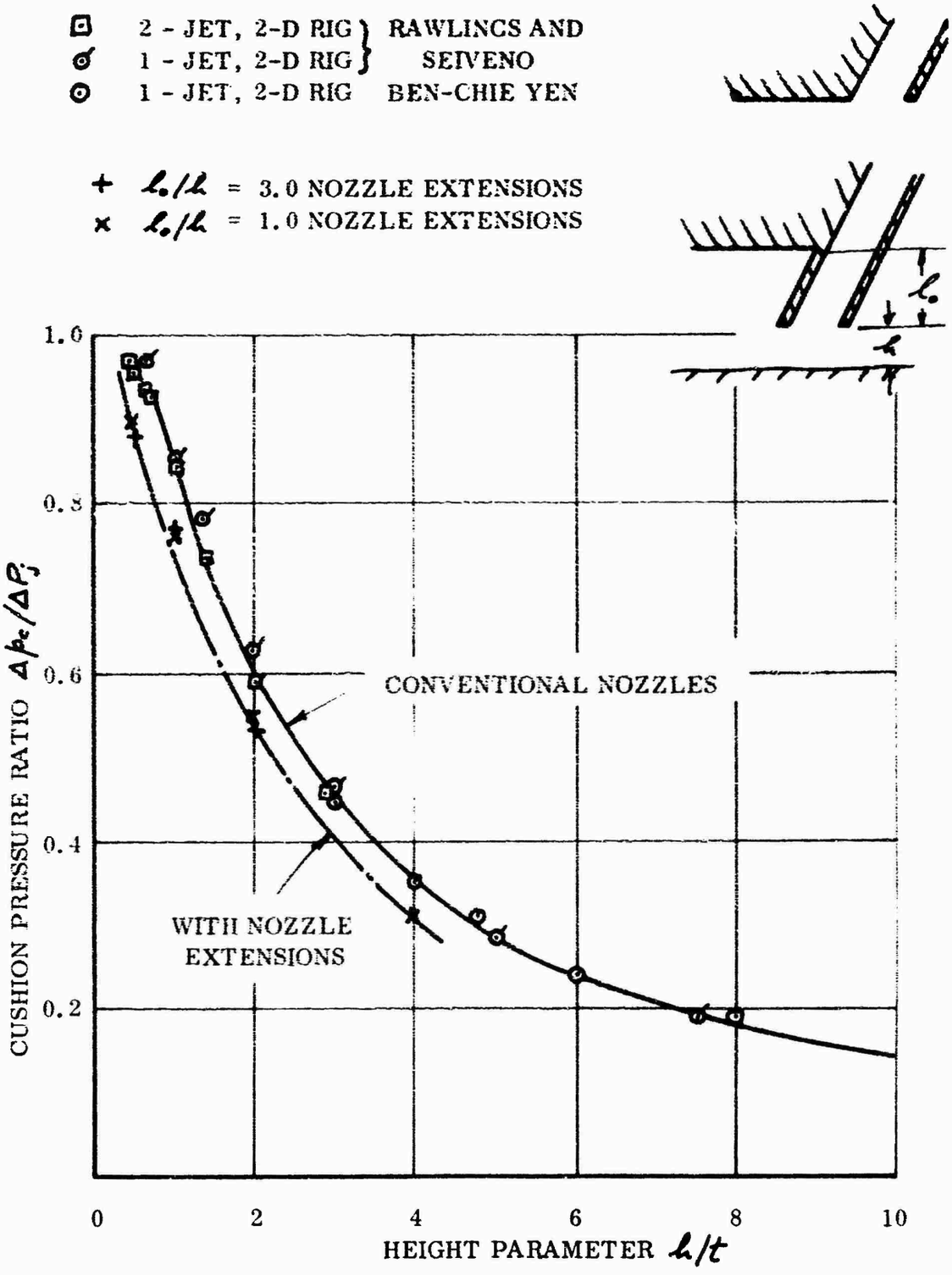

Figure 84. Effect of Nozzle Extensions on the Cushion Pressure Ratio ($\theta = 0^{\circ}$).

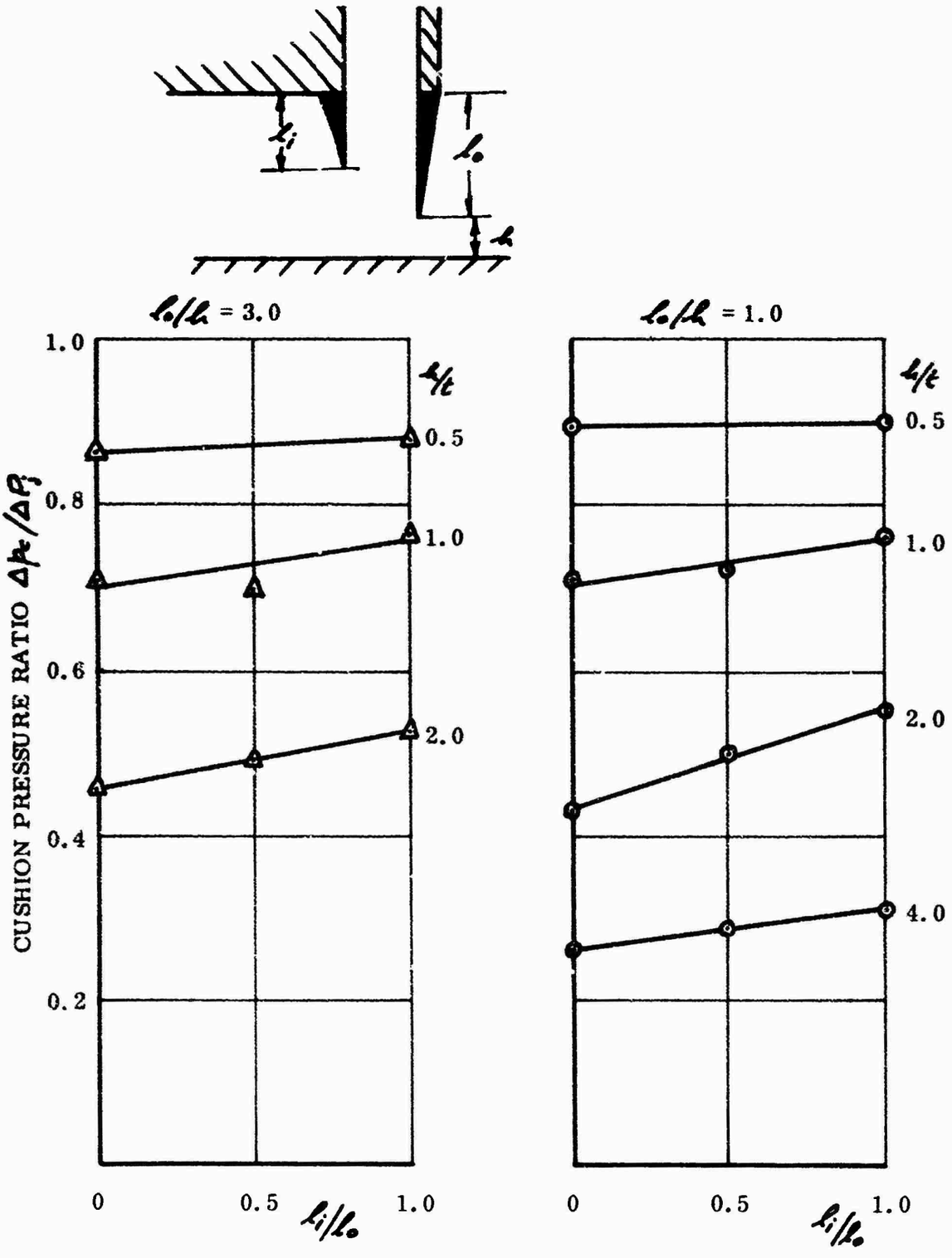

Figure 85. Effect of Exposing the Inner Surface of the Jet When Nozzle Extensions Are Used (Reference 23).

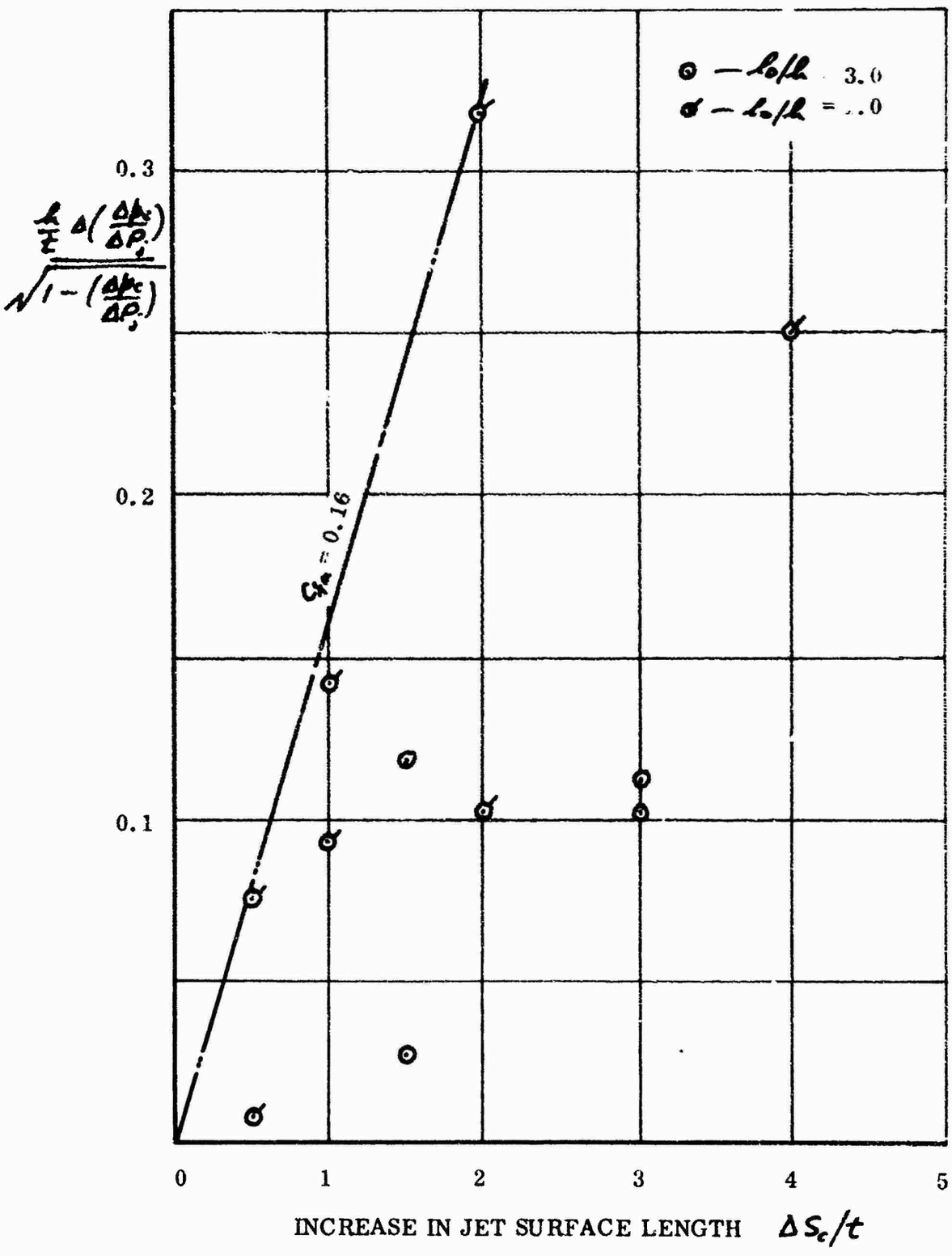

Figure 86. Reduced Aeronutronic Data of Figure 85.

Equation (221) has been used to plot the expression

$$\frac{h}{t}\,\Delta\left(\frac{\Delta p_c}{\Delta P_j}\right)\left(1-\frac{\Delta p_c}{\Delta P_j}\right)^{-\frac{1}{2}} = -\frac{\Delta S_c}{t}\,C_f \qquad (222)$$

in Figure 86. The scatter is very large, as we would expect in analyzing this type of data. Nevertheless an appropriate trend is detectable and all points fall on or below the $C_f = 0.16$ curve, indicating $v_i/v_j > 0$. Moreover, the $\ell_o/h = 1.0$ points are noticably higher, on the average, than the $\ell_o/h = 3.0$ ones; this again is reasonable because the entrained vortex flow would be virtually parallel to the jet in the latter case.

A GENERAL THEORY OF MIXING LOSS

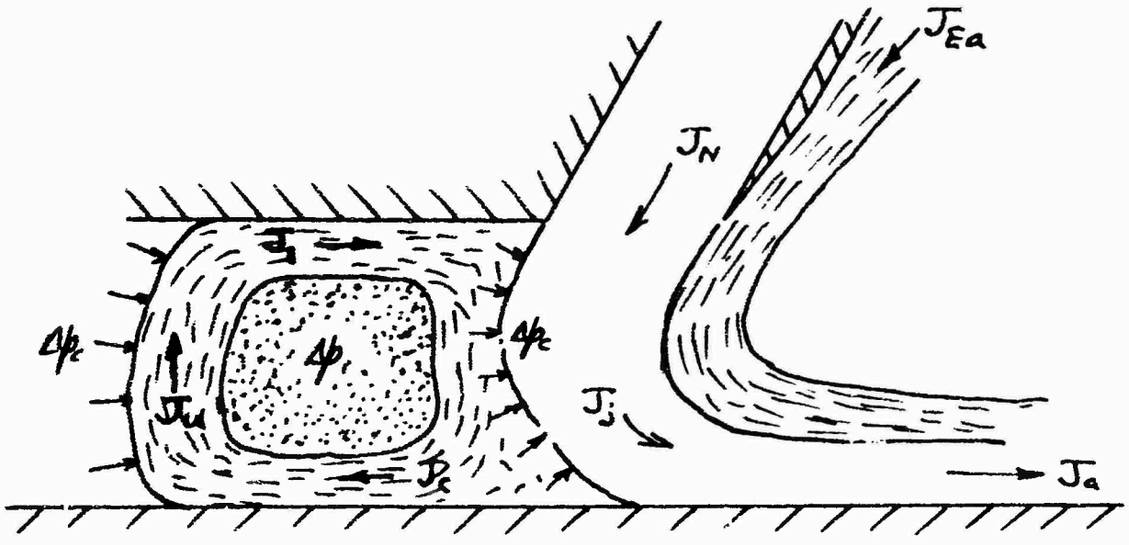

Figure 87. Mixing in the Annular Jet.

Under equilibrium conditions, it is generally agreed that viscous mixing causes the entrained flows illustrated in Figure 87. If S_c and S_a are distances along the jet surfaces on the cushion and ambient sides respectively, then from Reference 4, the entrained airflow ratio

$$n = \frac{\dot{m}_j}{\dot{m}_N} - 1 = \frac{1}{2}\,\frac{\partial n}{\partial (x/t)}\left[\frac{S_c}{t} + \frac{S_a}{t}\right].$$

For continuity of mass flow, the entrained cushion air must return to the cushion, and since some transfer of momentum has occurred, the momentum flux to ambient of the main part of the jet is accordingly reduced.

This must result in the cushion pressure being less than the value predicted for inviscid flow. We can regard this either as being caused by a reduction of the momentum flux to ambient (as in the previous section) or by a reduction in the curvature of the jet.

From a long term point of view, the best approach is likely to involve expressing the local jet velocity distribution in a suitable analytic form (such as the error-function distribution), weighting it for the effect of varying static pressure, and solving the resulting equations for the inward and outward flows.

In the present analysis we shall take a simpler approach, using the general concepts of Reference 4, but making the use of the general momentum relationship of Equation (101)

$$\Delta p_c = \frac{J_a}{RC}$$

We shall also assume that mixing on the ambient side of the jet does not influence J_a, because there is nominally no pressure change, so that all mixing effects are attributable to the cushion.

The entrainment of cushion air reduces J_a by an amount ΔJ_a as explained in the previous section, so that we may write

$$\Delta p_c = \Delta p_{c_{INVISCID}} - \frac{\Delta J_a}{Ch} - F \qquad (223)$$

where F = a cushion entrainment term which will be discussed later.

The flow picture of Figure 87 is similar to that of an overfed jet, as indicated in Figure 88. However, the big difference is that we do not obtain as low a cushion pressure, unless all the primary vortex momentum (J_c) is dissipated ($J_1 = 0$).

The momentum loss ΔJ_a is readily calculated when the entrainment function is known, and it is reasonable to assume that the momentum flux J_c into the cushion is equal to the momentum lost by the outgoing jet. Then knowing $\dot{m}_c$ and J_c we know the mean effective velocity v_c into the cushion.

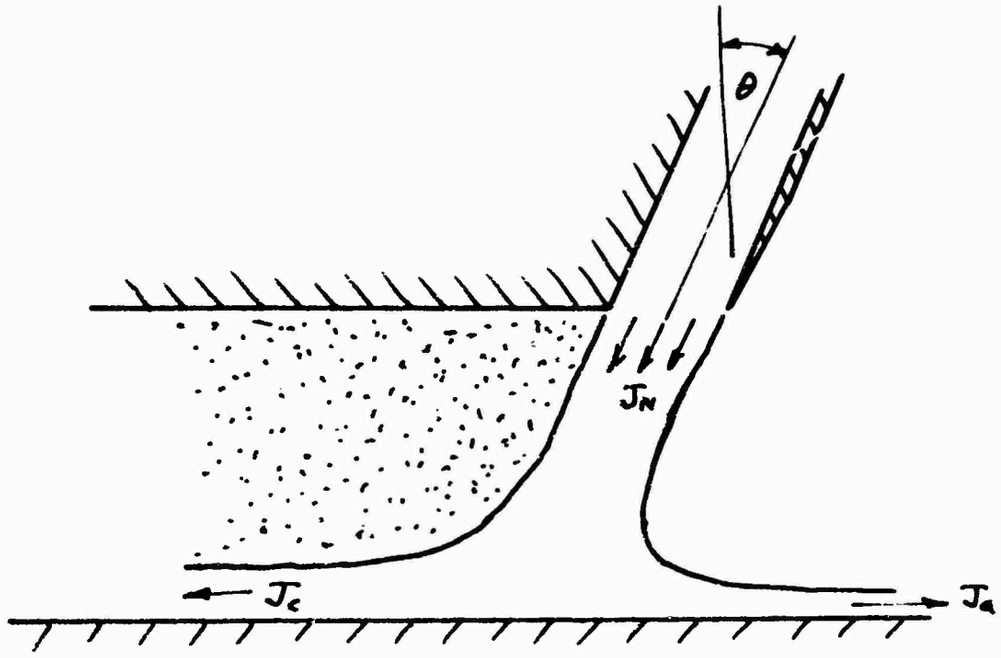

(a) Conventional Overfed Jet.

$$\Delta p_c = \frac{1}{hC}\left[J_N \sin\theta + J_a - J_c \right]$$

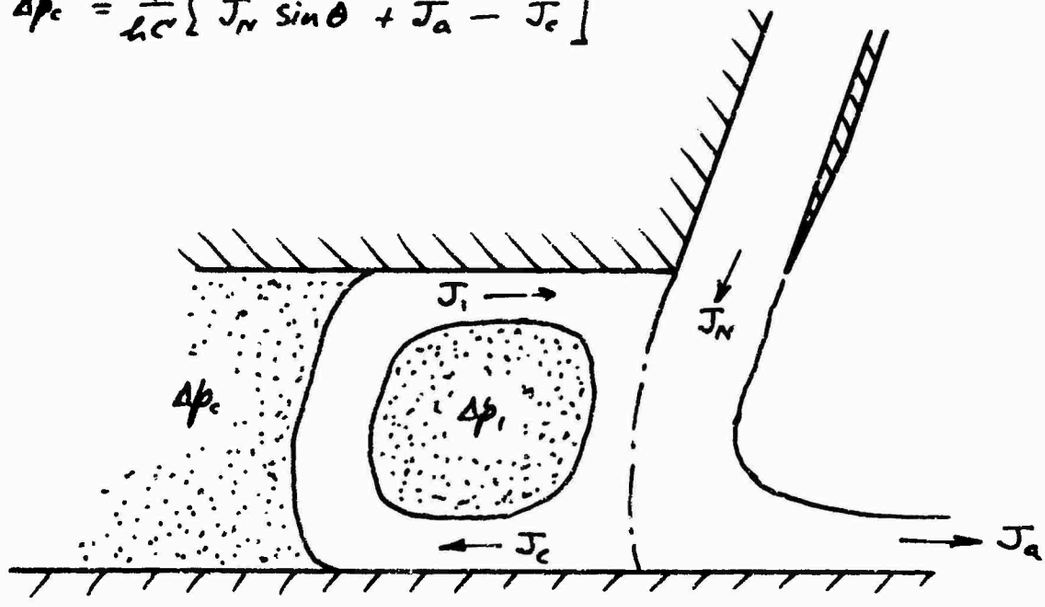

(b) Jet With Primary Vortex.

$$\Delta p_c = \frac{1}{hC}\left[J_a - (J_c - J_1) \right] \qquad \Delta p_1 = \Delta p_c - \left(\frac{J_c + J_1}{hC} \right)$$

Figure 88. Two Ways of Portraying the Overfed Jet.

The momentum flux, J_1 , back to the jet is less than J_c because of skin friction losses against the ground plane and base plate and because of air friction between the outside of the vortex and the inner cushion air. The inner air may be stationary or there may be a secondary vortex; possibly the former is true of a finite planform, and the latter of a two-dimensional test rig. When a secondary vortex exists the air friction will be much less, of course.

We now proceed to express this chain of reasoning mathematically, assuming that entrainment takes place over $\phi h/t$, where ϕh is the distance over which entrainment occurs. (From Figure 82, for example, we might expect $\frac{1}{4} < \phi < \frac{1}{2}$).

Now, for mixing at constant static pressure (Figure 87)

$$J_N = J_j + J_c \tag{224}$$

or, in terms of average values,

$$\dot{m}_N \dot{v}_N = (\dot{m}_j + \dot{m}_c)\dot{v}_c ;$$

$$\therefore \quad \dot{v}_c = \frac{\dot{v}_N}{1 + n/2} \tag{225}$$

since the entrained air mass flow is $\frac{n\dot{m}_N}{2}$;

$$\therefore \quad J_c = \frac{n \dot{m}_N \dot{v}_N / 2}{1 + n/2}$$

$$= \frac{n \dot{J}_N}{2(1 + n/2)} \tag{226}$$

and $$n = \partial n / \partial(x/t) \cdot \phi \, h/t .$$

$\dot{J}_N$ is the momentum flux at the nozzle. However, when the vehicle is close to the ground, mixing occurs only on the innermost portions of the jet, and it would be unrealistic to take $\dot{J}_N$ as the total value (J_N) for the whole jet, particularly in the zone of establishment ($\phi h/t < 5.2$). We should rather weight $\dot{J}_N$ to be representative of the velocity and mass flow pertaining to that part of the jet in which mixing actually occurs.

Using the vortex assumptions of Reference 4, and denoting C_{fa}, C_{fg} as the skin friction coefficients of the cushion air and ground respectively, then

referring to Figure 87

$$J_c - J_m = C_{fG} \cdot \tfrac{1}{2}\rho v_c^2 hC$$

$$J_m - J_1 = C_{fa} \cdot \tfrac{1}{2}\rho v_c^2 hC . \qquad (227)$$

The skin friction on the base plate is here neglected as being negligible, and for convenience we assume that the skin friction in both the ground and cushion regions can be based on the v_c velocity.

Then

$$J_m = J_c - C_{fG} \cdot \tfrac{1}{2}\rho v_c^2 hC$$

$$J_1 = J_m - C_{fa} \cdot \tfrac{1}{2}\rho v_c^2 hC$$

$$= J_c - \tfrac{1}{2}\rho v_c^2 hC(C_{fa} + C_{fG}); \qquad (228)$$

$$\therefore J_c - J_1 = \tfrac{1}{2}\rho v_c^2 hC(C_{fa} + C_{fG}) . \qquad (229)$$

Thus from Figure 88

$$\Delta p_c = \frac{J_m}{hC} - \tfrac{1}{2}\rho v_c^2 (C_{fa} + C_{fG}) . \qquad (230)$$

But from (210) and (224)

$$J_a = J_{a_{INVISCID}} - J_c\left(1 + \frac{\Delta p_j}{\tfrac{1}{2}\rho v_j^2}\right)^{1/2}; \qquad (231)$$

$$\therefore \Delta p_c = \Delta p_{c_{INVISCID}} - \frac{J_c}{hC}\left(1 + \frac{\Delta p_j}{\tfrac{1}{2}\rho v_j^2}\right)^{1/2} - \frac{\rho}{2}\left(\frac{J}{\dot{m}_c}\right)^2 (C_{fa} + C_{fG}) \qquad (232)$$

where J_c and $\dot{m}_c$ are given by Equations (225) and (226). Δp_j and v_j are of course mean effective values.

The solution of Equation (232) can be accomplished in varying degrees of accuracy, depending upon how detailed we care to make the analysis of J_N and $\dot{m}_c$. Using the simple values given by Equations (225) and (226) and assuming uniform total head in the jet we can obtain a solution which is applicable at large values of h/t.

$$\frac{\Delta p_c}{\Delta P_j} = \frac{\Delta p_c}{\Delta P_{j\,\text{INVISC.}}} - \frac{n}{1+n/2}\cdot\frac{t}{h}\cdot\frac{J_N}{2Ct\Delta P_j}\left(1-\frac{\Delta p_i}{\Delta P_j}\right)^{-1/2}$$

$$-\frac{C_{fa}+C_{fc}}{(1+n/2)^2}\cdot\left[\frac{\dot{m}_j}{Ct\,(2\rho\Delta P_j)^{1/2}}\right]^2. \qquad (233)$$

The non-dimensional ratios

$$\left(1-\frac{\Delta p_i}{\Delta P_j}\right)^{1/2}, \quad \frac{J_N}{2Ct\Delta P_j} \quad \text{and} \quad \frac{\dot{m}_j}{Ct\,(2\rho\Delta P_j)^{1/2}}$$

must be known before Equation (233) can be evaluated. However, they are of second-order importance, since they appear only in the viscous correction to the exact solution, and they can be derived with sufficient accuracy from exponential theory. We proceed as follows:

$$\frac{-\tau_z}{(2\rho\Delta P_j)^{1/2}} = e^{-z/R} \qquad (234)$$

$$\frac{\dot{m}_z}{Ct(2\rho\Delta P_j)^{1/2}} = \frac{1}{t}\int_0^z e^{-z/R}\,dz = \frac{R}{t}\left(1-e^{-z/R}\right). \qquad (235)$$

The mass flow on the cushion side of the point z is

$$\frac{\Delta\dot{m}_j}{Ct\,(2\rho\Delta P_j)^{1/2}} = \frac{R}{t}\left(e^{-z/R}-e^{-t/R}\right). \qquad (236)$$

Taking this value as average across the jet

$$\frac{\dot{m}_j}{Ct(2\rho\Delta P_j)^{1/2}} = \frac{e^{-3/R} - e^{-t/R}}{t/R - 3/R} . \tag{237}$$

If the amount of the jet affected is the same* as the quantity of air entrained, then from Equation (236) and (237)

$$n \cdot \frac{e^{-3/R} - e^{-t/R}}{t/R - 3/R} = R/t \cdot (e^{-3/R} - e^{-t/R}) \tag{238}$$

or $\quad 3/t = 1-n \quad$ and $\quad 3/R = t/R \cdot (1-n)$;

$$\therefore \quad \frac{\dot{m}_j}{Ct(2\rho\Delta P_j)^{1/2}} = \frac{e^{-(1-n)t/R} - e^{-t/R}}{nt/R} . \tag{239}$$

We can also calculate the average momentum flux and static pressure (Δp_j) in the mixing zone, using the same approach.

$$\frac{J_{j3}}{2Ct\Delta P_j} = \frac{1}{t}\int_0^3 e^{-2z/R}\,dz = \frac{R}{2t}(1 - e^{-2z/R}); \tag{240}$$

$$\therefore \quad \Delta J = \frac{R}{2t}(e^{-2z/R} - e^{-2t/R}) = \frac{R}{2t}(e^{-2t/R(1-n)} - e^{-2t/R}). \tag{241}$$

Averaging across the jet

$$\frac{\Delta \dot{J}_j}{2Ct\Delta P_j} = \frac{\frac{1}{2}(e^{-2t/R(1-n)} - e^{-2t/R})}{nt/R} . \tag{242}$$

---

* Actually, for entrainment on one side of a jet, it can be shown that $\Delta \dot{m}_N = 1.2\,\dot{m}_N$, using the Rouse data.

The local static pressure is

$$\frac{\Delta p_3}{\Delta P_j} = 1 - e^{-2\zeta/R} .$$

Thus, the arithmetric average in the region $t/R \geq \zeta/R > 1-n$ is

$$\frac{\Delta p_j}{\Delta P_j} = 1 - \tfrac{1}{2}\left(e^{-2t/R(1-n)} + e^{-2t/R}\right) \tag{243}$$

and

$$\left(1 - \frac{\Delta p_j}{\Delta P_j}\right)^{1/2} = \left(\frac{e^{-2t/R(1-n)} + e^{-2t/R}}{2}\right)^{1/2} . \tag{244}$$

Substituting these values in Equation (237),

$$\frac{\Delta p_c}{\Delta P_j} = \frac{\Delta p_c}{\Delta P_{j\,\text{inviscid}}} - \frac{R/h}{1+n/2} \cdot \frac{\tfrac{1}{2}\left(e^{-2t/R(1-n)} - e^{-2t/R}\right)}{\sqrt{\tfrac{1}{2}\left(e^{-2t/R(1-n)} + e^{-2t/R}\right)}}$$

$$- \frac{(C_{fa} + C_{fa})}{(1+n/2)^2} \cdot \frac{\left(e^{-t/R(1-n)} - e^{-t/R}\right)^2}{n^2 (t/R)^2} \tag{245}$$

$$(\phi h/t < 5.2)$$

$$e^{-2t/R(1-n)} - e^{-2t/R} = e^{-2t/R}\left(e^{2nt/R} - 1\right), \quad \text{etcetera},$$

so that Equation (245) becomes

$$\frac{\Delta p_c}{\Delta P_j} = \frac{\Delta p_c}{\Delta P_j} - \frac{R}{h} \cdot \frac{e^{-t/R}\left(e^{2nt/R} - 1\right)}{(2)^{1/2}(1+n/2)\left(e^{2nt/R} + 1\right)}$$

$$- \frac{C_{fa} + C_{fa}}{(1+n/2)^2} e^{-2t/R} \cdot \left(\frac{e^{nt/R} - 1}{n\, t/R}\right)^2 \tag{246}$$

$$(\phi h/t < 5.2).$$

Also, in the region $\phi h/t < 5.2$,

$$n = 0.08\phi h/t = 0.08\phi \frac{h}{R}\cdot\frac{R}{t}\ ; \tag{247}$$

$$\therefore\ nt/R = 0.08\phi h/R\ . \tag{248}$$

Substituting in (246),

$$\frac{\Delta p_c}{\Delta P_j} = \frac{\Delta p_c}{\Delta P_{j\ \text{INVISCID}}} - \frac{\frac{R}{t}\cdot\frac{e^{-t/R}}{2\pi}\left(e^{0.16\phi h/R} - 1\right)}{\left(1 + 0.04\phi\frac{h}{R}\cdot\frac{R}{t}\right)\left(e^{0.16\phi h/R} + 1\right)^{1/2}}$$

$$- \frac{(C_{f_a} + C_{f_G})e^{-2t/R}\left(e^{0.08\phi h/R} - 1\right)^2}{\left(1 + 0.04\phi\frac{h}{R}\cdot\frac{R}{t}\right)^2 (0.08\phi h/R)^2}\ . \tag{249}$$

Note that the two viscous mixing terms tend to zero as $h/t \to 0$.

Within the order of accuracy of this analysis, a further simplification is possible, by virtue of the fact that $0.16\,\phi h/R \ll 1.0$.

Thus, we can write

$$e^{0.16\phi h/R} - 1 = 0.16\,\phi h/R$$

$$\frac{\Delta p_c}{\Delta P_j} = \frac{\Delta p_c}{\Delta P_{j\ \text{INVISCID}}} - \frac{0.08\phi e^{-t/R}}{\left(1 + 0.04\phi\frac{h}{R}\cdot\frac{R}{t}\right)\left(1 + 0.04\phi\frac{h}{t}\right)}$$

$$- \frac{(C_{f_a} + C_{f_G})e^{-2t/R}}{\left(1 + 0.04\phi\frac{h}{R}\cdot\frac{R}{t}\right)^2}\ . \tag{250}$$

For $\phi h/t > 5.2$ we use the normal equations for J_N and $\dot{m}_j$ which gives

$$\frac{\Delta p_c}{\Delta P_j} = \frac{\Delta p_c}{\Delta P_{j\ inviscid}} - \frac{n}{1+n/2}\frac{t}{h}\cdot\frac{1-e^{-2t/R}}{2t/R\cdot e^{-t/R}}$$

$$- \frac{(C_{fa}+C_{fa})(1-e^{-t/R})^2}{(1+n/2)^2(t/R)^2} \qquad (251)$$

where $$n = 0.62(\phi h/t - 1)^{1/2}. \qquad (252)$$

Note that in the limit $t/h \to 0$,

$$\frac{\Delta p_c}{\Delta P_j} \to \frac{\Delta p_c}{\Delta P_{j\ inviscid}} - \frac{t}{h}\cdot\frac{n}{1+n/2} - \frac{C_f}{(1+n/2)^2}$$

$$\to \frac{\Delta p_c}{\Delta P_{j\ inviscid}} - \frac{0.62(\phi h/t)^{\frac{1}{2}} - t/h}{\frac{1}{2}+0.31(\phi h/t)^{\frac{1}{2}}} - \frac{C_f}{\left[\frac{1}{2}+0.31(\phi h/t)^{\frac{1}{2}}\right]^2}$$

$$\to \frac{\Delta p_c}{\Delta P_{j\ inviscid}} \to 0.$$

In practice the case of $\phi h/t > 5.2$ rarely occurs, since it implies $h/t > 10$, approximately. Thus Equation (250) is of most interest.

This equation is plotted in Figure 89 for the case of $\theta = 0^o$. It is evident that the loss in cushion pressure is very large when no secondary vortex exists, so that the full static air friction drag acts on the primary vortex. This extreme is unlikely in practice of course, but on the other hand, the secondary vortex cannot be expected to be loss-free so that the lower limit will not be approached either.

These limiting results are presented in Figure 90 in the conventional form of the cushion pressure ratio against height. The experimental points are seen to fall below the limit for $h/t < 2.0$, and it is thought that this deficiency probably represents diffusion losses in the nozzle, rather than a gross error

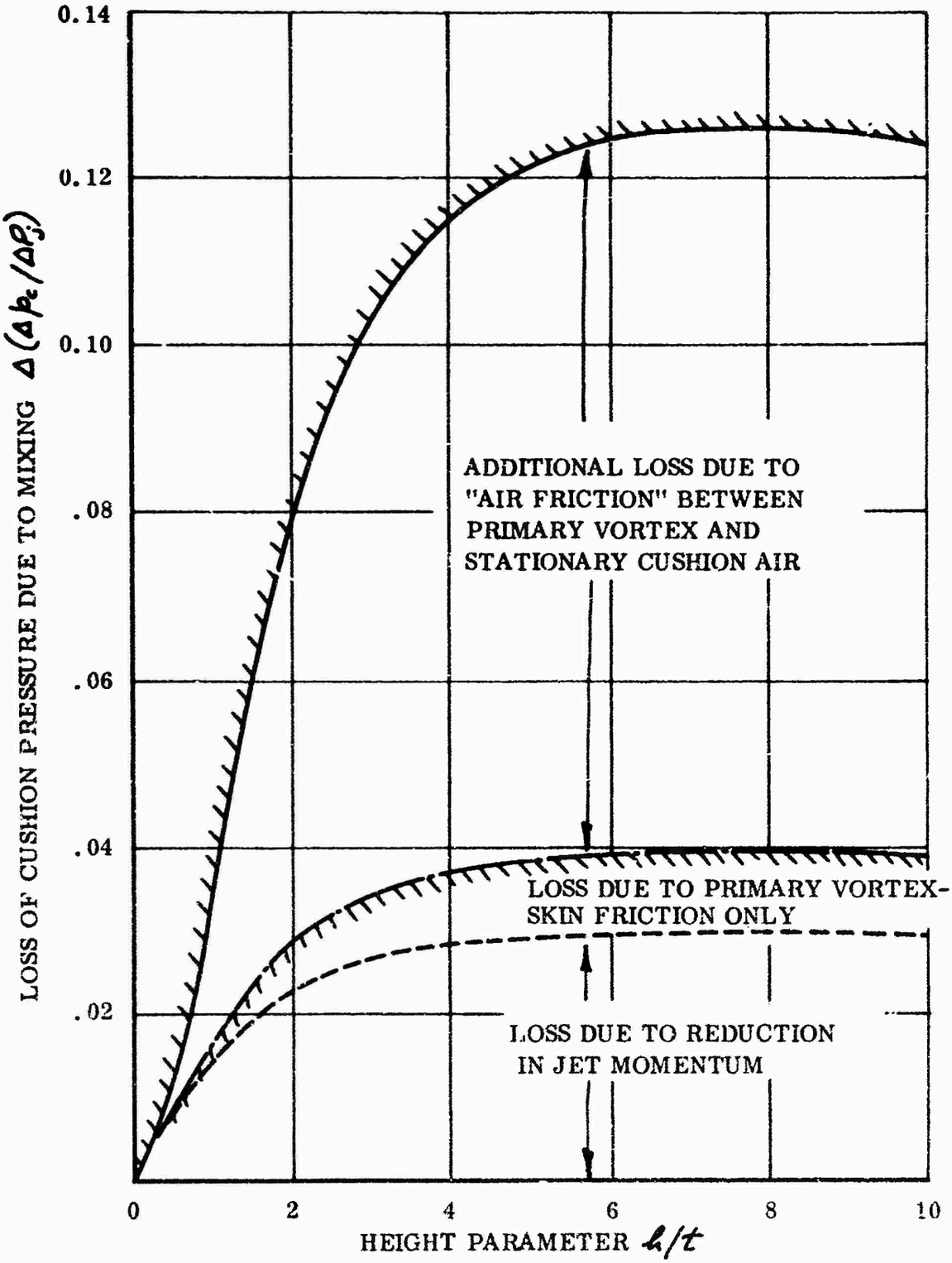

Figure 89. Theoretical Loss in Cushion Pressure Caused by Viscous Mixing ($\theta = 0^{o}$).

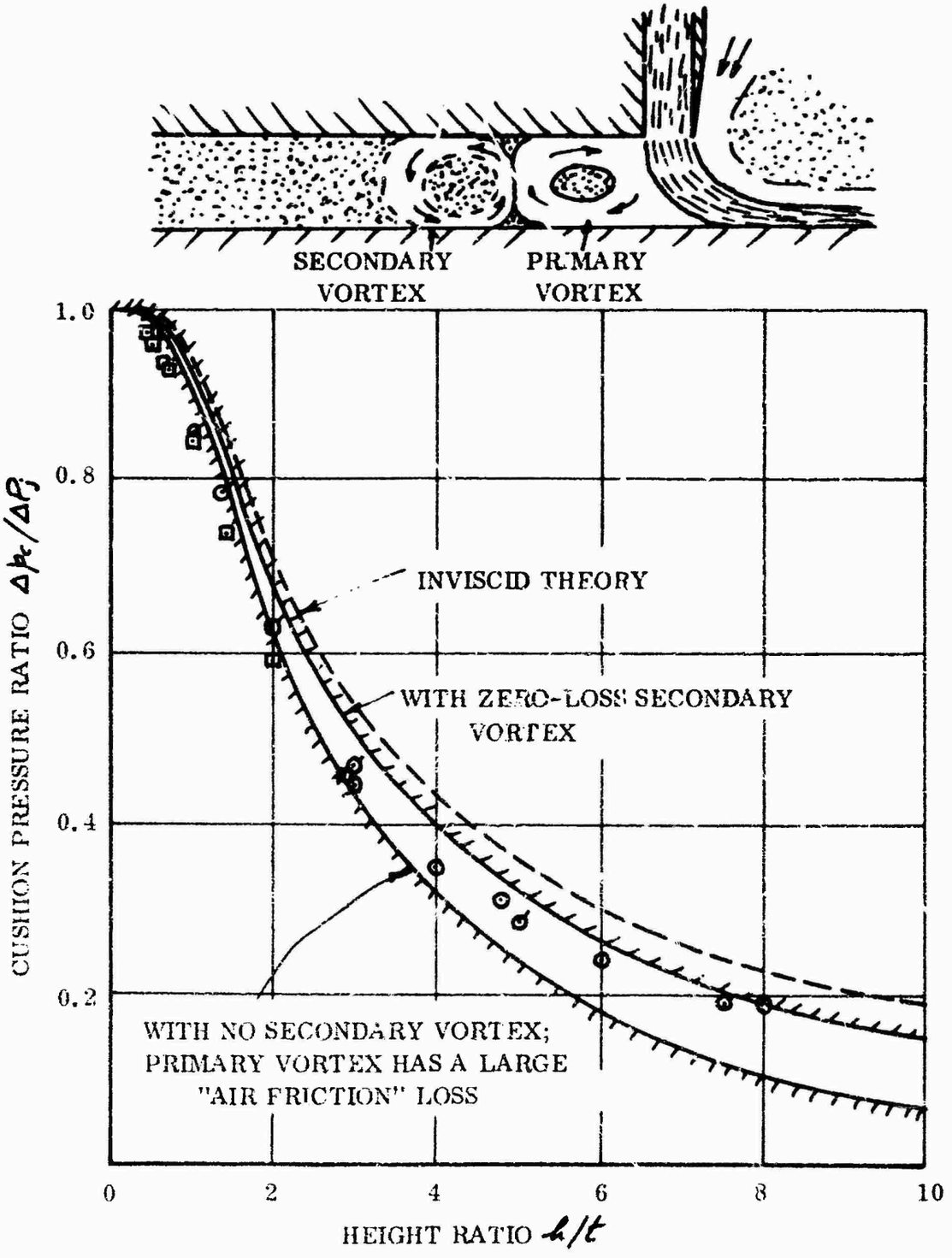

Figure 90. Comparison of Viscous Mixing Theory With Experiment for $\theta = 0^{\circ}$. (Experimental Points From Figure 84).

in the viscous mixing theory. Such diffusion losses are considered in the next chapter.

THE STATIC PRESSURE IN THE PRIMARY VORTEX

From Figure 88 the primary vortex pressure is

$$\Delta p_i = \Delta p_c - \frac{J_c + J_1}{hC}. \tag{253}$$

In general, $J_1 < J_c$, due to friction losses. However, the air must flow back to the jet, so that we can never have the condition $J_1 = 0$. At the present time, therefore, since we are necessarily ignorant of the exact value of the entrainment function n and the distance over which entrainment occurs, it seems sufficiently accurate to assume $J_1 = J_c$ and $J_1 = 0$ as the two extremes.

Since
$$J_c = \frac{n/2}{1+n/2}\dot{J}_N = \frac{n/2}{1+n/2}\cdot\frac{Ct\Delta P_j}{nt/R}\left(e^{-2t/R(1-n)} - e^{-2t/R}\right),$$

$$\frac{2J_c}{hC} = \Delta P_j e^{-2t/R}\cdot 0.16\,\phi\,; \tag{254}$$

$$\therefore \quad \frac{\Delta p_i}{\Delta p_c} = 1 - \frac{\Delta P_j}{\Delta p_c}\cdot 0.16\,\phi\, e^{-2t/R}$$

$$= 1 - \left\{\begin{matrix}0.16\\0.08\end{matrix}\right\}\phi\cdot\frac{e^{-2t/R}}{1-e^{-2t/R}} \tag{255}$$

where 0.16 is used when $J_1 = J_c$, and half that value when $J_1 = 0$.

Equation (255) is plotted in Figure 91 together with the available experimental data. The nature of this particular measurement inevitably gives rise to a great deal of scatter unless the experiment is specially designed for it, and it is noteworthy that the two Hydronautics[24] measurements, made during a program specially designed to study this effect, agree very well with the theory. The Aeronutronic data are very scattered, indicating the possibility of low accuracy, and the Iowa State data, while consistent, indicate much lower values than the other two. Thus a new and quite detailed experimental investigation is evidently necessary before any firm conclusions can be drawn.

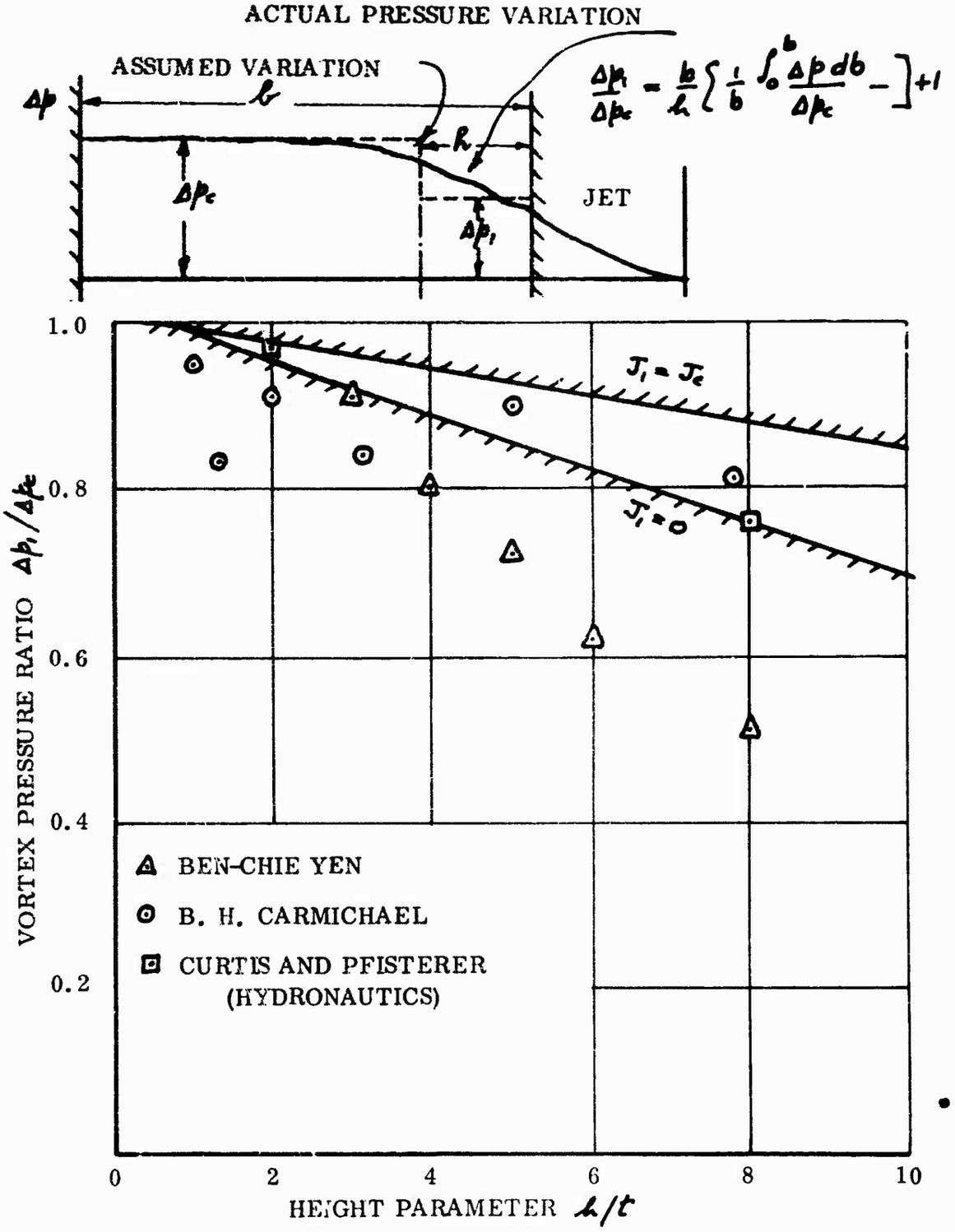

Figure 91. Primary Vortex Pressure as a Function of Hover Height ($\theta = 0^{o}$).

Chapter Seven

A SMALL PERTURBATION THEORY OF DIFFUSION LOSSES IN AN ANNULAR JET NOZZLE

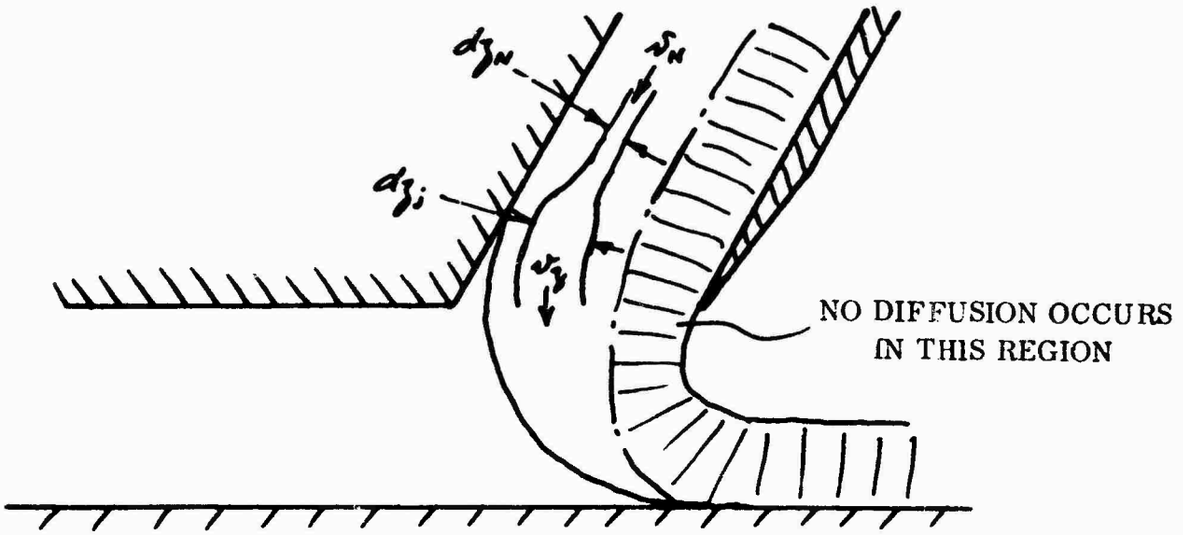

Figure 92. Basic Geometry of Nozzle Diffusion.

We come now to a second important source of loss; that due to the diffusion which occurs on the inside of the nozzle as the local velocity slows from v_N to v_3 .

The existence of such a diffusion loss was postulated by Payne in 1964[13] and was first measured in the present program. It appears to be a significant source of energy loss at normal operating heights but one which could easily escape experimental observation unless the experimenter was actually looking for it. (In this regard the Chaplin annular jet rig used by Payne, Inc. is a very powerful tool, because of its excellent flow distribution in the nozzle ducting upstream of the nozzle proper and because the pressure loss appears as a "gauge" reading .)

The existence of diffusion in the nozzle is easy to understand, of course, because the jet must balance the cushion pressure, which is necessarily higher than the static pressure in the nozzle. Typical wall pressure distributions obtained with the Chaplin test rig are illustrated in Figures 93 and 94.

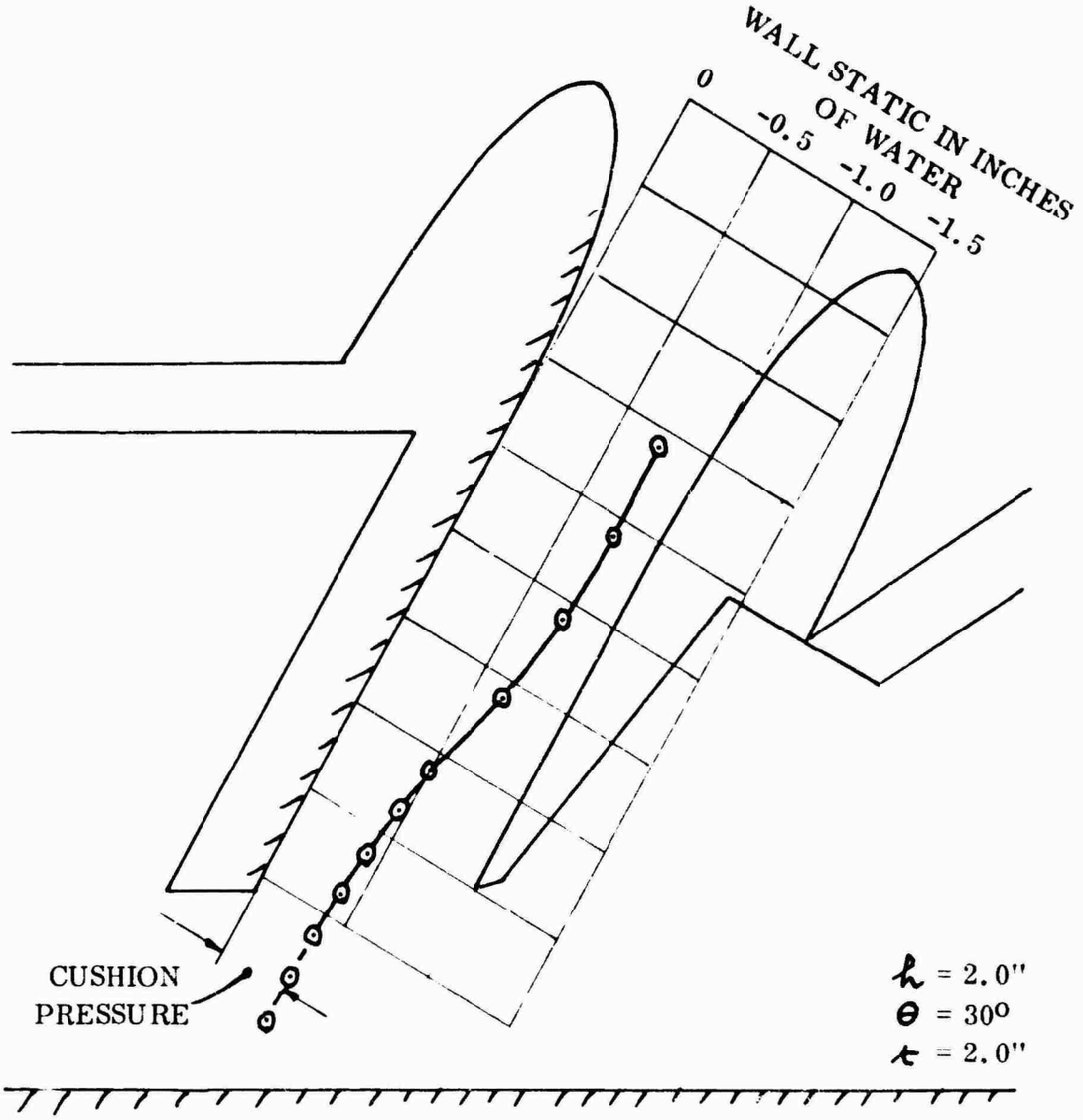

Figure 93. Static Pressure Distribution on the Inside Nozzle Wall.

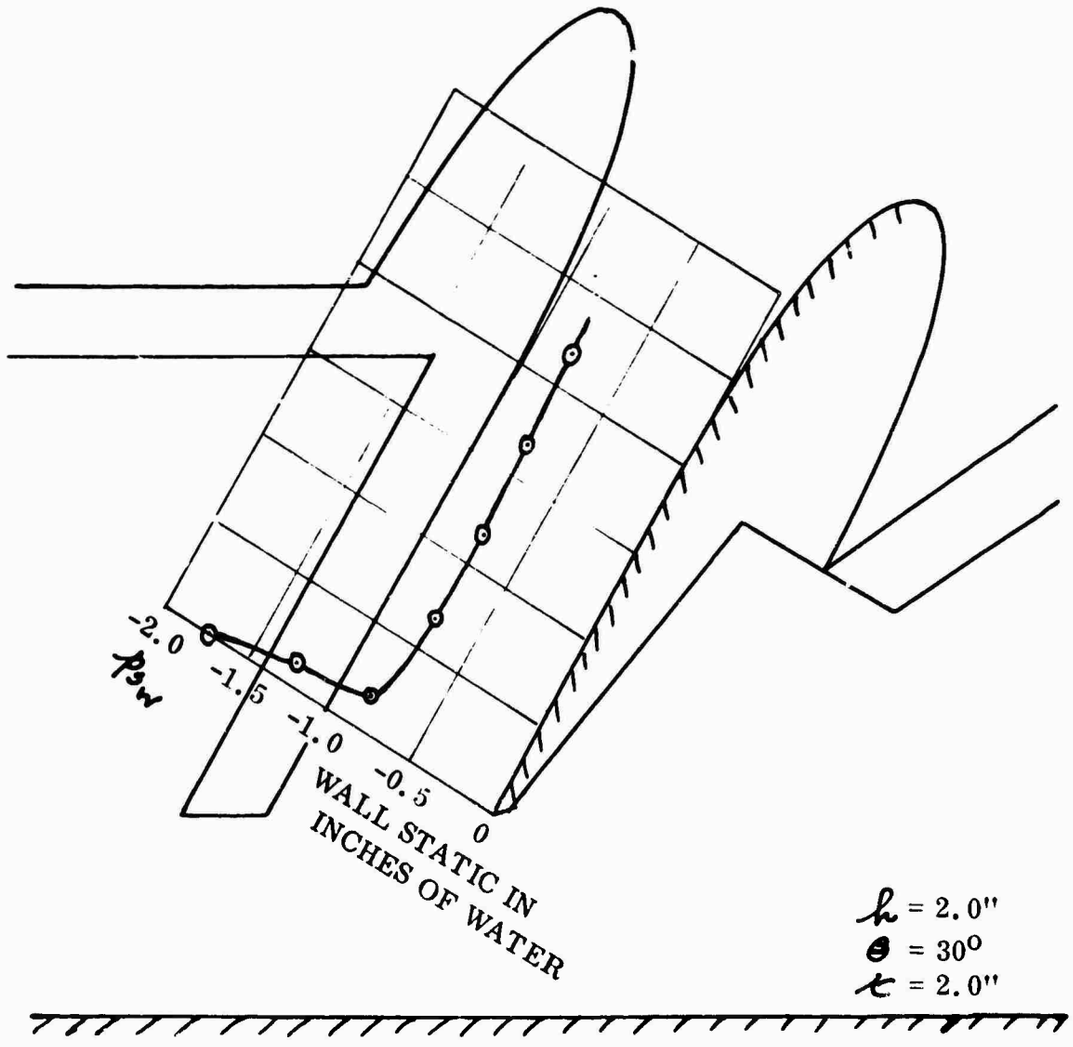

Figure 94. Static Pressure Distribution on the Outside Nozzle Wall.

The present state of diffusion theory can hardly be regarded as satisfactory, of course. However, the theory developed in Chapter Two enables us to obtain an estimate if we assume that diffusion takes place at constant static pressure.

If v_N is the velocity of a filament in the nozzle, before diffusion starts, and v_3 is the local velocity in the developed jet, then the total head loss ΔH is given by Equation (80)

$$\frac{\Delta H}{\Delta P_3} = \left(1 - \frac{v_3}{v_N}\right)^2 \left(1 - \frac{\Delta p_N}{\Delta P_3}\right) \tag{256}$$

where Δp_N = static pressure in the nozzle duct upstream of the diffusion section

ΔP_3 = total pressure at the same station.

APPROXIMATE SOLUTION FOR A "STRAIGHT" NOZZLE

In this section we assume a conventional straight nozzle and an "exponential" jet with an initially constant total head distribution.

Thus
$$\frac{\Delta p_3}{\Delta P_j} = 1 - e^{-z_3/R}. \tag{257}$$

The mass flow is given by

$$\dot{m}_j = Ct(2\rho\Delta P_j)^{\frac{1}{2}} \frac{1 - e^{-t/R}}{t/R} = \rho C t v_N ;$$

$$\therefore v_N = \left(\frac{2}{\rho}\Delta P_j\right)^{\frac{1}{2}} \frac{1 - e^{-t/R}}{t/R}. \tag{258}$$

For simplicity, we define

$$\frac{1 - e^{-t/R}}{t/R} = \frac{1}{\psi} \tag{259}$$

Since $v_3 = \left(\frac{2}{\rho}\Delta P_j\right)^{\frac{1}{2}} e^{-z/R}$,

$$\frac{v_3}{v_N} = \psi e^{-3/R}. \tag{260}$$

Also, since $\frac{\Delta p_N}{\Delta P_j} = 1 - \frac{1}{2}\rho v_N^2 / \Delta P_j$

$$\frac{\Delta p_N}{\Delta P_j} = 1 - 1/\psi. \tag{261}$$

From Equations (260) and (261),

$$\frac{\Delta H}{\Delta P_j} = \frac{(1 - \psi e^{-3/R})^2}{\psi}. \tag{262}$$

Note that $\Delta H = 0$ when

$$e^{-3/R} = \frac{1}{\psi} \tag{263}$$

$$3/R = \log \psi \tag{264}$$

Equation (262) is plotted in Figure 95 for a typical case.

This approach can be regarded as a "small perturbation" analysis, in that we neglect the change in v_3 caused by the loss in total head. A more exact treatment would result in larger calculated losses.

MEAN TOTAL PRESSURE LOSS

The mean total head change will be given by

$$\bar{\Delta P} = \Delta P_j - \frac{1}{t}\int_{3'}^{t} \Delta H \, dz ;$$

$$\therefore \quad \frac{\bar{\Delta P}}{\Delta P_j} = 1 - \frac{1}{\psi t}\int_{3'}^{t} (1 - 2\psi e^{-3/R} + \psi^2 e^{-2 3/R}) \, dz \tag{265}$$

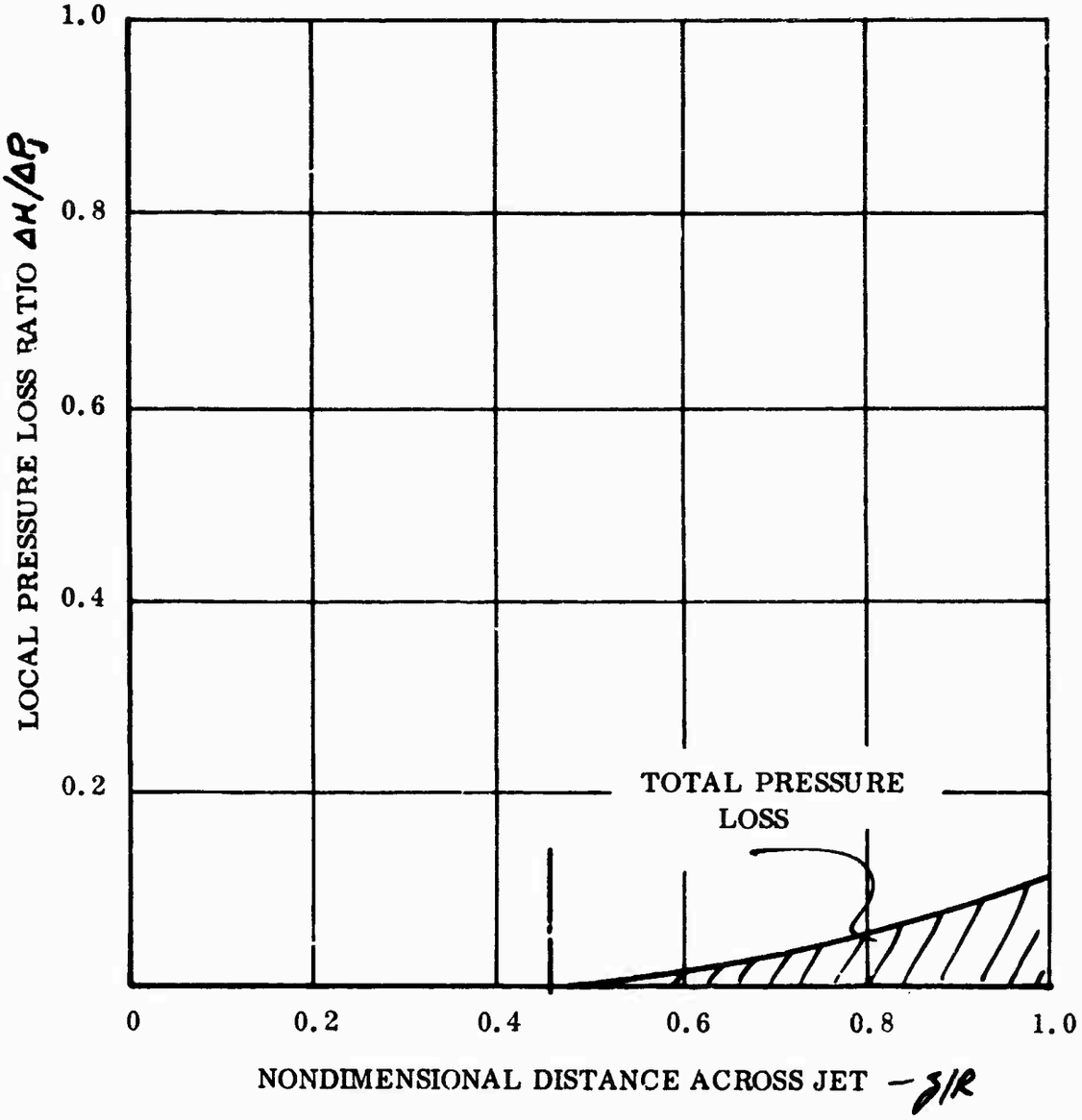

Figure 95. Approximate Total Pressure Loss Due to Diffusion for $t/R = 1.0$, in a Straight Nozzle. (Based on the Exponential Theory Static Pressure Distribution.)

$$\frac{\overline{\Delta P}}{\Delta P_j} = 1 - \frac{\rho/\epsilon}{\psi}\left[\epsilon/R - \log\psi - 2\left(1-\psi e^{-\epsilon/R}\right) + \tfrac{1}{2}\left(1-\psi e^{-2\epsilon/R}\right)\right]. \quad (266)$$

The loss component of Equation (266) is plotted in Figure 96. At a height corresponding to $\epsilon/R = 2.0$ for example, there is a 5% loss in mean total head. The actual cushion pressure loss will be somewhat greater than 5%, of course, because of the unfavorable ΔP_3 gradient resulting, even though this is offset, to some extent, by the thickening of the jet. It will also be greater by virtue of the "small perturbation" assumption, as noted earlier.

It is interesting to note that the actual pressure loss measured in the Chaplin rig (Chapter Four) was 4%, instead of the theoretical figure of 2.5%.

TOTAL POWER LOSS DUE TO DIFFUSION

Power is defined as

$$\mathcal{P} = \int_0^A \Delta P_v \, dA. \quad (267)$$

The power loss is

$$\Delta\mathcal{P} = \mathcal{P}_N - \mathcal{P}_j$$

or

$$\frac{\Delta\mathcal{P}}{\mathcal{P}_N} = 1 - \frac{\mathcal{P}_j}{\mathcal{P}_N}.$$

We are interested only in that part of the jet in which diffusion occurs, of course.

The power of this part is

$$\mathcal{P}_j' = \int_{z'}^{\epsilon_j} (\Delta P_j - \Delta H) v_3 \, dz$$

$$= \int_{z'}^{\epsilon_j} \Delta P_j v_3 \, dz - \int_{z'}^{\epsilon_j} \Delta H v_3 \, dz. \quad (268)$$

The power of the remainder of the jet is

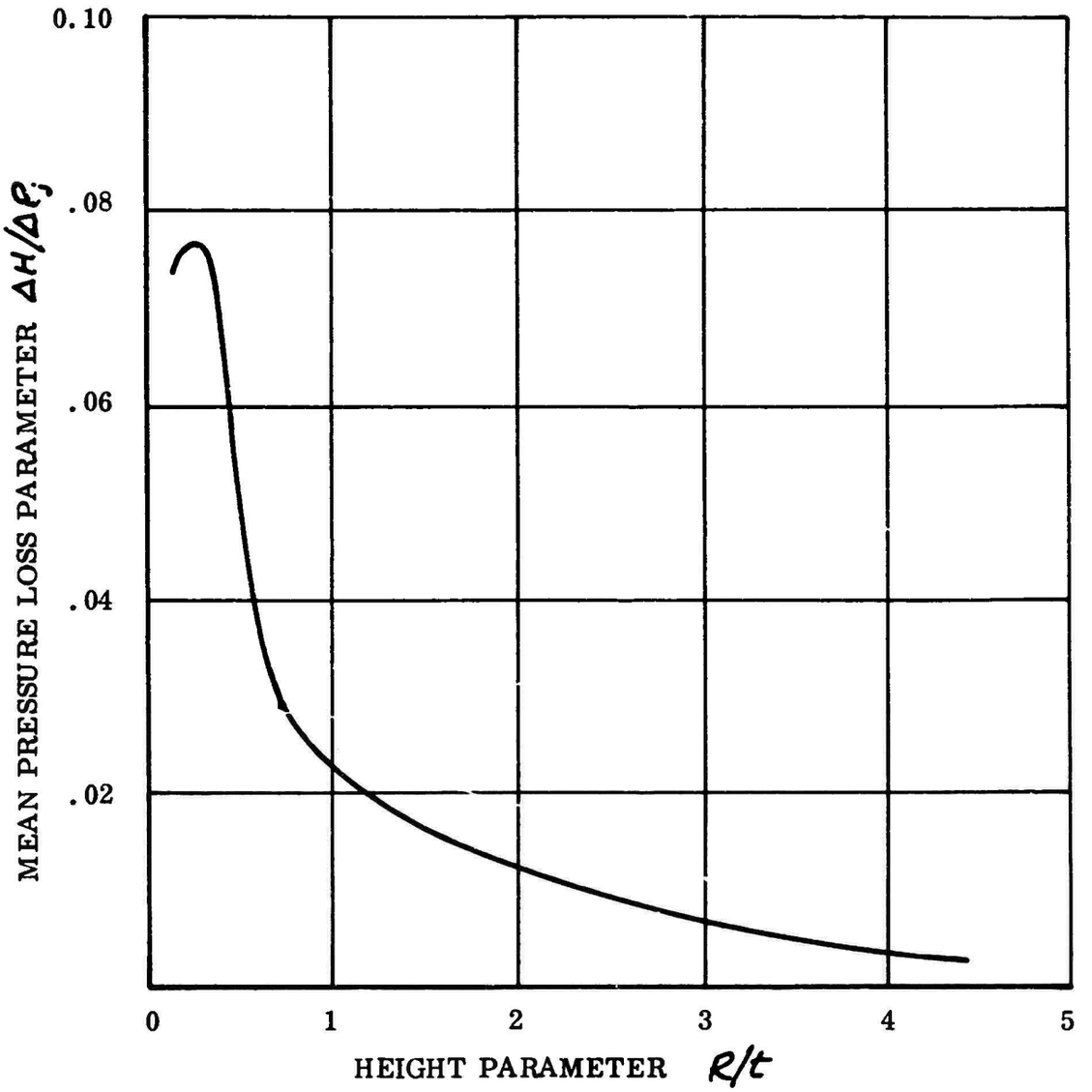

Figure 96. Mean Total Pressure Loss as a Function of the Height Parameter R/t for a Straight Nozzle. (Based on Approximate Exponential Theory Static Pressure Distribution.)

$$P_j - \Delta P_j' = \int_0^{z'} \Delta P_j v_z \, dz. \tag{269}$$

Thus, the total jet power is

$$P_j = \int_0^{t_j} \Delta P_j v_z \, dz - \int_{z'}^{t_j} \Delta H v_z \, dz_j. \tag{270}$$

The power before diffusion is

$$P_N = \Delta P_j v_N t. \tag{271}$$

This must equal the first integral of Equation (270), indicating that the jet thickness t_j is greater than the nozzle thickness. In fact, for continuity

$$v_N \, dz = v_j \, dz_j$$

$$dz_j = \frac{v_N}{v_z} \, dz.$$

Substituting in (270) and dividing (270) by (271)

$$\frac{\Delta P}{P_N} = \int_{z'}^{t} \frac{\Delta H \, v_N \, dz}{\Delta P_j \, v_N t}$$

$$= \frac{1}{t} \int_{z'}^{t} \frac{\Delta H}{\Delta P_j} \, dz$$

$$= \frac{1}{\psi t} \int_{z'}^{t} \left[1 - 2\psi e^{-z/R} + \psi^2 e^{-2z/R} \right] dz. \tag{272}$$

This is exactly the same as Equation (266).

Chapter Eight

COANDA JET FLOW

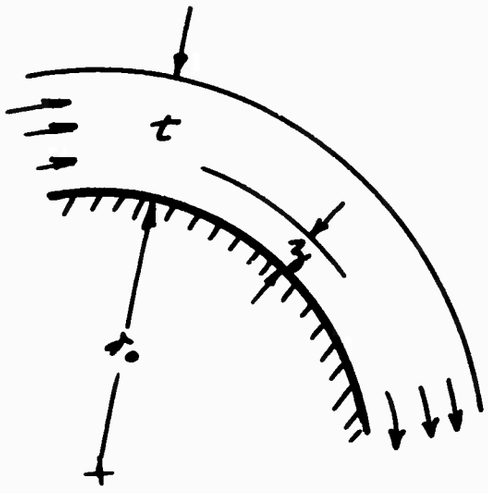

Figure 97. Basic Geometry.

From Equation (91), the equation governing Coanda flow can be taken as "free vortex" if the wall radius is constant; that is,

$$\frac{d\Delta p}{dz} + \frac{2}{r_o+z}\Delta p_z = \frac{2}{r_o+z}\Delta P_z, \tag{273}$$

for which the general solution is

$$\Delta p_z = e^{-2\int \frac{dz}{r_o+z}}\left[\int \frac{2\Delta P_z}{r_o+z} e^{2\int \frac{dz}{r_o+z}} dz + K\right] \tag{274}$$

$$= \frac{2}{(r_o+z)^2}\int_o^z \Delta P_z (r_o+z)\,dz + \frac{K}{(r_o+z)^2} \tag{275}$$

when $z = t$, $\Delta p_z = 0$;

$$\therefore \quad K = -2\int_o^t \Delta P_z (r_o+z)\,dz;$$

$$\therefore \quad \Delta p_z = \frac{-2}{(r_o+z)^2}\int_z^t \Delta P_z (r_o+z)\,dz. \tag{276}$$

SOLUTION FOR CONSTANT TOTAL HEAD

When $\Delta P_3 = \text{constant} = \Delta P_j$, say,

$$\frac{\Delta \phi_3}{\Delta P_j} = \frac{-2}{(\tau_0 + 3)^2}\left[\tau_0 \zeta + \zeta^2/2\right]_3^t$$

$$= -2\,\frac{\left[\frac{\tau_0}{t}(1 - 3/t) + \frac{1}{2}\left\{1 - (3/t)^2\right\}\right]}{\left(\tau_0/t + 3/t\right)^2}. \qquad (277)$$

At the wall, therefore,

$$\frac{\Delta \phi_w}{\Delta P_j} = -2(t/\tau_0) - (t/\tau_0)^2. \qquad (278)$$

The local velocity is given by

$$\frac{v_3}{\left(\frac{2}{\rho}\Delta P_j\right)^{1/2}} = \left(1 - \frac{\Delta \phi_3}{\Delta P_j}\right)^{1/2}$$

$$= \frac{\tau_0 + t}{\tau_0 + 3}, \qquad (279)$$

so that at the wall, the velocity is

$$\frac{v_w}{\left(\frac{2}{\rho}\Delta P_j\right)^{1/2}} = 1 + t/\tau_0. \qquad (280)$$

Since in parallel flow

$$\frac{v_N}{\left(\frac{2}{\rho}\Delta P_j\right)^{1/2}} = 1,$$

the velocity ratio

$$\frac{v_w}{v_N} = 1 + t/\tau_0. \qquad (281)$$

This ratio is a measure of whether separation will occur when a straight surface follows a curved one, as in Figure 98.

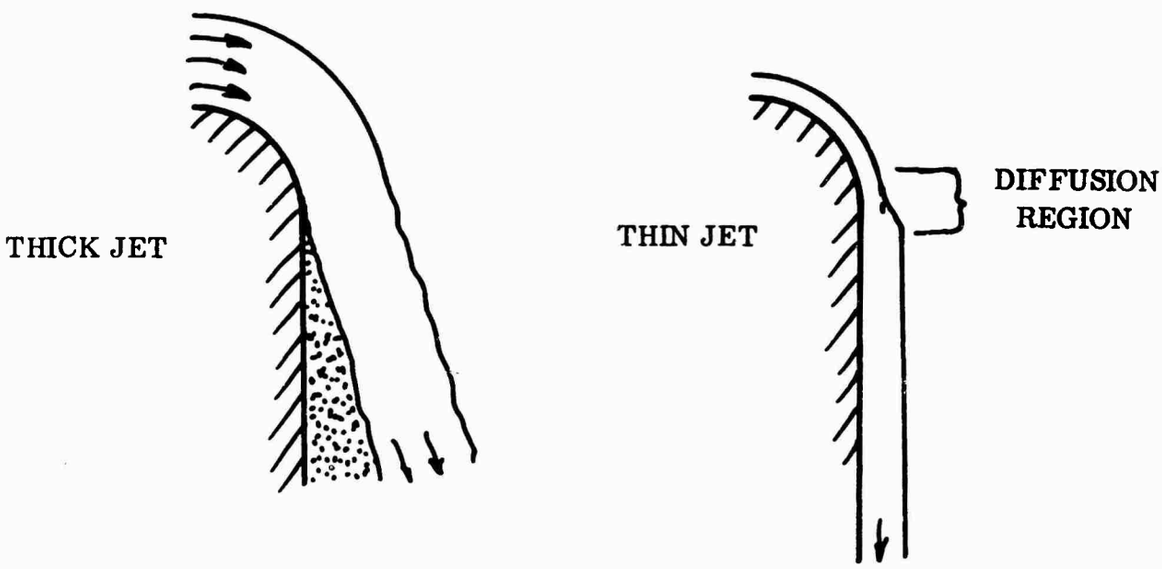

Figure 98. Separation of Coanda Flow.

Even if the diffusion is distributed, by careful blending of the radius and the straight section, we must expect separation when $\sqrt{w}/\sqrt{N} > 2.0$ ($t/r_0 > 1.0$). When the flat section is merely tangential, separation can be expected to occur at a lower value. In all cases there will be some loss of jet total head, of course.

Figure 99, derived from Equation (278) gives the wall static pressure as a function of the jet thickness ratio t/r_0 . In Reference 25 an experimental measurement is reported, in which a 1/8-inch jet, at an initial (nozzle) Mach number of 0.68, is deflected by a curved surface of radius 2.5 inches. The surface pressure is an average of

$$\frac{\Delta p_w}{\Delta P_j} = -0.1 .$$

The theoretical figure is, from Equation (278),

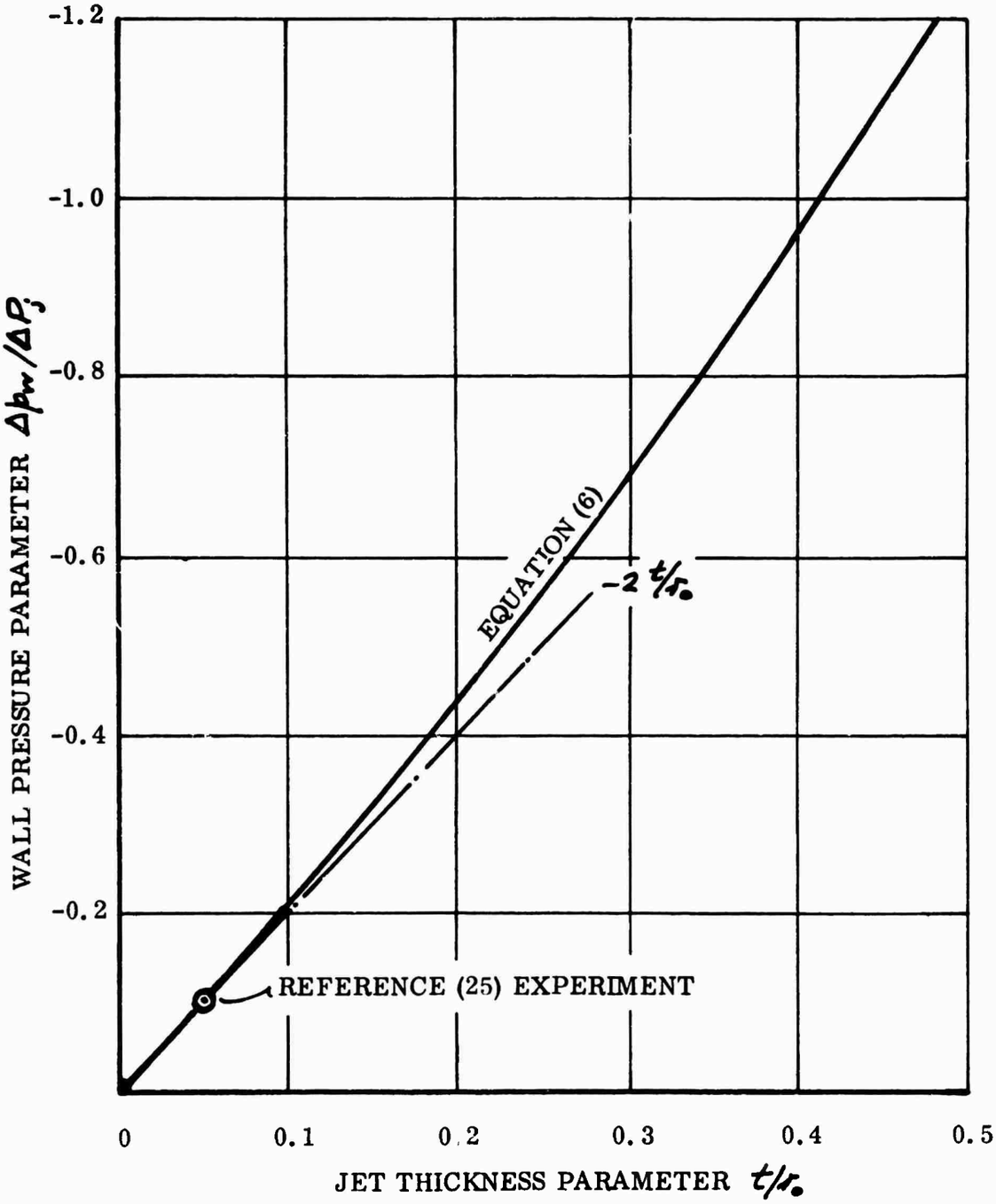

Figure 99. Variation of Wall Pressure With the Jet Thickness Parameter t/r_o .

$$\frac{\Delta p_w}{\Delta P_j} = -2 \times .05 - (.05)^2$$

$$= -0.1025$$

The agreement is therefore very good.

APPROXIMATE SOLUTION FOR THE BOUNDARY LAYER EFFECT

Let us define the loss of total head due to skin friction as

$$D_F = \int_0^t (\Delta P_j - \Delta P_\zeta)\, d\zeta = \int_0^t \phi(\zeta)\, d\zeta, \tag{282}$$

so that

$$\Delta P_\zeta = \Delta P_j - \phi(\zeta) \tag{283}$$

where $\phi(\zeta)$ is understood to be finite and positive near the wall, but equal to zero over most of the jet. Substituting (283) in Equation (276),

$$\Delta p_\zeta = \frac{-2}{(r_0+\zeta)^2} \int_\zeta^t [\Delta P_j - \phi(\zeta)](r_0+\zeta)\, d\zeta$$

$$= \frac{-2}{(r_0+\zeta)^2} \left[\int_\zeta^t \Delta P_j (r_0+\zeta)\, d\zeta - r_0 \int_\zeta^t \phi(\zeta)\, d\zeta - \int_\zeta^t \zeta \phi(\zeta)\, d\zeta \right]. \tag{284}$$

This is the same as Equation (277) when ζ is large enough not to include the boundary layer. When $\zeta = 0$, however, we have

$$\frac{\Delta p_w}{\Delta P_j} = \frac{\Delta p_w}{\Delta P_j}_{\text{INVISCID}} + \frac{2 D_F}{r_0 \Delta P_j} \tag{285}$$

where

$$D_F \simeq C_f \cdot \tfrac{1}{2} \rho v_w^2 \ell.$$

That is, $$D_F = C_{of}\,\ell(\Delta P_j - \Delta p_w);$$

$$\therefore \frac{\Delta p_w}{\Delta P_j} = \frac{\Delta p_w}{\Delta P_j}_{INVISCID} + 2C_f \ell/r_0\left(1 - \frac{\Delta p_w}{\Delta P_j}\right)$$

$$= \frac{\frac{\Delta p_w}{\Delta P_j}_{INVISCID} + 2C_f \ell/r_0}{1 + 2C_f \ell/r_0}. \qquad (286)$$

This solution is only approximate, of course, but it does show how skin friction causes the wall static pressure to increase as the jet moves around the curved surface, and why the flow eventually separates.

We can obviously solve the equations for the case of viscous entrainment on the outer surface of the jet. In this case, ΔP_3 decreases with increasing path length $\ell - r_0\theta$, and the thickness t increases. There is probably little point in doing this unless we use a realistic velocity distribution for the jet, however, and the magnitude of the task then renders it inappropriate for the present program. There does not seem to be any good reason why this approach should not adequately cover the Coanda flow problem, however, and enable both performance and stability to be predicted. Needless to say, such predictive ability would be highly valuable, not only where Coanda flow is required, but also where it is <u>not</u> desired.

From Equation (279), the local velocity in a (free vortex) Coanda flow is

$$v_3 = \left(\frac{2}{\rho}\Delta P_j\right)^{\frac{1}{2}} \cdot \frac{r_0 + t}{r_0 + z}. \qquad (287)$$

After diffusion, this reduces to

$$v_D = \left[2/\rho\,(\Delta P_j - \Delta H)\right]^{\frac{1}{2}}, \qquad (288)$$

ΔH being the total head loss, which is given by Equation (80).

That is, $$\Delta H/\Delta P_j = \left(1 - \frac{v_D}{v_3}\right)^2\left(1 - \Delta p_3/\Delta P_j\right); \qquad (289)$$

$$\therefore \Delta H = \tfrac{1}{2}\rho v_3^2\left(1 - \frac{v_D}{v_3}\right)^2. \qquad (290)$$

Let $q_o = \frac{1}{2}\rho v_o^2 \cdot \Delta P_j$, the nozzle dynamic head to ambient.

Then

$$\frac{\Delta H}{q_o} = \frac{v_3^2}{2/\rho \Delta P_j} \left[1 - \frac{(1 - \Delta H/\Delta P_j)^{1/2}}{v_3/(\frac{2}{\rho}\Delta P_j)^{1/2}} \right]^2$$

$$= \frac{v_3^2}{2/\rho \Delta P_j} - 2\frac{v_3}{(2/\rho \Delta P_j)^{1/2}}(1 - \Delta H/\Delta P_j)^{1/2} + 1 - \frac{\Delta H}{\Delta P_j} .$$

Noting that $\Delta P_j = q_o$ and $(2/\rho \Delta P_j)^{1/2} = v_o$,

$$\frac{2\Delta H}{q_o} = 1 - 2\left(\frac{v_3}{v_o}\right)\left(1 - \frac{\Delta H}{q_o}\right)^{1/2} + \left(\frac{v_3}{v_o}\right)^2 \qquad (291)$$

or $$0 = 2\left(1 - \frac{\Delta H}{q_o}\right) - 2\left(\frac{v_3}{v_o}\right)\left(1 - \frac{\Delta H}{q_o}\right)^{1/2} + \left(\frac{v_3}{v_o}\right) - 1 . \qquad (292)$$

$1 - \Delta H/\Delta P_j$ is obviously similar to the conventional diffuser loss ($1 - \eta_D$).

$$\therefore \quad 2\eta_D - 2\left(\frac{v_3}{v_o}\right)\eta_D^{1/2} + \left(\frac{v_3}{v_o}\right)^2 - 1 = 0, \qquad (293)$$

$$\eta_D^{1/2} = \frac{1}{2}\frac{v_3}{v_o} + \left[\frac{1}{2} - \frac{1}{4}\left(\frac{v_3}{v_o}\right)^2\right]^{1/2}, \qquad (294)$$

and $$\eta_D = \frac{1}{2} + \frac{v_3}{v_o}\left[\frac{1}{2} - \frac{1}{4}\left(\frac{v_3}{v_o}\right)^2\right]^{1/2}. \qquad (295)$$

This function is plotted in Figure 100.

The average diffusion efficiency over the jet is therefore

$$\bar{\eta}_D = \frac{1}{2} + \frac{1}{t}\int_0^t \frac{v_3}{v_o}\left[1/2 - \frac{1}{4}\left(\frac{v_3}{v_o}\right)^2\right]^{1/2} dz \qquad (296)$$

$$= \frac{1}{2} + \frac{1}{2^{1/2}t}\int_0^t \frac{v_3}{v_o}\left[1 - \frac{1}{2}\left(\frac{v_3}{v_o}\right)^2\right]^{1/2} dz . \qquad (297)$$

$$\eta_D = \frac{1}{2} + \frac{v_z}{v_0}\sqrt{\frac{1}{2} - \frac{1}{4}\left(\frac{v_z}{v_0}\right)^2}$$

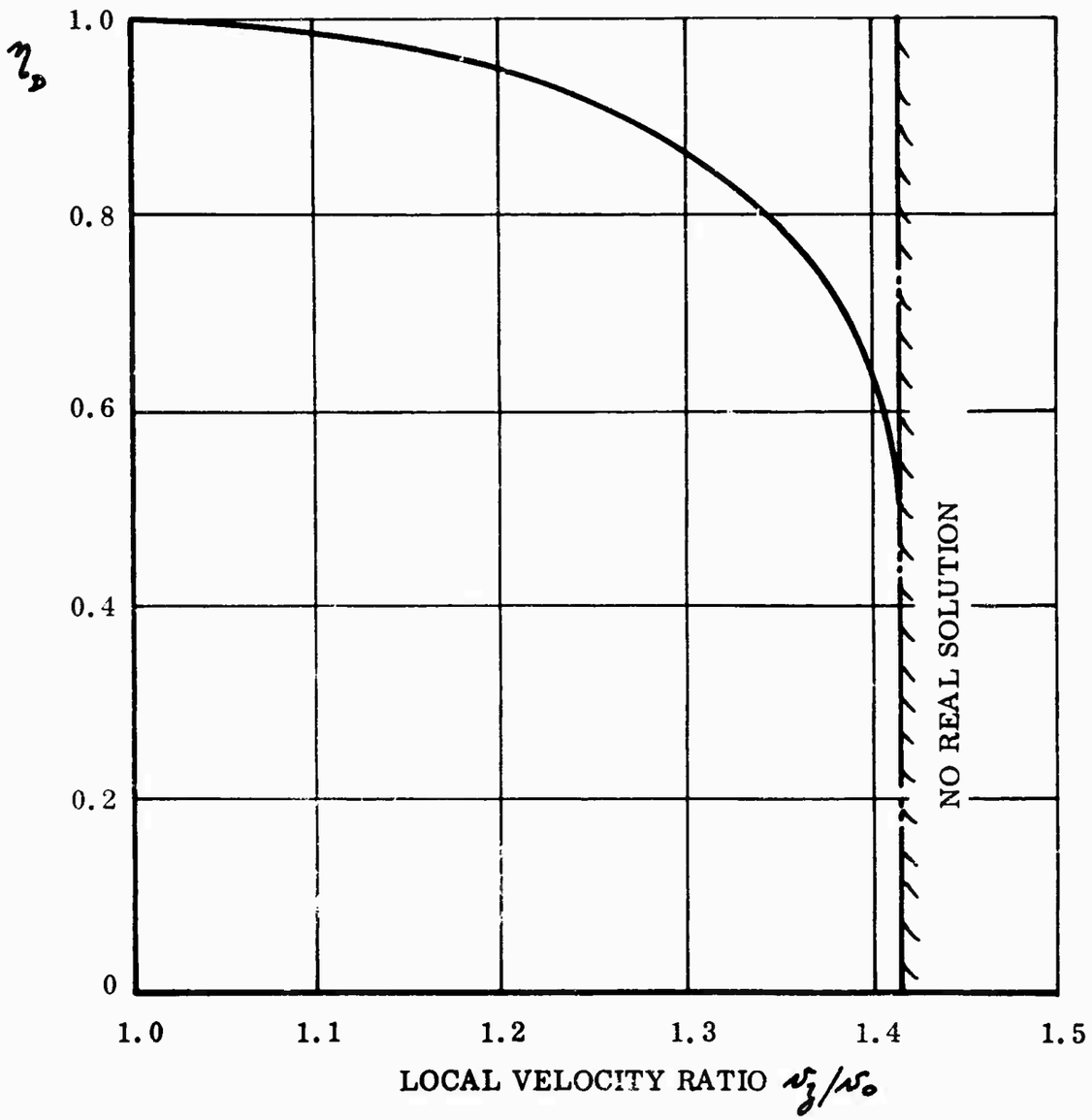

Figure 100. Variation of Local Diffusion Efficiency η_D With Local Velocity Ratio.

As indicated in Figure 100, there is no solution when

$$\left(\frac{v_3}{v_0}\right)^2 > 2.0.$$

That is, $$v_3/v_0 > 2^{1/2}$$

or $$r_0 + t > 2^{1/2}(r_0 + z).$$

This is most critical at the wall ($z = 0$), so that the requirement for a solution is

$$1 + t/r_0 < 2^{1/2}$$

or $$t/r_0 < 0.414. \qquad (298)$$

If we had used "small perturbation" theory, assuming that the total pressure loss did not reduce the velocity after diffusion, we should have obtained the result $t/r_0 < 1.0$ for a real solution. Note that the Equation (298) "stability" limit corresponds to

$$\left(\frac{\Delta p_w}{\Delta P_i}\right)_{MAX.} = -1.0. \qquad (299)$$

Substituting Equation (287) in (297)

$$\bar{\eta}_D = 1/2 + \frac{1}{2^{1/2} t}\int_0^t \frac{r_0 + t}{r_0 + z}\left[1 - \tfrac{1}{2}\left(\frac{r_0 + t}{r_0 + z}\right)^2\right]^{1/2} dz. \qquad (300)$$

Let $$X = \frac{r_0 + t}{r_0 + z}.$$

Then $$z = \frac{r_0 + t}{X} - r_0$$

$$\frac{dz}{dX} = -\frac{r_0 + t}{X^2}$$

$$\bar{\eta}_D = \frac{1}{2} + \frac{1}{2^{\frac{1}{2}}t}\int_{x_0}^{x_t} -\frac{t_0 x t}{X}\left[1 - X^2/2\right]^{\frac{1}{2}} dx$$

$$= \frac{1}{2} + \frac{1}{2}\left(\frac{t_0}{t}+1\right)\left[-(2-X^2)^{\frac{1}{2}} + 2^{\frac{1}{2}}\log\left|\frac{2^{\frac{1}{2}}+(2-X^2)^{\frac{1}{2}}}{X}\right|\right]_{X_0}^{X_t}.$$

Now

$$X_0 = 1 + t/t_0$$

$$X_t = 1.$$

$$\therefore \bar{\eta}_D = \frac{1}{2} + \frac{1}{2}\left(\frac{t_0}{t}+1\right)\left[\left(2 - \overline{1+t/t_0}^{\,2}\right)^{\frac{1}{2}} - 1 + 2^{\frac{1}{2}}\log\left|1+2^{\frac{1}{2}}\right| - 2^{\frac{1}{2}}\log\left|\frac{2^{\frac{1}{2}}+\left(2-\overline{1+t/t_0}^{\,2}\right)^{\frac{1}{2}}}{1+t/t_0}\right|\right]. \qquad (301)$$

It can be shown that $\eta_D \to 1.0$ as $t/t_0 \to 0$, as should be expected.

Chapter Nine

TWO-DIMENSIONAL FLOW IN A CURVED DUCT WITH CONSTANT TOTAL HEAD

The flow in a two-dimensional curved duct involves sudden diffusions when the curves are radii, tangential to straight ducts. These can be treated by the diffusion theory developed in Chapter Two.

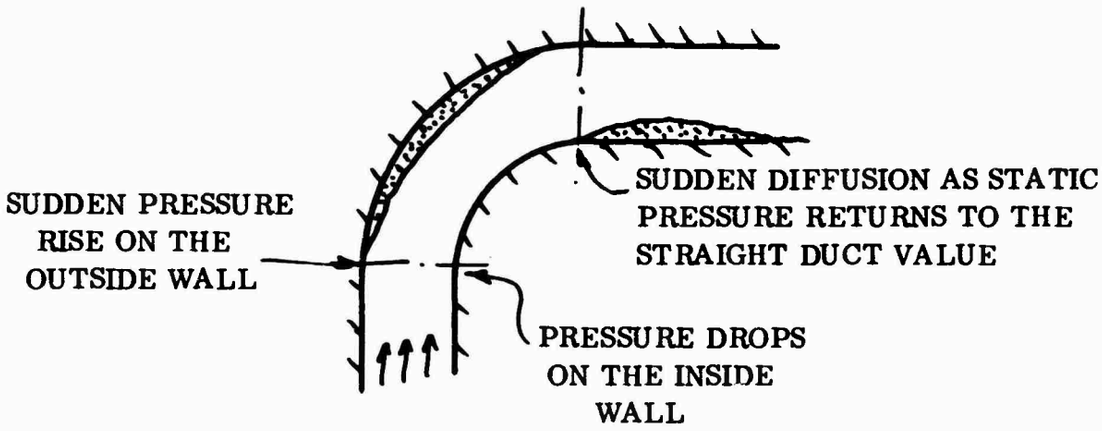

Figure 101. Flow Separation in a Curved Duct.

The physical picture is illustrated in Figure 101. In real (three-dimensional) ducts, the pressure differential across the bend generates secondary flows in the boundary layer of the side walls, and sometimes in the middle as well, and these secondary flows can mask the simple picture shown in Figure 101.

In this chapter we confine our attention to the simplest possible case; a duct of constant thickness, which corresponds to the free-vortex flow of an annular jet. There is no reason why the more sophisticated general theory should not be applied, of course, provided that we remember to include the equation for continuity; that is, to take account of the variation in mean velocity as the distance between the walls varies. This would enable us to solve problems of the type sketched in Figure 102 and to determine the optimum duct bend geometry for minimum loss.

In addition, there is no need to limit the theory to the constant total head case of this paper, of course.

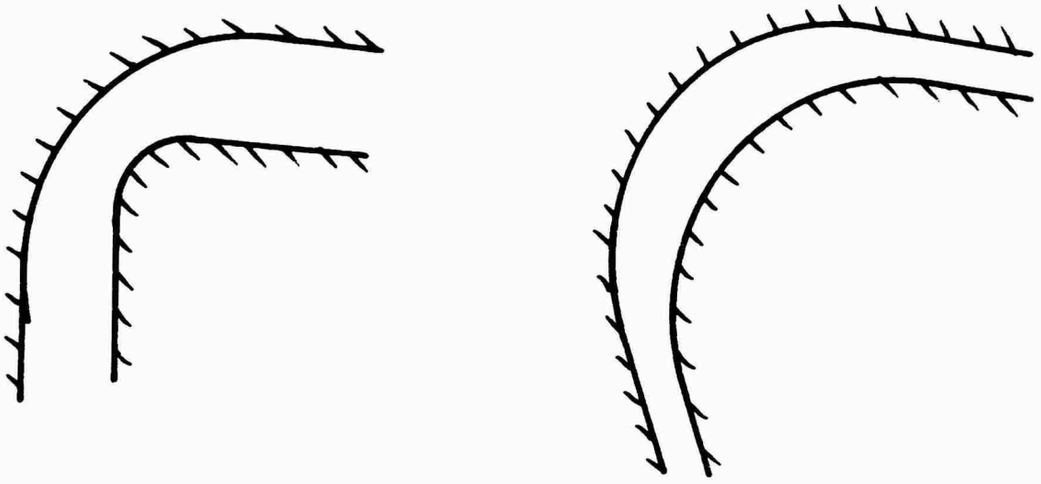

Figure 102. Cases Solvable Using the General Theory Developed in This Investigation.

STATIC PRESSURE AND VELOCITY DISTRIBUTION

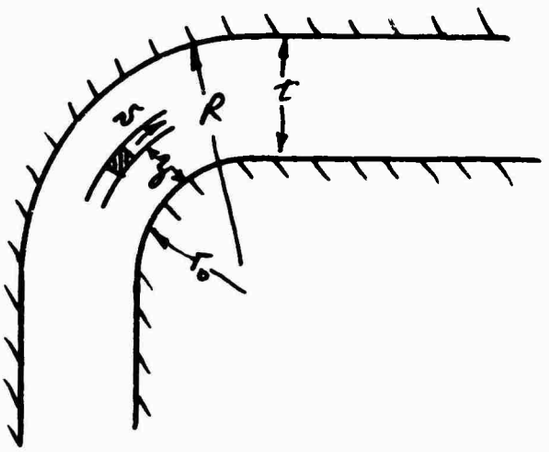

Figure 103. Assumed Geometry.

From Equation (91) the local static pressure in the bend is given by

$$\frac{d\Delta p_z}{dz} + \frac{2}{r_0 + z}\Delta p_z = \frac{2}{r_0 + z}\Delta P_z \; ; \tag{302}$$

$$\therefore \quad \Delta p_z = \frac{2\int (r_0 + z)\Delta P_z \, dz + K}{(r_0 + z)^2} \; . \tag{303}$$

If $\Delta P_z = \text{constant} = \Delta P$, say,

$$\frac{\Delta p_z}{\Delta P} = \frac{2r_0 z + z^2}{(r_0 + z)^2} + \frac{K}{(r_0 + z)^2} \; . \tag{304}$$

The local velocity is

$$\frac{v_z}{\left(\frac{2}{\rho}\Delta P\right)^{1/2}} = \left(1 - \frac{\Delta p_z}{\Delta P}\right)^{1/2} = \frac{(r_0^2 - K)^{1/2}}{r_0 + z} \; . \tag{305}$$

The mass flow is

$$\dot{m} = \rho C \int_0^t v_z \, dz = C(2\rho\Delta P)^{1/2} \int_0^t \frac{r_0^2 - K}{r_0 + z} \, dz \; ;$$

$$\therefore \quad \frac{\dot{m}}{C(2\rho\Delta P)^{1/2}} = (r_0^2 - K)^{1/2} \log\left|1 + t/r_0\right| \; . \tag{306}$$

But if the duct width before the bend is also t,

$$\dot{m} = \rho C t v_0 = Ct\left(2\rho\,\overline{\Delta P - \Delta p_0}\right)^{1/2} \; . \tag{307}$$

Equating (306) and (307),

$$1 - \Delta p_3/\Delta P_0 = \frac{r_0^2 - K}{t^2} \cdot [\log|1 + t/r_0|]^2 ;$$

$$\therefore \quad K = r_0^2 - \frac{t^2(1 - \Delta p_0/\Delta P)}{[\log|1 + t/r_0|]^2} . \qquad (308)$$

Substituting for K in Equation (304),

$$\frac{\Delta p_3}{\Delta P} = 1 - \frac{(t/r_0)^2(1 - \Delta p_0/\Delta P)}{(1 + 3/r_0)^2[\log|1 + t/r_0|]^2} , \qquad (309)$$

which tends to $\Delta p_0/\Delta P$ as $r_0 \to \infty$.

From Equation (305),

$$\frac{v_3}{(2/\rho \Delta P)^{1/2}} = \frac{t/r_0 \cdot (1 - \Delta p_0/\Delta P)^{1/2}}{(1 + 3/r_0)\log|1 + t/r_0|} ; \qquad (310)$$

or, since $v_0^2 = \frac{2}{\rho}\Delta P (1 - \Delta p_0/\Delta P)$,

$$\frac{v_3}{v_0} = \frac{t/r_0}{(1 + 3/r_0)\log|1 + t/r_0|} . \qquad (311)$$

As $t/r_0 \to 0$,

$$\frac{v_3}{v_0} \longrightarrow \frac{1}{1 + 3/r_0} \longrightarrow 1.0 .$$

The wall velocity values given by Equation (311) are plotted in Figure 104.

THE CONSTANT VELOCITY STREAMLINE

A streamline exists, near the center of the duct, along which there is no change in velocity; that is, $v_{3s} = v_0$. From Equation (311) this is given by

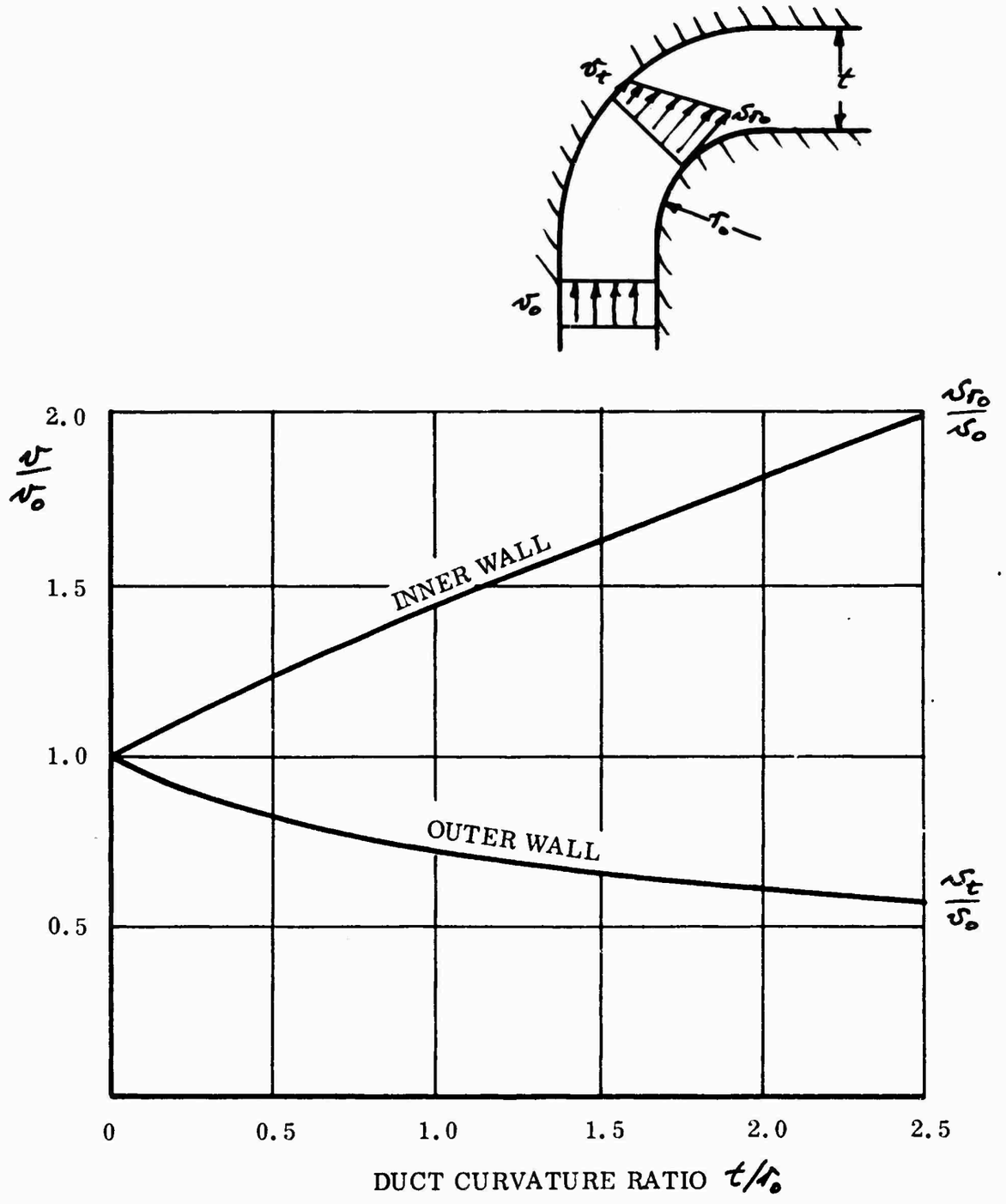

Figure 104. Variation of Inner and Outer Bend Velocities With Duct Aspect Ratio. (Constant Upstream Total Head and No Diffusion Loss.)

$$\left(\frac{\delta}{r_0}\right)_s = \frac{t/r_0}{\log(1 + t/r_0)} - 1 ;$$

$$\therefore \left(\frac{\delta}{t}\right)_s = \frac{\delta}{r_0} \cdot \frac{r_0}{t} = \frac{1}{\log(1 + t/r_0)} - \frac{1}{t/r_0} . \quad (312)$$

In the limit $t/r_0 \to 0$,

$$\frac{\delta}{t_s} \to 1/2$$

as should be expected. The general solution to (312) is plotted in Figure 105.

MASS FLOW DISTRIBUTION AROUND THE BEND

By integrating Equation (310) across the duct on either side of the constant velocity streamline we can obtain expressions for the mass flow on either side of the constant velocity streamline.

$$\frac{\dot{m}_{OUTER}}{\dot{m}_{TOTAL}} = \frac{\log\left[(1 + r_0/t)\log(1 + t/r_0)\right]}{\log(1 + t/r_0)} \quad (313)$$

$$\frac{\dot{m}_{INNER}}{\dot{m}_{TOTAL}} = \frac{\log\left[t/r_0 / \log(1 + t/r_0)\right]}{\log(1 + t/r_0)} . \quad (314)$$

These Equations are plotted in Figure 106.

TOTAL HEAD LOSS ON THE OUTSIDE OF THE CONSTANT VELOCITY STREAMLINE

From Equation (80) the total head loss in a constant pressure diffusion is

$$\frac{\Delta H}{\Delta P} = \left(1 - \frac{v_s}{v_0}\right)^2 \left(1 - \frac{\Delta p_0}{\Delta P}\right) . \quad (315)$$

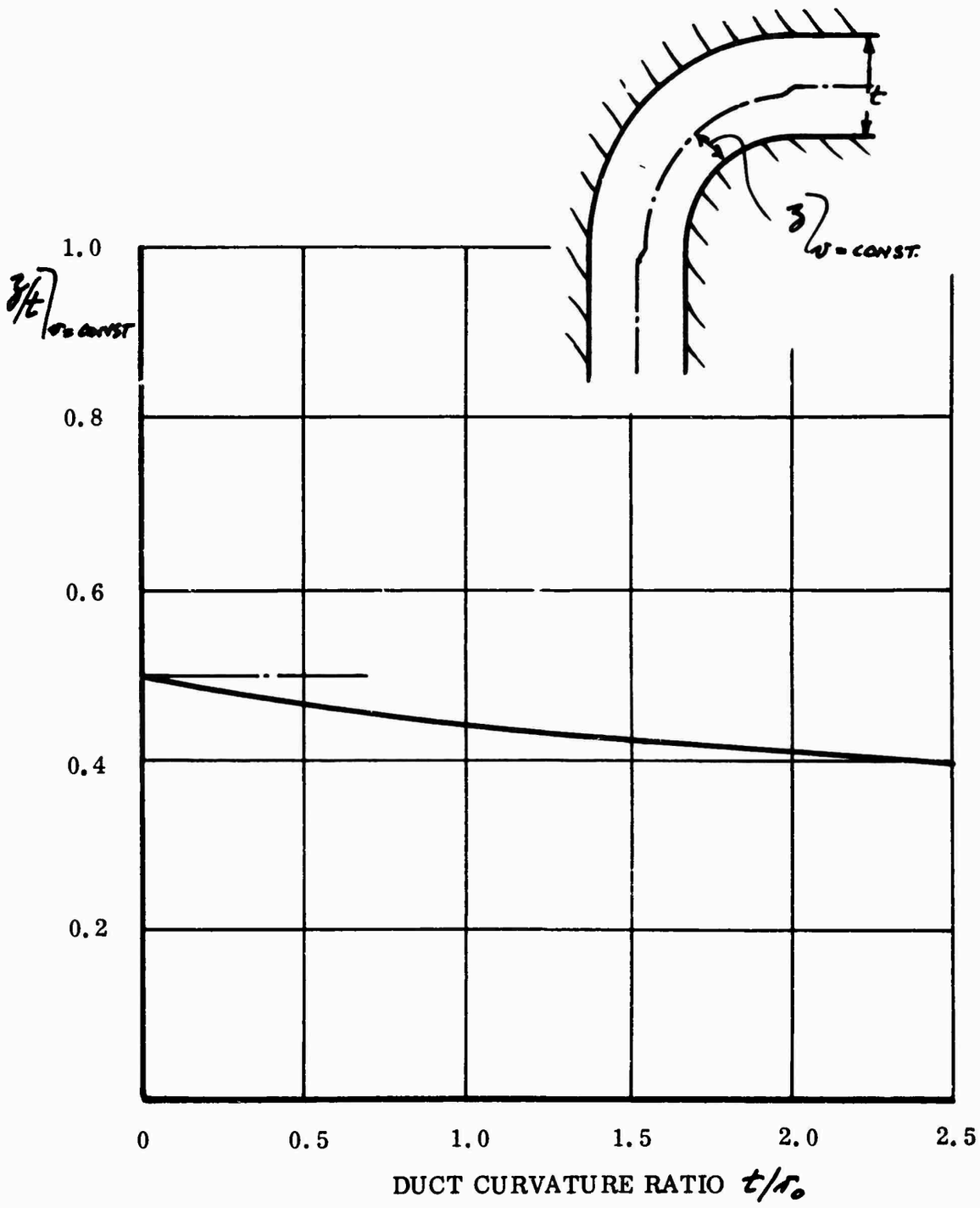

Figure 105. Position of the Constant Velocity Streamline.

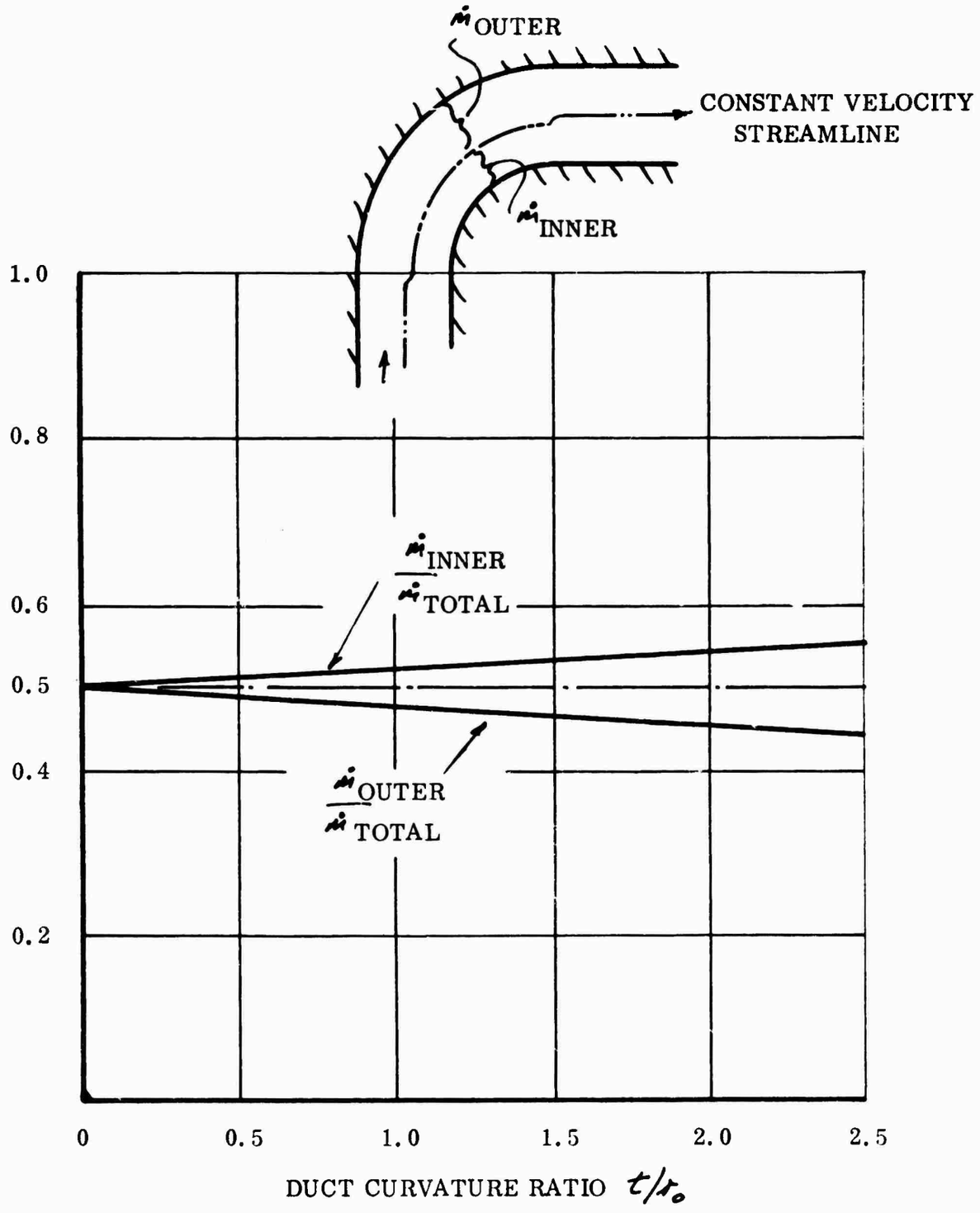

Figure 106. Ratio of Mass Flow on One Side of the Constant Velocity Streamline to the Total Mass Flow.

Since $\Delta P\left(1 - \frac{\Delta H_0}{\Delta P}\right) = q_0$, this is more conveniently expressed as

$$\frac{\Delta H}{q_0} = \left(1 - \frac{v_\beta}{v_0}\right)^2. \tag{316}$$

Substituting Equation (311), the mean loss is

$$\left(\frac{\bar{\Delta H}}{q_0}\right)_{OUTER} = \frac{1}{t/H_0 - \beta_s/H_0} \int_{\beta_s/H_0}^{t/H_0} \left[1 - \frac{t/H_0}{(1+\beta/H_0)\log(1+t/H_0)}\right]^2 d\beta/H_0$$

$$= \frac{1 - t/H_0 + \frac{2t/H_0}{\log(1+t/H_0)}\log\frac{t/H_0}{\log(1+t/H_0)} - \frac{(t/H_0)^2}{(1+t/H_0)[\log(1+t/H_0)]^2}}{1 + t/H_0 - \frac{t/H_0}{\log(1+t/H_0)}} \tag{317}$$

TOTAL HEAD LOSS ON THE INSIDE OF THE CONSTANT VELOCITY STREAMLINE

For this case, Equation (315) becomes

$$\frac{\Delta H}{\Delta P}_{INNER} = \left(1 - v_0/v_\beta\right)^2\left(1 - \Delta p_\beta/\Delta P\right). \tag{318}$$

But $$\Delta P\left(1 - \Delta p_\beta/\Delta P\right) = \Delta P - \Delta p_\beta = \tfrac{1}{2}\rho v_\beta^2$$
$$= q_0\left(v_\beta/v_0\right)^2;$$

$$\therefore \frac{\Delta H}{q_0} = \left(v_\beta/v_0 - 1\right)^2. \tag{319}$$

$$\therefore \left(\frac{\bar{\Delta H}}{q_0}\right)_{\text{INNER}} = \frac{1}{z_B/r_0}\int_0^{z_B/r_0}\left[\frac{t/r_0}{(1+z/r_0)\log(1+t/r_0)} - 1\right]^2 d\,z/r_0$$

$$= \frac{\dfrac{t/r_0}{\log(1+t/r_0)}\left[\dfrac{t/r_0}{\log(1+t/r_0)} - 2\log\left\{\dfrac{t/r_0}{\log(1+t/r_0)}\right\}\right] - 1}{\dfrac{t/r_0}{\log(1+t/r_0)} - 1} \quad (320)$$

MEAN TOTAL PRESSURE LOSS ACROSS THE DUCT

Summing Equations (317) and (320) across the entire duct

$$\left(\frac{\Delta H}{q_0}\right)_{\text{TOTAL}} = \frac{(t/r_0)^2}{(1+t/r_0)[\log(1+t/r_0)]^2} - 1. \quad (321)$$

Equation (321) is plotted in Figure 107.

THE LOSS INCREMENT DUE TO SKIN FRICTION

We can obtain an approximate figure for the total head loss due to skin friction from the relationship

$$t\,\bar{\Delta H}_{SF} = C_f\left[\tfrac{1}{2}\rho v_{r_0}^2\,\theta r_0 + \tfrac{1}{2}\rho v_t^2\,\theta(r_0+t)\right] \quad (322)$$

$$\frac{\bar{\Delta H}_{SF}}{q_0} = \theta C_f r_0/t\left[\left(\frac{v_{r_0}}{v_0}\right)^2 + (1+t/r_0)\left(\frac{v_t}{v_0}\right)^2\right] \quad (323)$$

$$= \theta C_f \cdot \frac{t}{r_0}\cdot\left[1 + \frac{1}{1+t/r_0}\right]\left[\log(1+t/r_0)\right]^{-2}. \quad (324)$$

This result is overplotted in Figure 107 for $\theta = 90^0$ and $C_f = .004$.

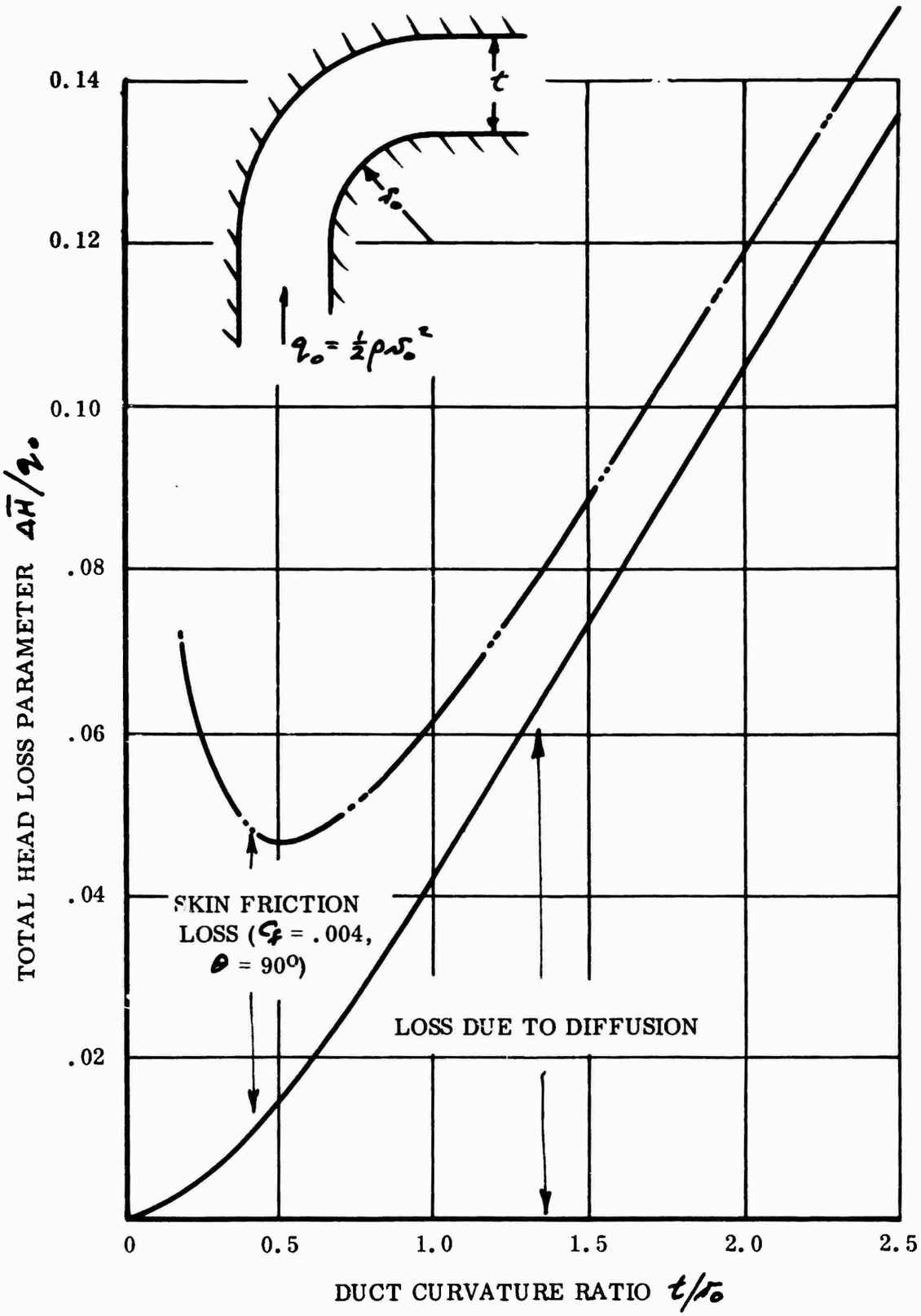

Figure 107. Average Total Head Loss Around a Constant Duct Thickness Bend.

COMPARISON WITH EXPERIMENT

The writers of this report are not aware of any two-dimensional flow measurements of curved duct losses, so that direct comparison with experiment is impossible. Reference 26 presents data for rectangular ducts of various finite aspect ratios and, as shown in Figure 108, these results fair into the two-dimensional solution very convincingly. However, an appropriately planned experimental program is essential before the basic hypothesis used in the foregoing analysis can be substantiated. Such a program would then permit embarkment upon the analysis of the secondary flows in the three-dimensional case.

It is perhaps worth pointing out that extensions of the present analysis to the more general case offer hope of defining duct bend shapes for minimum loss.

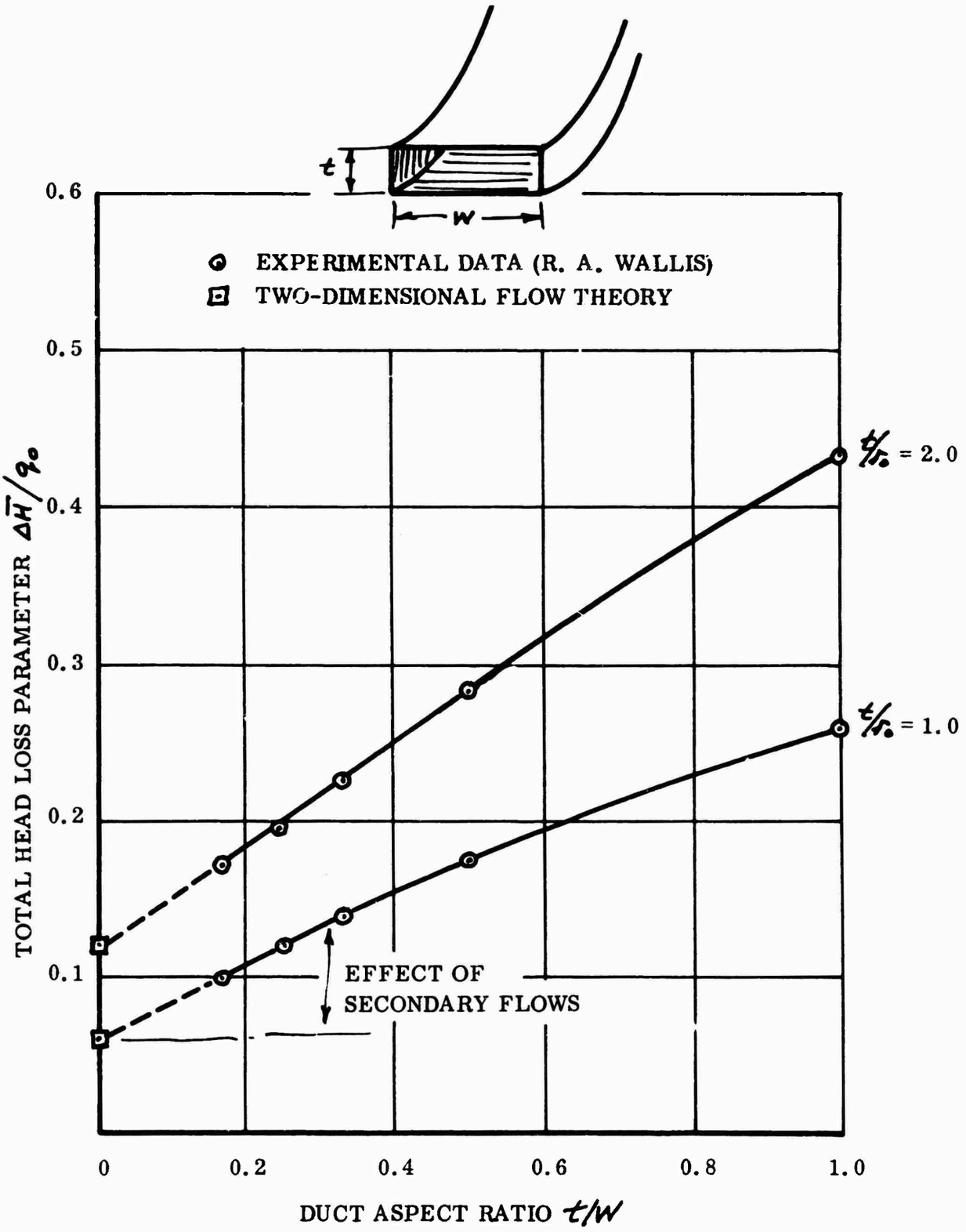

Figure 108. Comparison Between Theory and Experiment for a Right-Angle Bend.

Chapter Ten

FLOW INTO A TWO-DIMENSIONAL FLUSH INTAKE

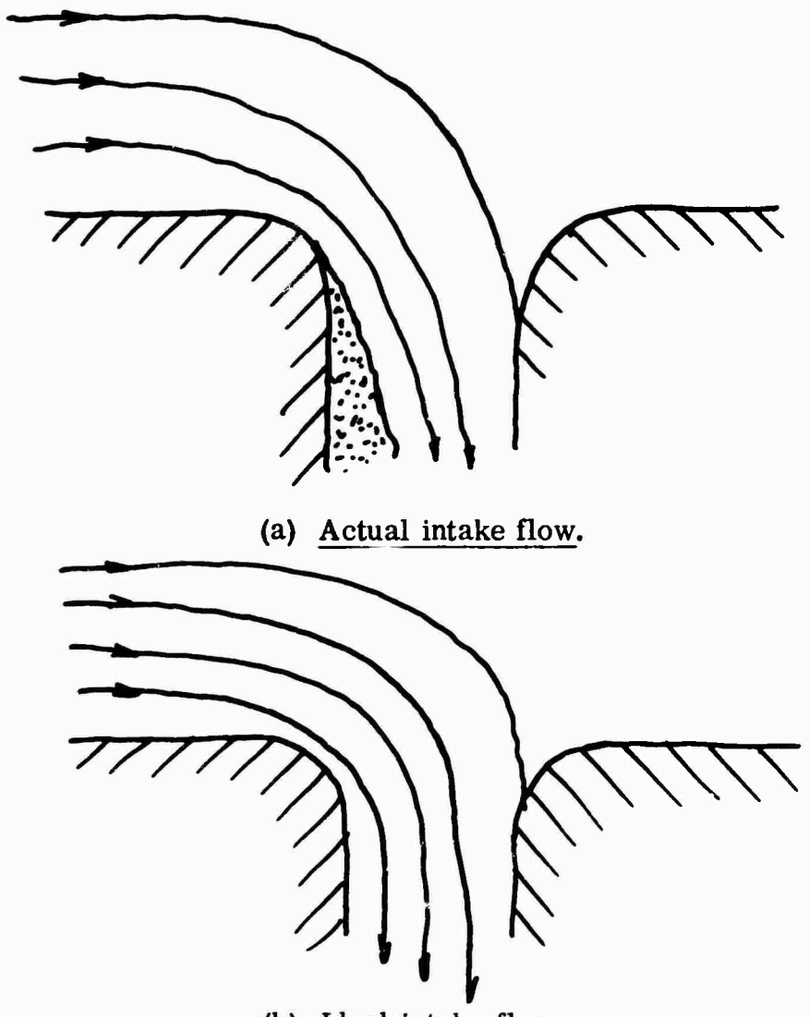

(a) Actual intake flow.

(b) Ideal intake flow.

Figure 109. Flow Into a Flush Intake.

An intake which is at right angles to the free-stream velocity is often highly desirable from a practical weight and size point of view, but is difficult to design for high intake efficiency. This is mainly because of the flow breakaway which occurs on the leading edge of such an intake, as indicated in Figure 109(a), in contrast to the hoped-for inviscid flow picture of Figure 109(b). Even the latter would present problems, however, in that the

velocity would vary across the plane of the intake.

In this chapter we attempt to lay the foundations for the analysis of such flows, using the same basic approaches that have proven successful for curved jet flows. The subject is complicated by the important effect of the upstream boundary layer, and by separation due to sudden diffusion on the intake lip. Thus, although we shall develop the theory far enough to obtain closed form solutions, we will not attempt to "fill in" all the details, this being beyond the scope of the present program. Sufficient work has been done to indicate that this approach should yield good results, however, and to show that its use will improve our predictive ability. To cite only two examples, it is found that the "momentum drag" is not equal to the product of the free stream velocity and the intake mass flow, and that the efficiency of a horizontal intake will decrease as the free-stream velocity increases, due to leading edge diffusion. Both these points might be of importance to a vehicle such as the XV-4A, for example.

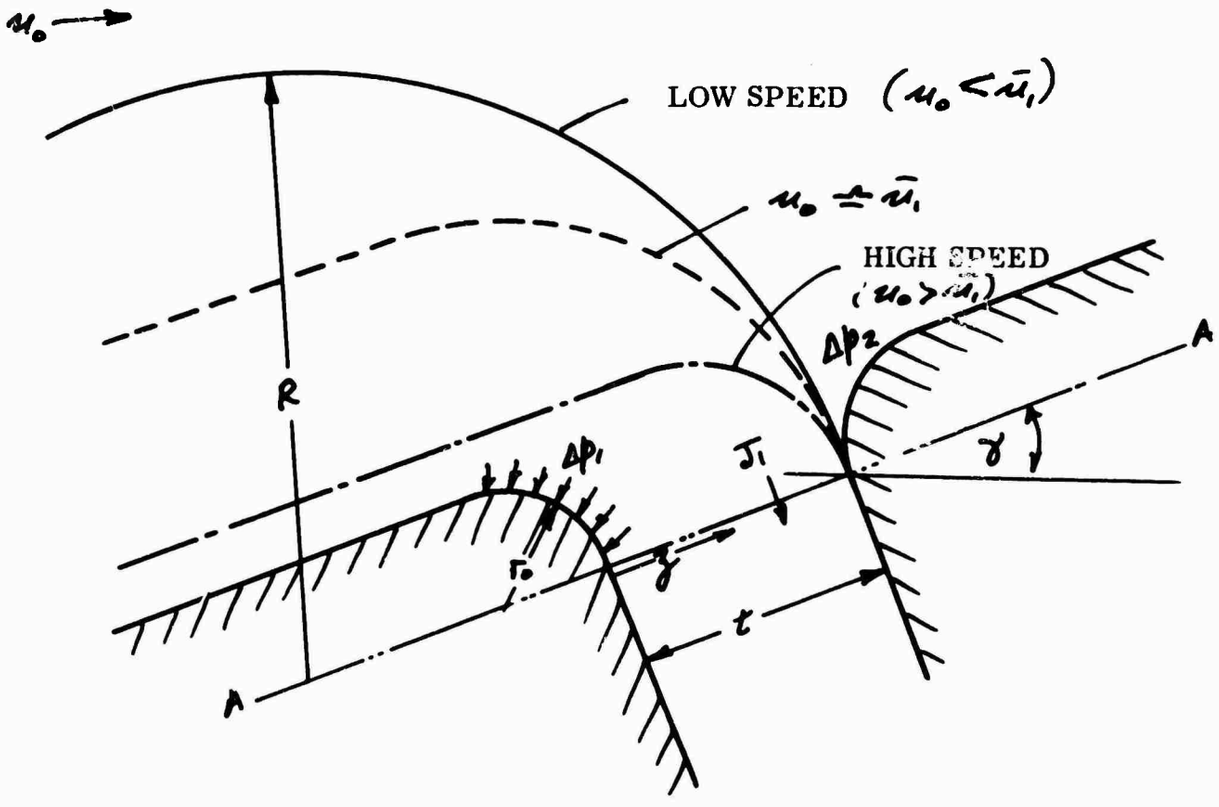

Figure 110. Flow Into a Flush Intake.

Two-dimensional flow into a flush intake must of necessity adhere to the body surface upstream of the intake, as illustrated in Figure 110. Thus, if the external flow is undefined, so that the surface pressure distribution is unknown, we are unable to calculate the effects due to the tilt angle. For small angles these effects will presumably be of second order, however.

The flow illustrated in Figure 110 must satisfy the equation of curvilinear flow. That is,

$$\frac{d\phi}{dz} + \frac{2}{r_0 + \eta z}\Delta p_3 = \frac{2}{r_0 + \eta z}\Delta P_3 . \qquad (325)$$

The curvature gradient η will depend upon the intake velocity ratio ($\bar{u}_1/u_0$), as indicated in Figure 110, the flow direction being reversed from the conventional annular jet direction. If we retain the annular jet assumption of constant boundary radius, then solutions can be obtained in the same way as in the earlier chapters. It is possible that the constant radius assumption is an unnecessary restriction, however, and that the results can be made more general in future work.

Additionally, the free-vortex and exponential theory approximations are still of value; the first is applicable in the region $\bar{u}_1/u_0 \simeq 1.0$, and the second is correct as $\bar{u}_1/u_0 \to 0$. For $\bar{u}_1/u_0 > 1.0$, the general theory must be used.

MOMENTUM EQUATIONS

The geometry shown in Figure 110 assumes that a straight-walled duct follows the radiused inlet. Thus the line A-A theoretically makes a discontinuity at which the static pressure field changes, being some function of z above A-A and uniform below. In practice, the boundary layer will thicken on the upstream wall, of course, in such a way as to avoid this discontinuity. In fact, if the velocity at the r_0 surface significantly exceeds the mean duct velocity, flow separation will occur at the point where the r_0 radius is tangential to the duct.

Noting this reservation, the horizontal momentum balance for $\gamma = 0$ gives

$$\int_{r_0}^{R} \rho u^2 dy = r_0 (\Delta p_2 - \Delta p_1). \qquad (326)$$

If $\bar{u} = \frac{1}{R-r_0}\int_{r_0}^{R} u\,dy$ and $\lambda = \frac{\frac{1}{R-r_0}\int_{r_0}^{R} u^2 dy}{\left[\frac{1}{R-r_0}\int_{r_0}^{R} u\,dy\right]^2}$,

then

$$\int_{r_0}^{R} \rho u^2 dy = \lambda \rho \bar{u}^2 (R-r_0) = r_0(\Delta p_2 - \Delta p_1) \tag{327}$$

$$R/r_0 = 1 + \frac{\Delta p_2 - \Delta p_1}{\rho \lambda \bar{u}^2}. \tag{328}$$

Since $R = r_0 + \eta t$, $R/r_0 = 1 + \eta t/r_0$,

$$\eta t/r_0 = \frac{\Delta p_2 - \Delta p_1}{\rho \bar{u}^2 \lambda}. \tag{329}$$

If we were to base the calculation of η on continuity of mass flow, then

$$(R-r_0)\bar{u} = t\bar{u};$$

$$\therefore \quad \frac{R}{r_0} = t/r_0\left(\frac{\bar{u}_1}{\bar{u}}\right) + 1 = 1 + \eta t/r_0;$$

$$\therefore \quad \eta = \frac{\bar{u}_1}{\bar{u}}. \tag{330}$$

This is not the same as Equation (329). Thus η differs depending on whether we assume conservation of momentum or mass flow. We do not know at the present time which is the more correct.

THE FLOW EQUATION FOR CONSTANT TOTAL HEAD

The total head distribution ΔP_3 may be considered constant and equal to ($\frac{1}{2}\rho u_0^2$) if the upstream boundary layer is of negligible thickness. The solution to (325) is therefore

$$\frac{\Delta p_3}{\frac{1}{2}\rho u_0^2} = (r_0 + \eta z)^{-2/\eta}\left[2\int_0^3 (r_0 + \eta z)^{\frac{2}{\eta}-1} dz + \frac{k}{\frac{1}{2}\rho u_0^2}\right] \tag{331}$$

$$\frac{\Delta p_3}{\tfrac{1}{2}\rho u_0^2} = (r_0 + \eta z)^{-2/\eta}\left[\{(r_0+\eta z)^{2/\eta}\}_0^3 + \frac{K}{\tfrac{1}{2}\rho u_0^2}\right]$$

$$= 1 - \left(\frac{r_0}{r_0+\eta z}\right)^{2/\eta} + \frac{K}{\tfrac{1}{2}\rho u_0^2 (r_0+\eta z)^{2/\eta}} \qquad (332)$$

$$\frac{\Delta p_1}{\tfrac{1}{2}\rho u_0^2} = \frac{K}{\tfrac{1}{2}\rho u_0^2 r_0^{2/\eta}};$$

$$\therefore \quad \frac{\Delta p_3}{\tfrac{1}{2}\rho u_0^2} = 1 - \left(1 - \frac{\Delta p_1}{\tfrac{1}{2}\rho u_0^2}\right)\left(\frac{r_0}{r_0+\eta z}\right)^{2/\eta} \qquad (333)$$

$$\frac{\Delta p_2}{\tfrac{1}{2}\rho u_0^2} = 1 - \left(1 - \frac{\Delta p_1}{\tfrac{1}{2}\rho u_0^2}\right)\left(\frac{r_0}{r_0+\eta t}\right)^{2/\eta}. \qquad (334)$$

INTAKE MASS FLOW

The local velocity is

$$\frac{v_3}{u_0} = \left(1 - \frac{\Delta p_3}{\tfrac{1}{2}\rho u_0^2}\right)^{1/2}$$

$$= \left(1 - \frac{\Delta p_1}{\tfrac{1}{2}\rho u_0^2}\right)^{1/2}\left(\frac{r_0}{r_0+\eta z}\right)^{1/\eta}. \qquad (335)$$

Thus the elemental mass flow is

$$dm_j = \rho b v_3 dz = \rho b dz u_0 \left(1 - \frac{\Delta p_1}{\tfrac{1}{2}\rho u_0^2}\right)^{1/2}\left(\frac{r_0}{r_0+\eta z}\right)^{1/\eta};$$

$$\therefore \quad m_1 = \rho b u_0 \left(1 - \frac{\Delta p_1}{\tfrac{1}{2}\rho u_0^2}\right)^{1/2}\int_0^t \left(\frac{r_0}{r_0+\eta z}\right)^{1/\eta} dz \qquad (336)$$

$$\frac{m_1}{b} = \frac{r_0 \rho u_0}{1-\eta}\left(1 - \frac{\Delta p_1}{\tfrac{1}{2}\rho u_0^2}\right)^{1/2}\left[\left(\frac{r_0/t}{r_0/t+\eta}\right)^{\frac{1-\eta}{\eta}} - 1\right]. \qquad (337)$$

Δp_1 appears as an arbitrary constant because the mass flow is arbitrary, so far as the intake is concerned. The actual value of $\dot{m}_1$ depends upon the depression existing in the intake, due to the fan or other air-moving device.

Writing $\dot{m}/\rho = \rho t \bar{u}_1$,

$$\frac{\bar{u}_1}{u_0} = \frac{r_0/t}{1-\eta}\left(1 - \frac{\Delta p_1}{\frac{1}{2}\rho u_0^2}\right)^{\frac{1}{2}}\left[\left(\frac{r_0/t}{r_0/t+\eta}\right)^{\frac{1-\eta}{\eta}} - 1\right] \quad (338)$$

or $$1 - \frac{\Delta p_1}{\frac{1}{2}\rho u_0^2} = \left(\frac{\bar{u}_1}{u_0}\right)^2 \cdot \left(\frac{1-\eta}{r_0/t}\right)^2 \left[\left(\frac{r_0/t}{r_0/t+\eta}\right)^{\frac{1-\eta}{\eta}} - 1\right]^{-2}. \quad (339)$$

Substitution of this in Equation (333) gives the static pressure distribution in terms of η and ($\bar{u}_1/u_0$) only, the latter being easily eliminated (Equation 330) for the case of conservation of mass flow.

THE FLOW CURVATURE PARAMETER η FOR CONSERVATION OF MOMENTUM

From Equation (334)

$$\frac{\Delta p_2 - \Delta p_1}{\frac{1}{2}\rho u_0^2} = 1 - \left(1 - \frac{\Delta p_1}{\frac{1}{2}\rho u_0^2}\right)\left(\frac{r_0/t}{r_0/t+\eta}\right)^{2/\eta} - \frac{\Delta p_1}{\frac{1}{2}\rho u_0^2}$$

$$= \left(1 - \frac{\Delta p_1}{\frac{1}{2}\rho u_0^2}\right)\left[1 - \left(\frac{r_0/t}{r_0/t+\eta}\right)^{2/\eta}\right] \quad (340)$$

$$= \left(\frac{\bar{u}_1}{u_0}\right)^2 \frac{(1-\eta)^2}{(r_0/t)^2} \frac{\left[1 - \left(\frac{r_0/t}{r_0/t+\eta}\right)^{2/\eta}\right]}{\left[\left(\frac{r_0/t}{r_0/t+\eta}\right)^{\frac{1-\eta}{\eta}} - 1\right]^2}. \quad (341)$$

Equating this to $2\eta/r_0/t$, as in Equation (329)(the conservation of momentum criterion)

$$\left(\frac{u_0}{\bar{u}_1}\right)^2 = \frac{1}{2}\frac{(1-\eta)^2}{\eta\, r_0/t} \frac{\left[1 - \left(\frac{r_0/t}{r_0/t+\eta}\right)^{2/\eta}\right]}{\left[\left(\frac{r_0/t}{r_0/t+\eta}\right)^{\frac{1-\eta}{\eta}} - 1\right]^2}. \quad (342)$$

This is explicit in the sense that defining η and r_0/t automatically defines the intake velocity ratio (u_1/u_0).

Since we cannot expect to have $R > \infty$ or $R < r_0$, these limits define the real range of η values. In the latter case, $\eta = 0$, of course, while for

$$R \to \infty \quad , \quad r_0 + \eta t \to \infty ;$$

$$\therefore \quad \eta \longrightarrow \infty .$$

The conservation of mass flow relationship for η is given by Equation (330). This is compared with Equation (347) in Figure 111, and the difference between the two is seen to be appreciable for low values of $\bar{u}_1/u_0$. This may be interpreted as indicating a limitation of the constant flow radius assumption, or that the differential pressures Δp_1 and Δp_2 act over a greater depth than the assumed value of r_0 . The latter is felt to be most probable at the present time; but in the work which follows we derive solutions for the conservation of momentum case only, since the conservation of mass flow solutions turn out to be the same, except for the relationship between η and $\bar{u}_1/u_0$.

THE STATIC PRESSURE DISTRIBUTION Δp_3

From Equations (334) and (339),

$$\frac{\Delta p_3}{\frac{1}{2}\rho u_0^2} = 1 - \frac{2\eta}{r_0/t} \frac{\left(\frac{r_0/3}{r_0/3+\eta}\right)^{2/\eta}}{\left[1 - \left(\frac{r_0/3}{r_0/3+\eta}\right)^{3/\eta}\right]} . \qquad (343)$$

Note that the intake velocity ratio does not appear explicitly.

From Equation (335) this gives

$$\frac{v_3}{\bar{u}_1} = \frac{v_3}{u_0} \cdot \frac{u_0}{\bar{u}_1} = \frac{1-\eta}{r_0/t} \frac{\left(\frac{r_0/3}{r_0/3+\eta}\right)^{1/\eta}}{\left[1 - \left(\frac{r_0/t}{r_0/t+\eta}\right)^{\frac{1-\eta}{\eta}}\right]} . \qquad (344)$$

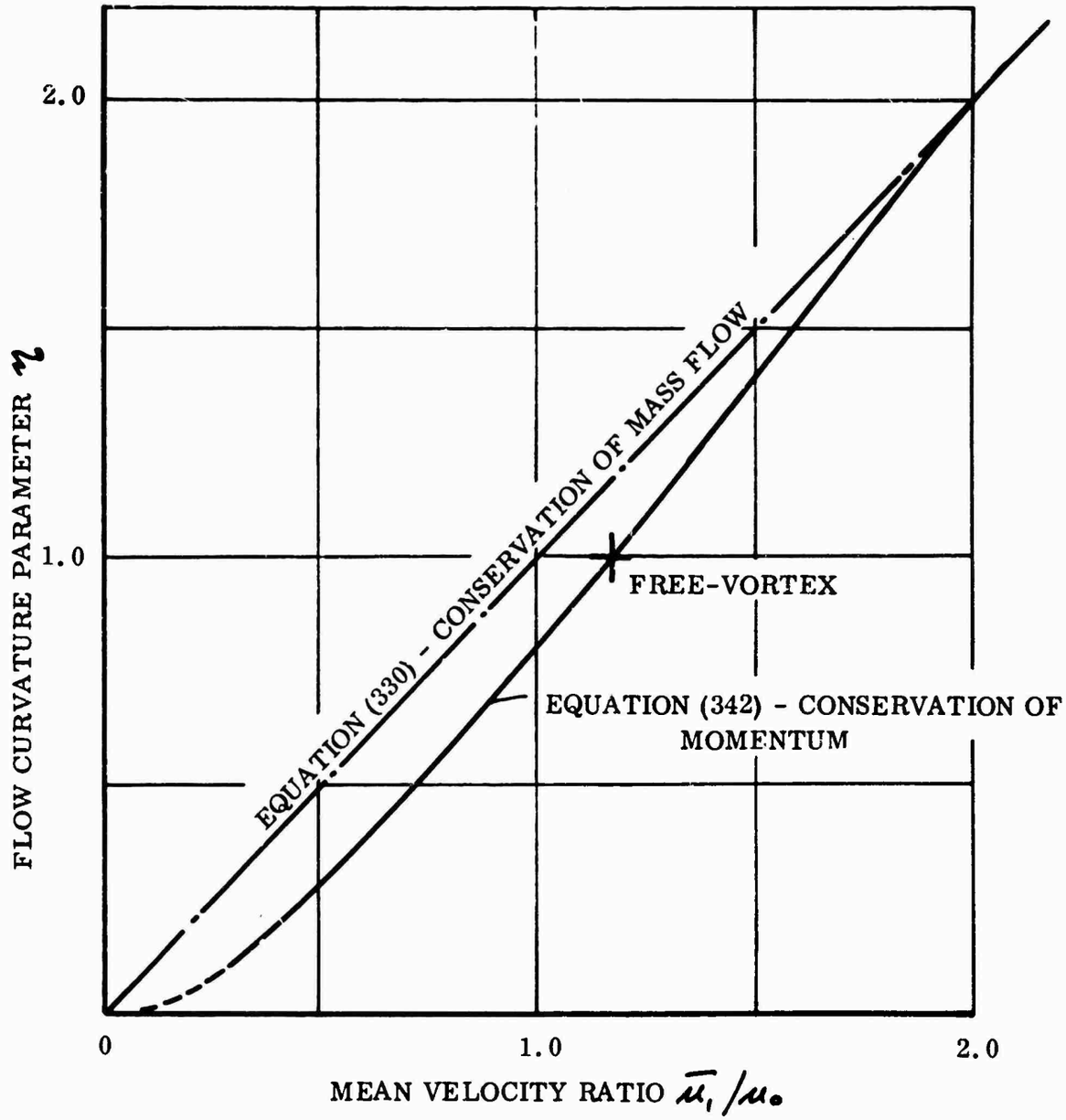

Figure 111. Variation of η With $\bar{u}_1/u_0$, for Uniform Inflow (ΔP_j = Constant).

LIMIT SOLUTIONS FOR $\eta = 0$, Δp_3 = CONSTANT.

From the exponential theory solutions of Chapter Four

$$\frac{\Delta p_3}{\tfrac{1}{2}\rho u_0^2} = e^{-2z/R}\left[\frac{2}{R}\int e^{2z/R}\,dz + \frac{K}{\tfrac{1}{2}\rho u_0^2}\right] \tag{345}$$

$$= 1 + \frac{K}{\tfrac{1}{2}\rho u_0^2}\,e^{-2z/R}. \tag{346}$$

When $z = 0$, $\Delta p_3 = \Delta p_1$;

$$\therefore \frac{\Delta p_1}{\tfrac{1}{2}\rho u_0^2} = 1 + \frac{K}{\tfrac{1}{2}\rho u_0^2};$$

$$\therefore \frac{\Delta p_3}{\tfrac{1}{2}\rho u_0^2} = 1 - \left(1 - \frac{\Delta p_1}{\tfrac{1}{2}\rho u_0^2}\right)e^{-2z/R}. \tag{347}$$

The local velocity is therefore

$$\frac{v_z}{u_0} = \left(1 - \frac{\Delta p_1}{\tfrac{1}{2}\rho u_0^2}\right)^{1/2} e^{-z/R}, \tag{348}$$

and the intake mass flow is

$$\dot{m} = \rho b u_0 \left(1 - \frac{\Delta p_1}{\tfrac{1}{2}\rho u_0^2}\right)^{1/2} \int_0^t e^{-z/R}\,dz$$

$$= \rho b u_0 \left(1 - \frac{\Delta p_1}{\tfrac{1}{2}\rho u_0^2}\right)\left(1 - e^{-t/R}\right). \tag{349}$$

Since $\dot{m} = \rho b t \bar{u}_1$,

$$\left(1 - \frac{\Delta p_1}{\tfrac{1}{2}\rho u_0^2}\right)^{1/2} = \frac{\bar{u}_1}{u_0}\,\frac{t/R}{1 - e^{-t/R}}. \tag{350}$$

Substituting in the static pressure and velocity equations,

$$\frac{\Delta p_z}{\tfrac{1}{2}\rho u_0^2} = 1 - \left(\frac{\bar{u}_1}{u_0}\right)^2 \left(\frac{r}{R}\right)^2 \frac{e^{-2(z/r)(r/R)}}{\left[1 - e^{-r/R}\right]^2} \tag{351}$$

$$\frac{v_z}{\bar{u}_1} = \frac{v_z}{u_0} \cdot \frac{u_0}{\bar{u}_1} = \frac{r/R}{1 - e^{-r/R}} \cdot e^{-(z/r)(r/R)} . \tag{352}$$

It is of interest to note that the local velocity ratio $v_z/\bar{u}_1$ is independent of the flow ratio ($\bar{u}_1/u_0$). The function ($v_z/\bar{u}_1$) is plotted in Figure 112.

SOLUTIONS FOR $n = 1.0$, Δp_z = CONSTANT

The free-vortex solutions of Chapter Four give

$$\frac{\Delta p_z}{\tfrac{1}{2}\rho u_0^2} = (r_0 + z)^{-2} \left[2\left(r_0 z + \frac{z^2}{2}\right) + \frac{K}{\tfrac{1}{2}\rho u_0^2}\right] . \tag{353}$$

When $z = 0$, $\Delta p_z = \Delta p_1$;

$$\therefore \quad \frac{\Delta p_1}{\tfrac{1}{2}\rho u_0^2} = \frac{K}{\tfrac{1}{2}\rho u_0^2 r_0^2} ;$$

$$\therefore \quad \Delta p_z = \frac{(2r_0 z + z^2)}{(r_0 + z)^2} + \frac{\Delta p_1}{\tfrac{1}{2}\rho u_0^2}\left(\frac{r_0}{r_0 + z}\right)^2 . \tag{354}$$

The local velocity is therefore

$$\frac{v_z}{u_0} = \left[1 - \frac{2r_0 z + z^2}{(r_0 + z)^2} - \frac{\Delta p_1}{\tfrac{1}{2}\rho u_0^2}\left(\frac{r_0}{r_0 + z}\right)^2\right]^{1/2}$$

$$= \frac{r_0}{r_0 + z}\left(1 - \frac{\Delta p_1}{\tfrac{1}{2}\rho u_0^2}\right)^{1/2} . \tag{355}$$

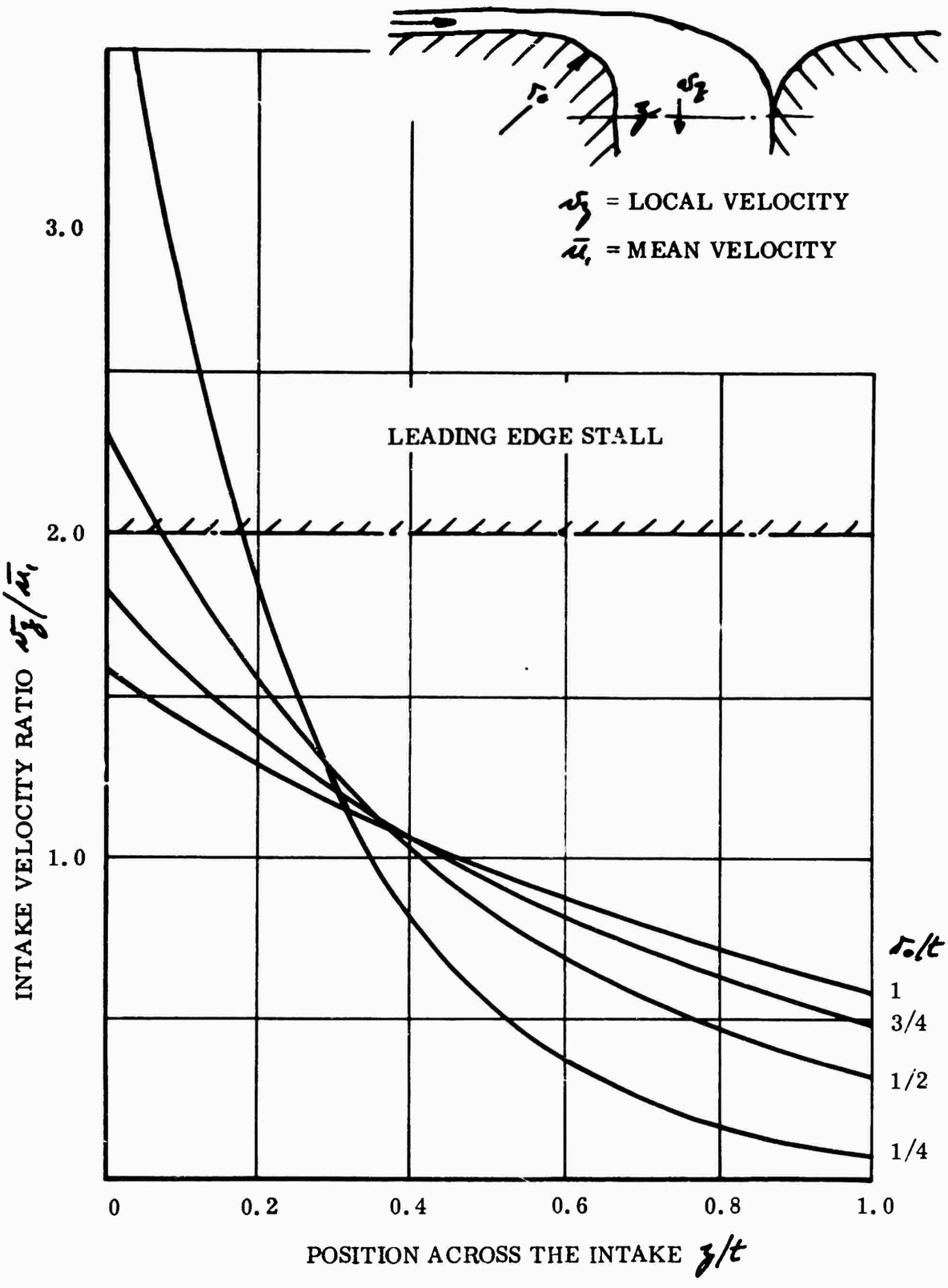

Figure 112. Variation of Inlet Velocity With Intake Lip Radius. (Exponential Theory for $u_o/\bar{u}_1 \to \infty$)

Thus, the mass flow is

$$\dot{m}_1 = \rho b r_0 u_0 \left(1 - \frac{\Delta p_1}{\frac{1}{2}\rho u_0^2}\right)^{1/2} \log\left(1 + t/r_0\right) \qquad (356)$$

$$= \rho b t \bar{u}_1 .$$

$$\therefore \left(1 - \frac{\Delta p_1}{\frac{1}{2}\rho u_0^2}\right)^{1/2} = \frac{(t/r_0)(\bar{u}_1/u_0)}{\log(1 + t/r_0)} . \qquad (357)$$

Substituting this in the static pressure and velocity equations,

$$\frac{\Delta p_z}{\frac{1}{2}\rho u_0^2} = 1 - \left(\frac{r_0}{r_0 + z}\right)^2 \frac{(t/r_0)^2 (\bar{u}_1/u_0)^2}{\left[\log(1 + t/r_0)\right]^2} \qquad (358)$$

$$\frac{v_z}{\bar{u}_1} = \frac{v_z}{u_0} \cdot \frac{u_0}{\bar{u}_1} = \left(\frac{r_0/t}{r_0/t + z/t}\right) \frac{t/r_0}{\log(1 + t/r_0)} . \qquad (359)$$

Once again the velocity ratio $v_z/\bar{u}_1$ is independent of ($u_0/\bar{u}_1$). Equation (359) is plotted in Figure 113.

THE FLOW EQUATION WITH AN UPSTREAM BOUNDARY LAYER

When the upstream boundary layer is significant, in relation to the size of the intake, the total head distribution in the on-coming flow cannot be regarded as constant. Thus, Equation (331) now has the integral

$$\int_0^z (r_0 + \eta z)^{\frac{2}{\eta} - 1} \Delta P_z \, dz \qquad (360)$$

instead of

$$\int_0^z (r_0 + \eta z)^{\frac{2}{\eta} - 1} dz . \qquad (361)$$

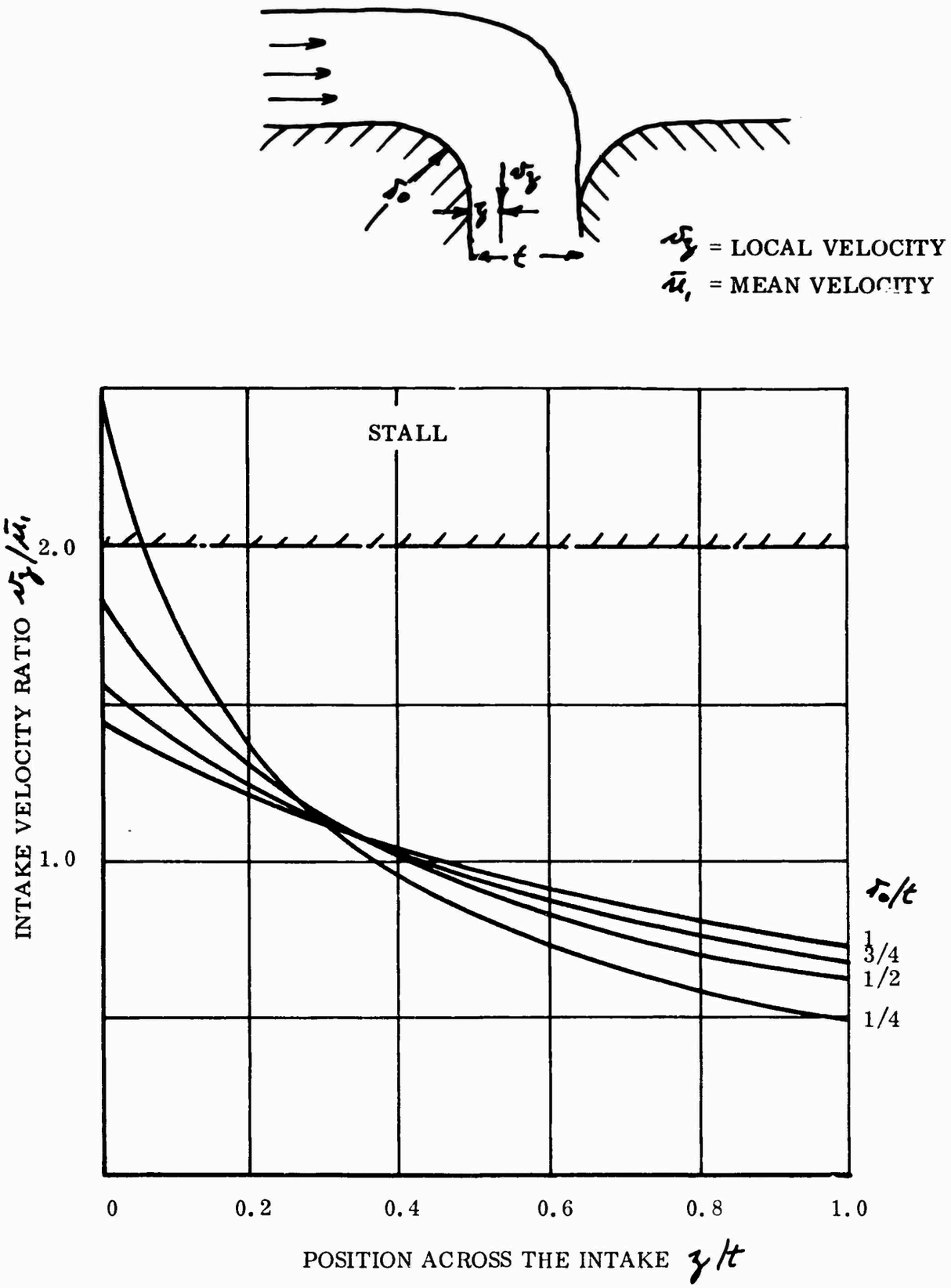

Figure 113. Variation of Inlet Velocity With Intake Lip Radius. (Free-Vortex Theory for $u_o/\bar{u}_1 \doteq 1.0$.)

In addition, the value of the curvature parameter (η) will be larger, from Equation (329).

The appearance of ΔP_z in the integral means that it must be analytic ($\Delta P_z = f(z)$), so that we have to make appropriate idealizations for $f(z)$. There is nothing particularly difficult about this; we have already accomplished it for jet flows, but the reduction to numerical results is time-consuming, and is not within the terms of reference at the present program.

SOLUTION FOR A THIN UPSTREAM BOUNDARY LAYER

We may write $$\Delta P_z = \tfrac{1}{2}\rho u_o^2 - \phi(z) \qquad (362)$$

where $\phi(z) = 0$ over most of the intake, but is finite when $z \to 0$. The general solution to Equation (325) then becomes

$$\frac{\Delta P_z}{\frac{1}{2}\rho u_o^2} = (r_o + \eta z)^{-2/\eta}\left[2\int_0^z (r_o+\eta z)^{\frac{2}{\eta}-1} dz - 2\int_0^z (r_o+\eta z)\frac{\phi(z)}{\frac{1}{2}\rho u_o^2} dz + \frac{K}{\frac{1}{2}\rho u_o^2}\right]. \qquad (363)$$

Now, since $\phi(z)$ is only finite when $z \to 0$,

$$(r_o+\eta z)^{\frac{2}{\eta}-1}\frac{\phi(z)}{\frac{1}{2}\rho u_o^2} \doteq r_o^{\frac{2}{\eta}-1}\left[1+(2-\eta)z/r_o\right]\frac{\phi(z)}{\frac{1}{2}\rho u_o^2};$$

$$\therefore \int_0^z (r_o+\eta z)^{\frac{2}{\eta}-1}\frac{\phi(z)}{\frac{1}{2}\rho u_o^2} dz \doteq \frac{r_o^{\frac{2}{\eta}-1}}{\frac{1}{2}\rho u_o^2}\int_0^z \phi(z)\,dz. \qquad (364)$$

Note that this approximation improves as the boundary layer gets thinner, r_o gets larger, or η approaches 2.0 or zero.

Now at constant static pressure there is a simple relationship between the skin friction drag and the boundary layer momentum.

$$\frac{D_F}{b} = \rho\int_0^\infty (u_o u - u^2)\,dy$$

and writing $\Delta P_0 = \frac{1}{2}\rho u_0^2$, this becomes

$$\frac{D}{\rho b} = \int_0^\infty \left\{ \left[\frac{2}{\rho}\Delta P_0 \cdot \frac{2}{\rho}\cdot \overline{\Delta P_0 - \phi(3)} \right]^{1/2} - \frac{2}{\rho}\left[\Delta P_0 - \phi(3)\right] \right\} dy$$

$$= \frac{2\Delta P_0}{\rho} \int_0^\infty \left\{ \left(1 - \frac{\phi(3)}{\Delta P_0}\right)^{1/2} - 1 + \frac{\phi(3)}{\Delta P_0} \right\} dy \cdot \quad (365)$$

If $\frac{\phi(3)}{\Delta P_0} \ll 1.0$, $\left(1 - \frac{\phi(3)}{\Delta P_0}\right)^{1/2} = 1 - \frac{1}{2}\frac{\phi(3)}{\Delta P_0}$;

$$\therefore \frac{D_F}{b} = \Delta P_0 \int_0^\infty \frac{\phi(3)\,dy}{\Delta P_0} = \int_0^\infty \phi(3)\,dy \cdot \quad (366)$$

Thus, Equation (363) becomes

$$\frac{\Delta p_3}{\frac{1}{2}\rho u_0^2} = \left[1 - \left(\frac{r_0}{r_0 + \eta 3}\right)^{2/\eta} - \frac{2 r_0^{2/\eta - 1}(D_F/b)}{\frac{1}{2}\rho u_0^2 (r_0 + \eta 3)^{2/\eta}} + \frac{K}{\frac{1}{2}\rho u_0^2 (r_0 + \eta 3)^{2/\eta}} \right] \cdot$$

When $3 = 0$, $\Delta p_3 = \Delta p_1$;

$$\therefore \frac{K}{\frac{1}{2}\rho u_0^2} = r_0^{2/\eta} \frac{\Delta p_1}{\frac{1}{2}\rho u_0^2} + \frac{2 r_0^{2/\eta - 1}(D_F/b)}{\frac{1}{2}\rho u_0^2} ;$$

$$\therefore \frac{\Delta p_3}{\frac{1}{2}\rho u_0^2} = 1 - \left(\frac{r_0}{r_0 + \eta 3}\right)^{2/\eta} + \frac{\Delta p_1}{\frac{1}{2}\rho u_0^2}\left(\frac{r_0}{r_0 + \eta 3}\right)^{2/\eta} + \frac{2(D_F/b)}{\frac{1}{2}\rho u_0^2}\left(\frac{r_0}{r_0 + \eta 3}\right)^{2/\eta}$$

$$= 1 - \left(\frac{r_0}{r_0 + \eta 3}\right)^{2/\eta} \left[1 - \frac{\Delta p_1}{\frac{1}{2}\rho u_0^2} - \frac{2(D_F/b)}{\frac{1}{2}\rho u_0^2} \right] \cdot \quad (367)$$

Thus the square bracket replaces $\left(1 - \Delta p_1 / \frac{1}{2}\rho u_0^2\right)$ in the previous constant total head analysis, and the rest of the reasoning can be followed as before.

MOMENTUM DRAG

The momentum of the free-stream air swallowed by the intake is initially

$$\int_{r_0}^{R} \rho u^2 dy.$$

Now

$$\int_{r_0}^{R} \rho u dy = \dot{m}.$$

Thus, the momentum drag can be written as

$$D_M = \int_{r_0}^{R} \rho u^2 dy = \lambda \rho \bar{u}_0^2 (R - r_0)$$

$$= \lambda \dot{m}_1 \bar{u}_0. \qquad (368)$$

This is quite different from the traditional value $\mu_0 \dot{m}_1$, particularly if the intake is mounted some way back from the leading edge of a body or if there is any drag-producing structure (such as a sharply radiused leading edge) in front of it, whereby the mean velocity $\bar{u}_0$ is reduced. Even without drag effects, however, distortion of the velocity profile by the presence of the body will result in λ differing from unity, and hence changing the momentum drag. It is easy to see from the studies of λ in Chapter Two that this could influence the momentum drag by a factor of two in certain cases. Thus the reported momentum drag anomalies may be nothing more than the use of an inapplicable analysis.

SOME EXPERIMENTAL MEASUREMENTS

The efficiency of a ram intake is usually stated as the ram pressure recovery ratio (η_R). The flow is approximately one-dimensional; therefore the total pressure in the intake may be written as

$$p_1 + \tfrac{1}{2}\rho u_1^2 = p_a + \tfrac{1}{2}\rho u_0^2 \cdot \eta_R$$

$$\eta_R = \frac{-p_1 - p_a}{\tfrac{1}{2}\rho u_0^2} + \left(u_1/u_0\right)^2$$

$$\eta_R = \frac{\Delta p_1}{\frac{1}{2}\rho u_0^2} + \left(\frac{u_1}{u_0}\right)^2 \tag{369}$$

where Δp_1 is the mean static pressure rise relative to ambient and u_1 is the mean velocity in the intake.

Intake Power Efficiency

For a flush intake the ram pressure recovery ratio does not have precise meaning. Instead, as a measure of efficiency we consider the power content of the swallowed air in relation to its power at free stream velocity. Power over an area A is given by

$$\mathcal{P} = \int^A \Delta P . u \, dA \tag{370}$$

and we define the efficiency as

$$\eta_P = \frac{\int^{A_1} \Delta P_1 u_1 \, dA_1}{\int^{A_0} \Delta P_0 u_0 \, dA_0} \tag{371}$$

$$= \frac{1}{\frac{1}{2}\dot{m} u_0^2} \int_0^{A_1} \left(\Delta p_1 u_1 + \tfrac{1}{2}\rho u_1^3\right) dA_1 \tag{372}$$

where $\dot{m}$ is the mass flow into the intake.

That is,

$$\eta_P = \frac{\text{Duct airflow power above ambient}}{\text{Duct airflow power with no loss}} .$$

If Δp_1 is constant over the duct area A, Equation (372) becomes

$$\eta_P = \frac{\Delta p_1}{\frac{1}{2}\rho u_0^2} + \frac{\rho}{\dot{m} u_0^2} \int_0^{A_1} u_1^3 \, dA_1 , \tag{373}$$

and if u_1 is constant also, Equation (373) reduces to Equation (369). Thus, the intake power efficiency and the ram pressure recovery ratio are identical under these conditions. However, the power efficiency has the advantage of

having an exact meaning, both in this special case and generally.

At low value of the free-stream velocity ($u_\infty \to 0$), the efficiency has a large negative value since ΔP_1 will become negative when the free-stream total head is insufficient to compensate for losses in the duct.

Experimental Measurement of Intake Power Efficiency

As a simple experiment to establish the power efficiency for a two-dimensional flow, an intake was constructed in the floor of the Eiffel tunnel at Payne, Inc. The aperture was connected by a short length of ducting to an antechamber exhausted by the intake of a centrifugal blower. The general arrangement and dimensions are shown in Figures 114 and 115. The air flow was examined by means of total and static pressure measurements at the throat of the intake, at the mouth of the intake, and at points near the tunnel floor upstream of the intake. Additionally, the direction of the flow at the intake mouth was established.

These measurements were made with a directional probe. This instrument does not sense static pressure directly, and a calibration was necessary to obtain static pressure data.

Calibration of Yaw Probe, for Static Pressure Measurement

The sensing head of the yaw probe is cylindrical, 0.120-inch diameter, with three pressure tappings at angles approximately -30°, 0°, $+30^\circ$ to the reference direction. The method of use consists of rotating the probe about its axis until the pressures in the side tappings are equal. The center tap (and reference direction) is then in line with the flow and senses the total pressure of the flow.

The pressure around a cylinder in incompressible flow is given by

$$p_r = p_s + C_p \cdot \tfrac{1}{2} \rho v^2 \qquad (374)$$

where C_p is a coefficient depending only on angular position around the cylinder with respect to the flow direction. For the probe as used, the angular position of the taps is constant and therefore C_p is constant. Thus, the common pressure in the side taps is given by

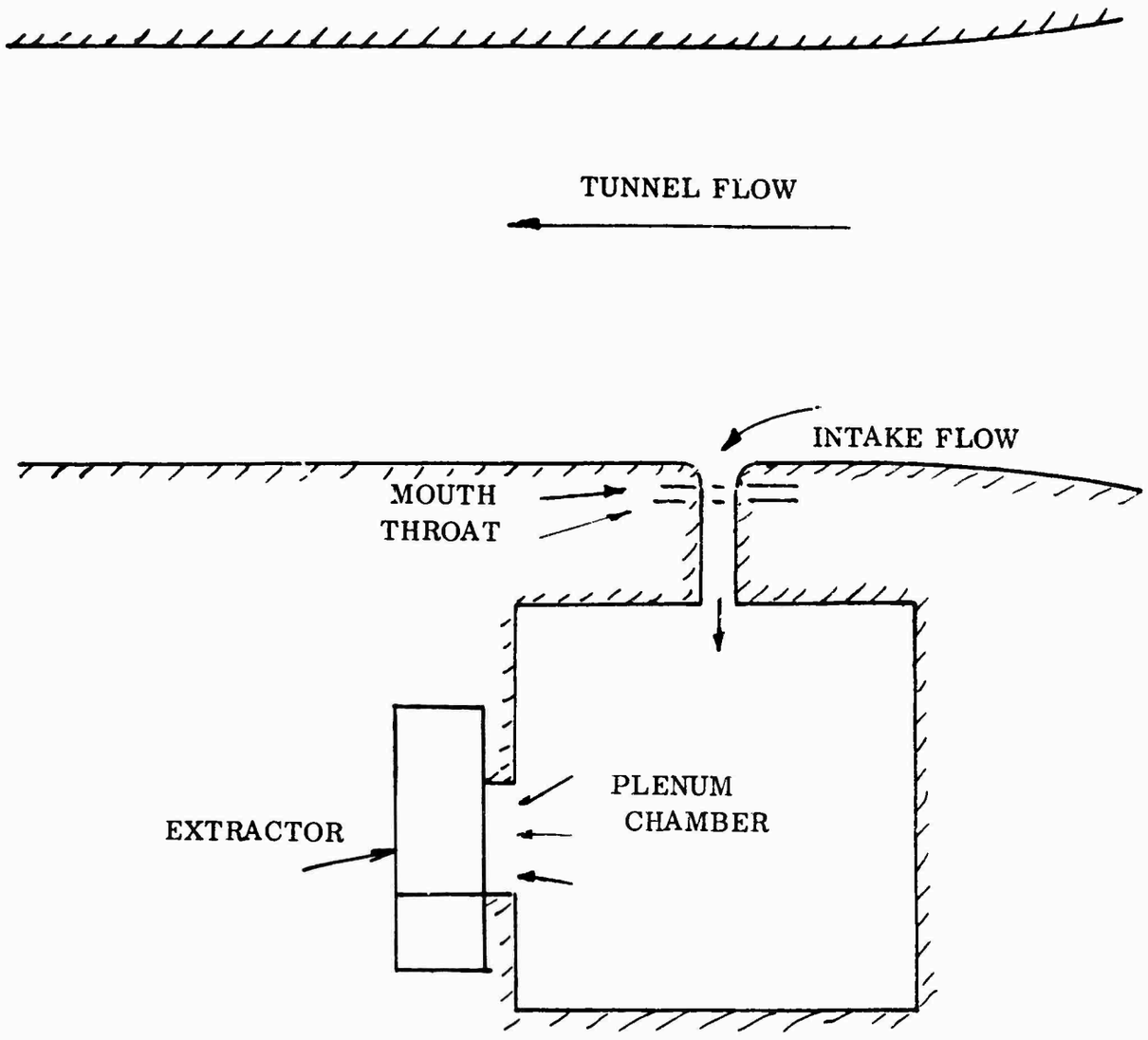

Figure 114. Arrangement of Intake in Floor of Wind Tunnel.

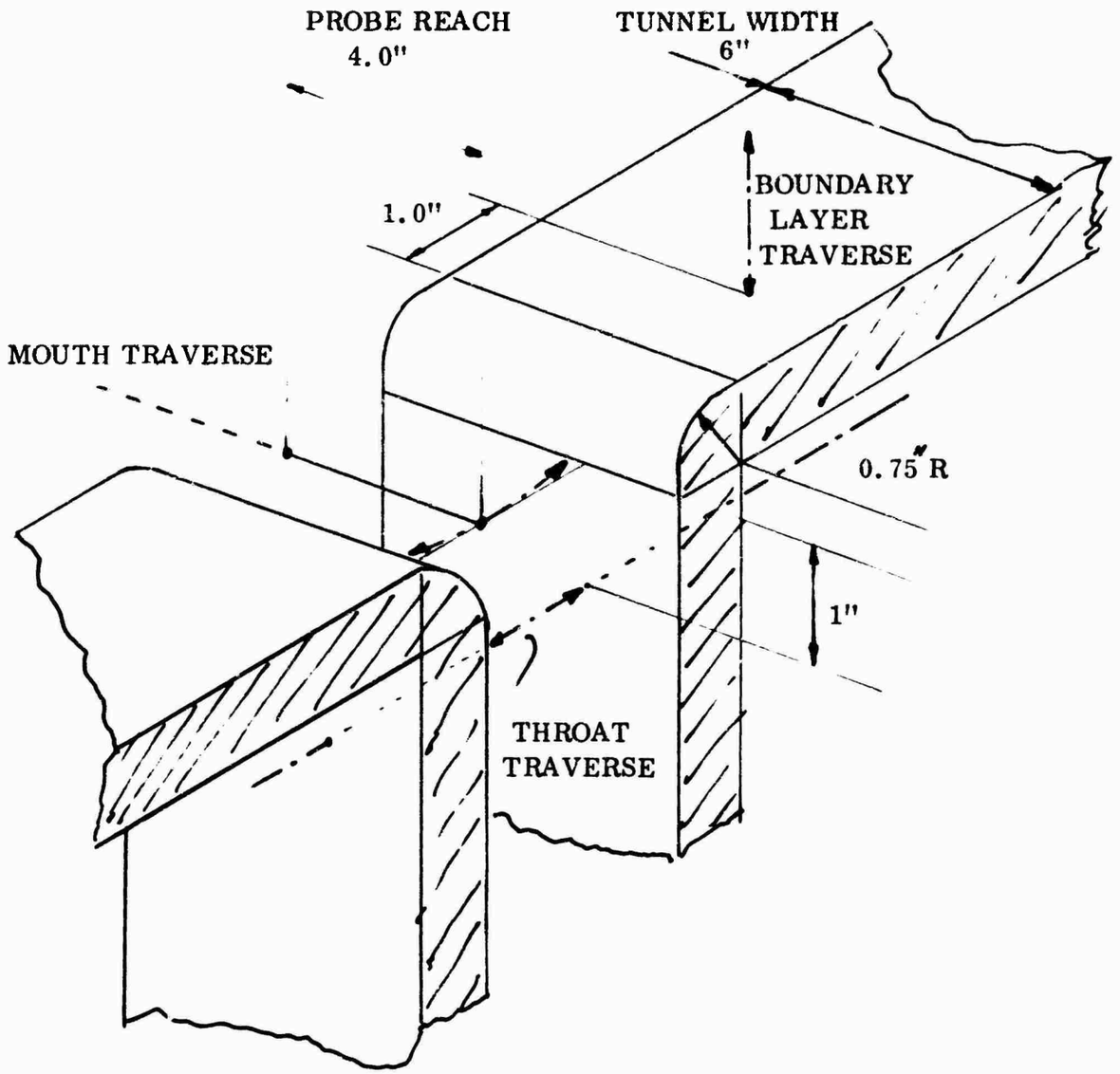

Figure 115. Location of Measuring Stations.

$$p_T = p_s + C_p(p_a - p_s) \qquad \text{when } p_a = P$$

$$1 - C_p = \frac{p_T - p_a}{p_s - p_a} . \tag{375}$$

C_p was determined by setting up the probe in the main tunnel flow and measuring $p_T - p_a$, $p_s - p_a$.

The actual values were

$$1 - C_p = \frac{p_T - p_a}{p_s - p_a} = \frac{4.47}{2.75} = 1.63$$

$$C_p = -0.63 . \tag{376}$$

In general

$$p_T = p_s + C_p(P - p_s)$$

$$p_s = \frac{p_T - C_p . P}{1 - C_p}$$

$$= \frac{p_T - P}{1 - C_p} + P$$

$$= 0.612(p_T - P) + P \tag{377}$$

and $$\tfrac{1}{2}\rho v^2 = -0.612(p_T - P) . \tag{378}$$

In the tunnel experiments, ΔP_1 of Equation (371) is, with respect to the tunnel static pressure (Δp_o), representing the total pressure above ambient sensed in the intake with forward motion u_o. Thus, if ΔP is the measured total pressure with respect to room static,

$$\Delta P_1 = \Delta P - \Delta p_0$$

$$= \tfrac{1}{2}\rho u_0^2 + \Delta P. \qquad (379)$$

Therefore, the expression for η_p becomes

$$\eta_p = \frac{\int_0^x \tfrac{1}{2}\rho u_0^2 u_1\, dx + \int_0^x \Delta P u_1\, dx}{\tfrac{1}{2}\dot{m} u_0^2}$$

$$= 1 + \frac{1}{\tfrac{1}{2}\dot{m} u_0^2} \int_0^t \Delta P u_1\, dx . \qquad (380)$$

Since ΔP is essentially negative, $\int_0^t \Delta P u_1\, dx$ represents the power lost in the intake flow, and the term $\frac{2}{\dot{m}u_0^2}\int_0^t \Delta P u_1\, dx$ may be called the power loss factor of the intake. Obviously as the tunnel speed is reduced the power loss factor becomes increasingly negative and leads to negative values of η_p. The experimental data are given on Figures 116, 117 and 118, showing the pressure and velocity distributions at the mouth and throat of the intake. The power loss factor was computed from the throat measurements.

Here the values were as follows:

Volume flow	$\int_0^t u_1\, dx$	= 16.0 ft^2/ second
Mass flow	$\dot{m} = \rho\int_0^t u\, dx$	= 0.0373 slug/second/ft
Power loss	$\int_0^t \Delta P u\, dx$	= 37.7 ft lb/second/ft
Free stream power	$\tfrac{1}{2}\dot{m}u_0^2$	= 151 ft lb/second/ft
Tunnel speed	u_0	= 90.0 ft/second
Power loss factor	$1 - \eta_p$	= 0.25
Intake power efficiency	η_p	= 0.75

Comparison with Theoretical Values

The velocity distribution in this intake mouth has been calculated by the methods of the previous section and is shown in Figures 119, 120 and 121.

In Figure 122 the experimental plot of the velocity normal to the intake plane is compared with the theoretical curve. The lack of agreement near the upstream wall is compared in Figure 123 with the velocity profile in the boundary layer in the tunnel 1 inch upstream of the start of the intake radius, and Figure 124 shows the total pressure gradient. The nominal thickness (where the velocity

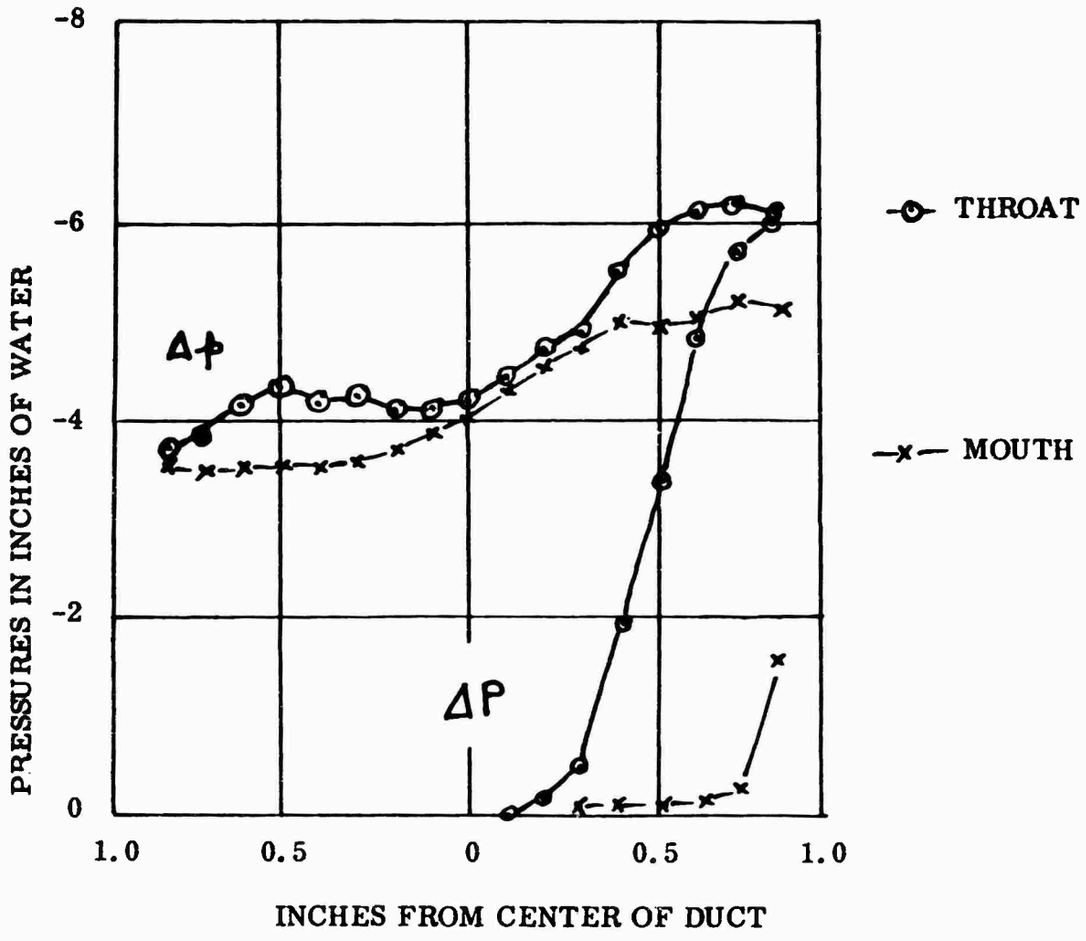

Figure 116. Total and Static Pressures in Intake.

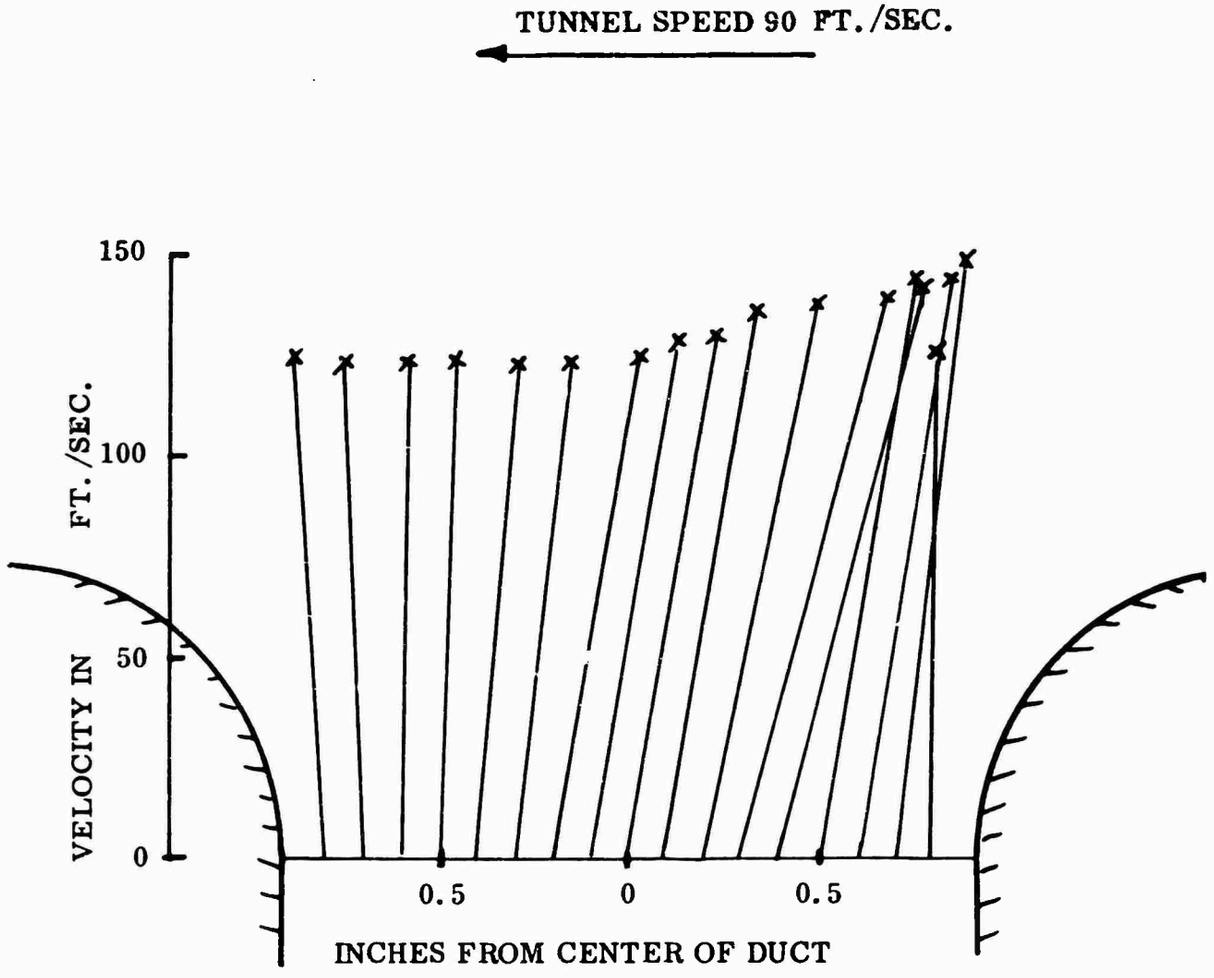

Figure 117. Velocity Vector Profile at Mouth of Intake.

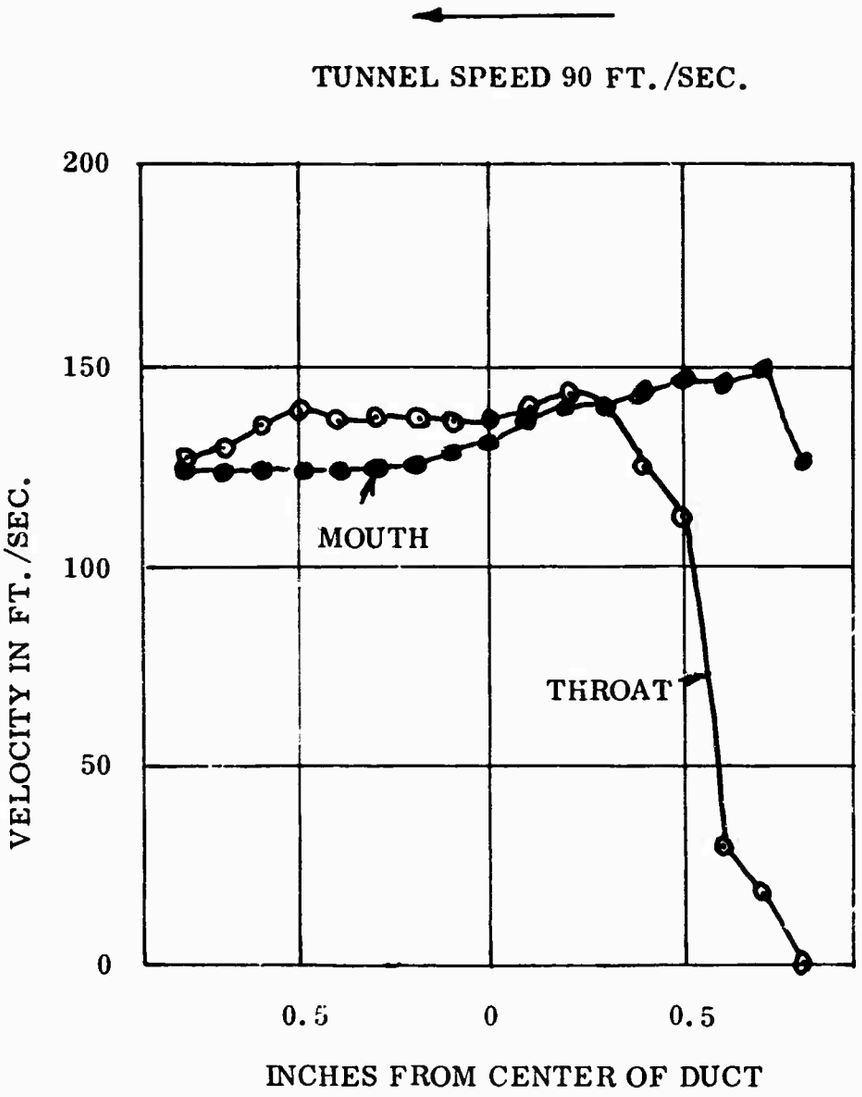

Figure 118. Velocities at Mouth and at Throat of Intake.

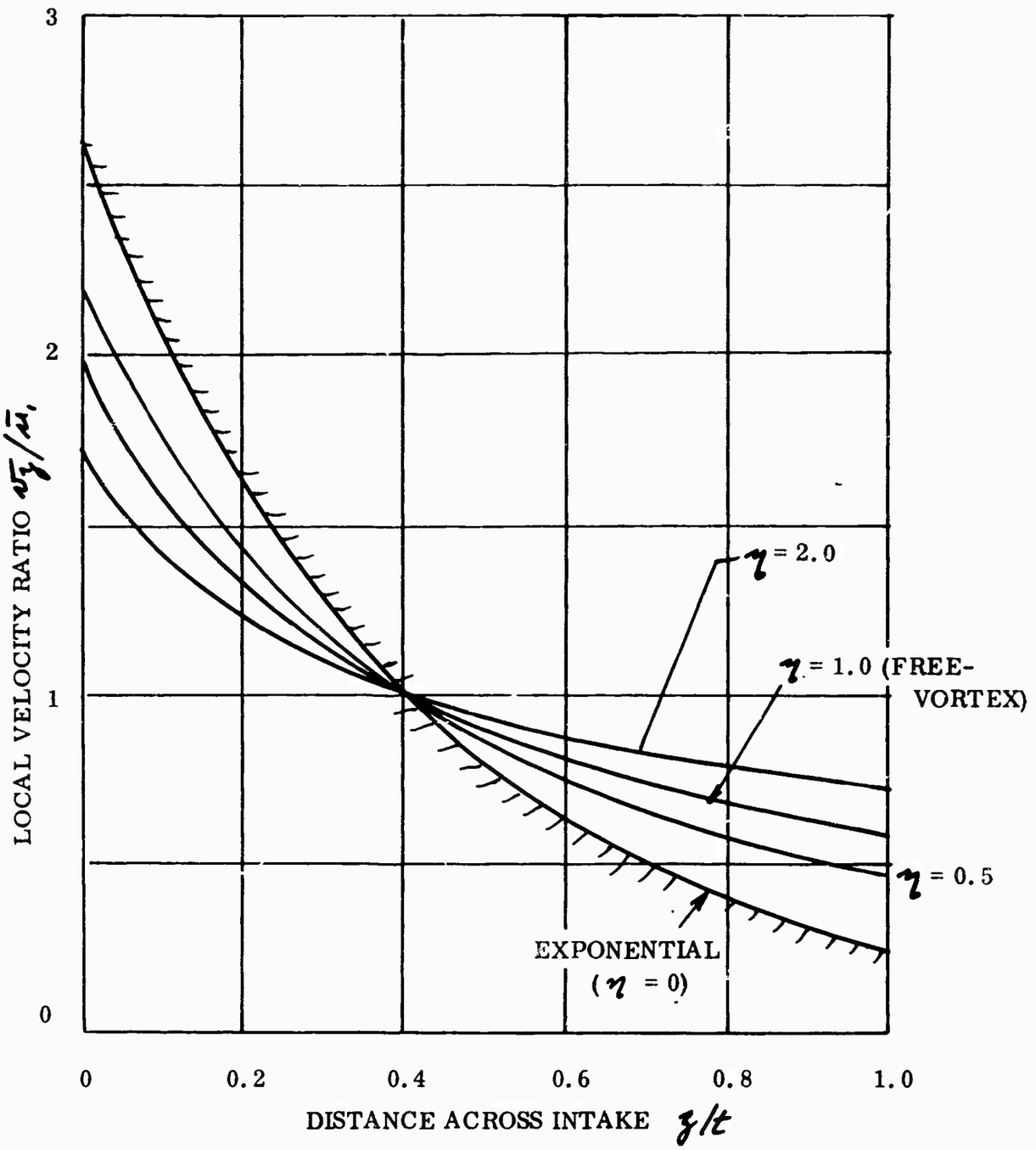

Figure 119. Theoretical Velocity Distributions for the Test Intake (Uniform Inflow).

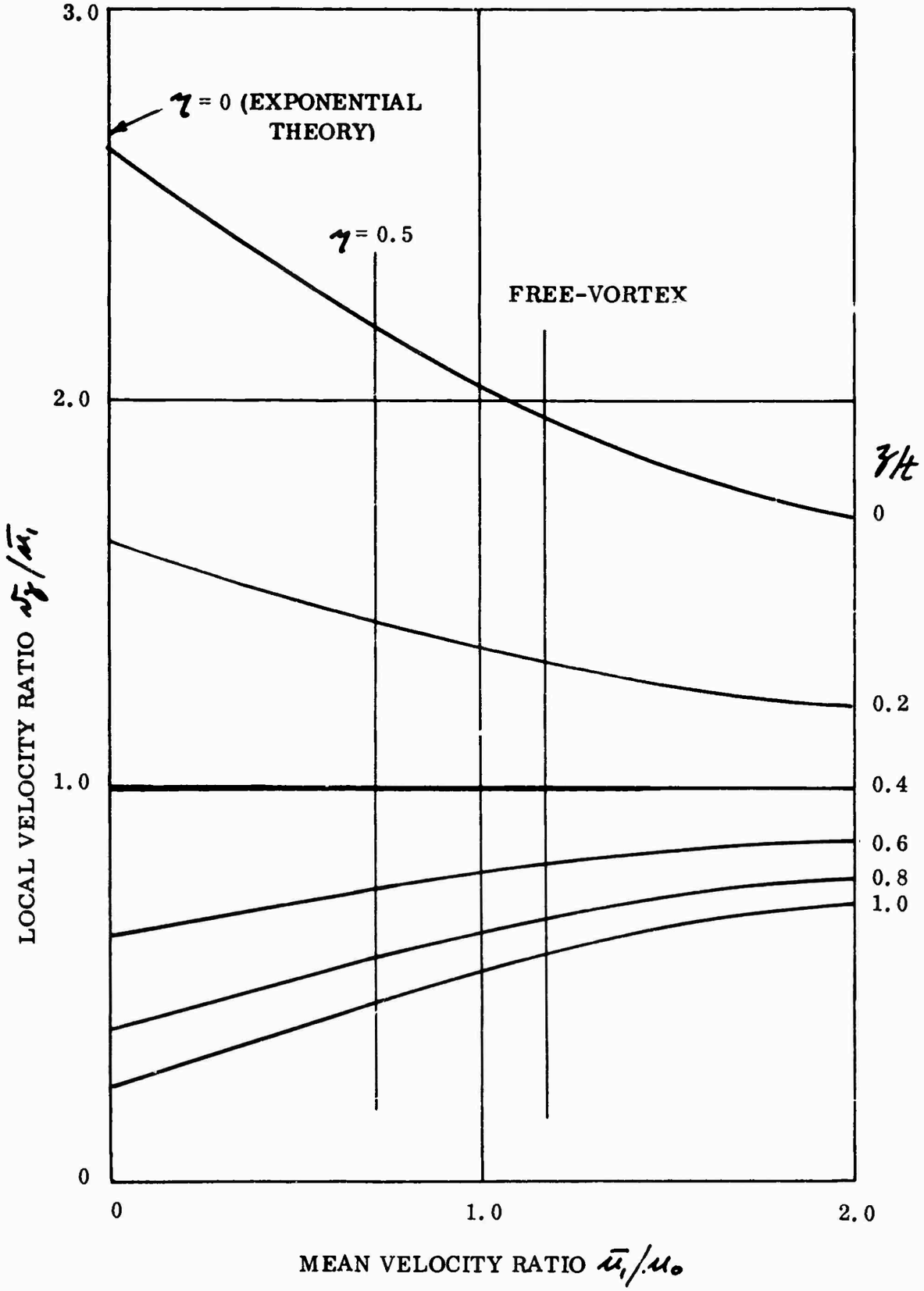

Figure 120. Cross-Plot of Intake Velocity Ratio, as a Function of $\bar{u}_1/u_0$, for the Test Intake. (Conservation of Momentum Correlation Between η and $\bar{u}_1/u_0$.)

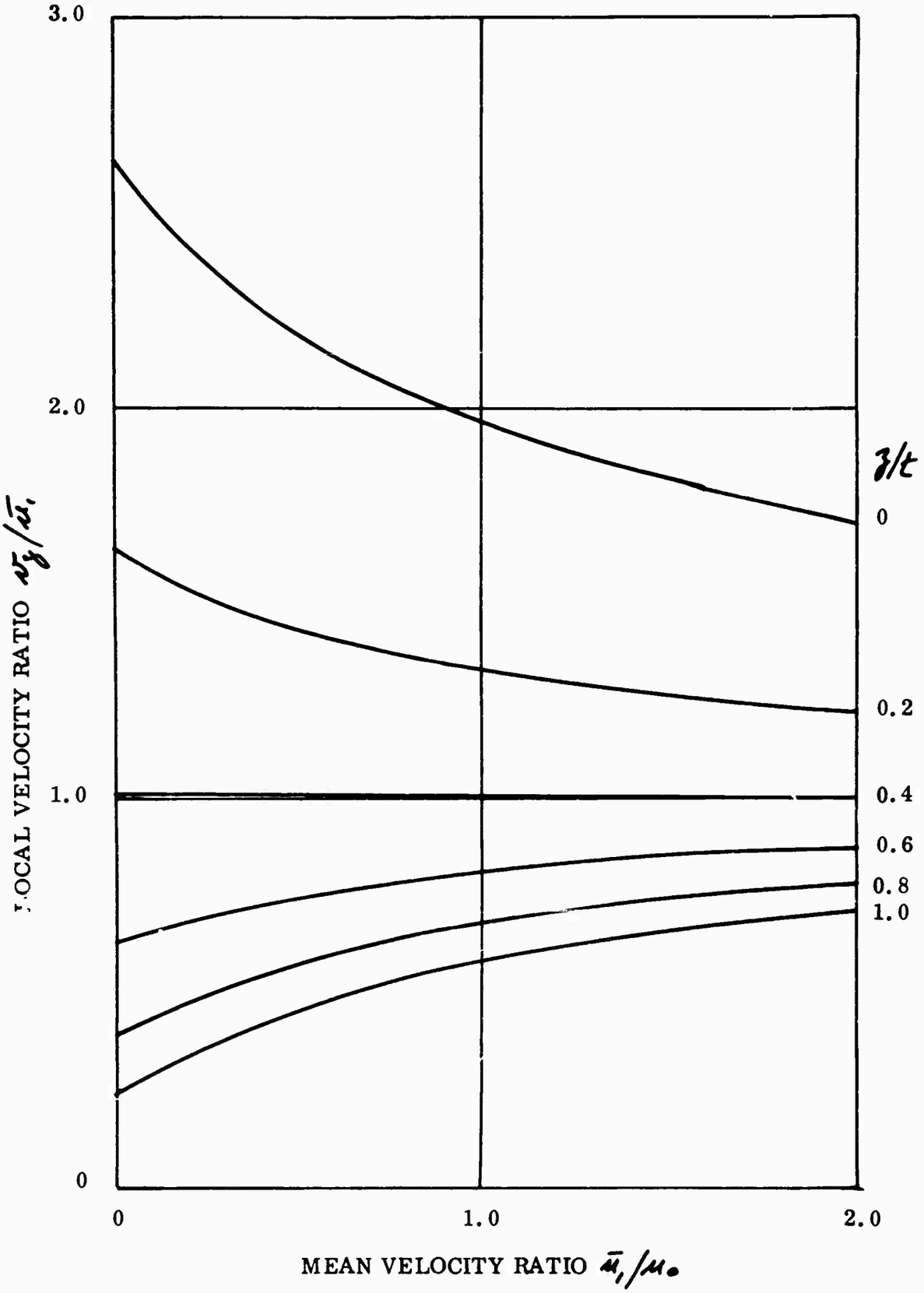

Figure 121. Cross-Plot of Intake Velocity Ratio, as a Function of $\bar{u}_1/u_\infty$, for the Test Intake. (Conservation of Mass Flow Correlation Between η and $\bar{u}_1/u_\infty$.)

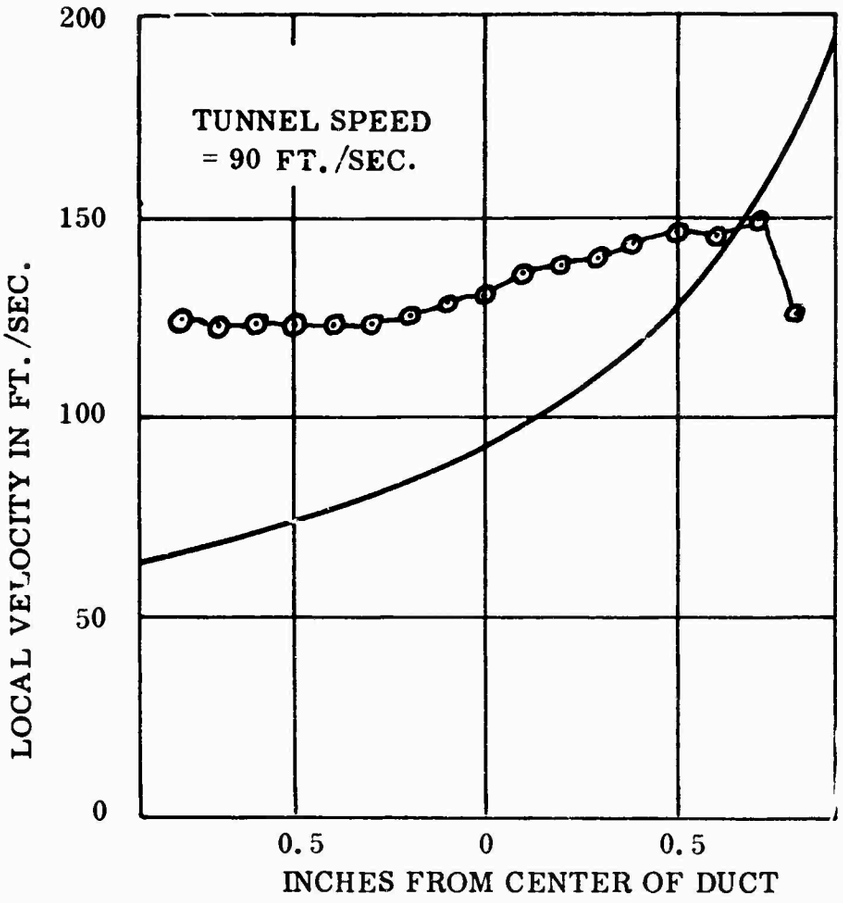

Figure 122. Comparison of Experimental and Theoretical Velocity at Mouth.

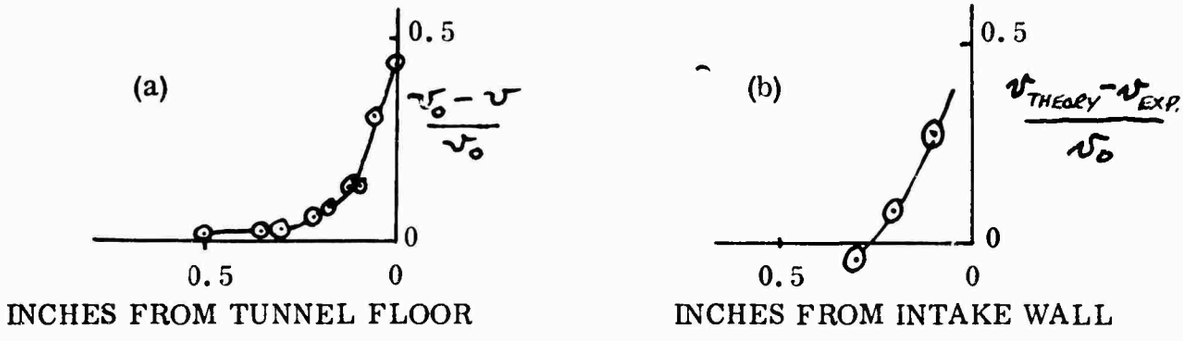

Figure 123. Resemblance Between
(a) Velocity Profile in Upstream Boundary Layer and
(b) Velocity Difference (Theoretical-Experimental) Near Upstream Wall of Intake Throat.

is 0.95 of the tunnel speed) is 0.14 inches and thus must be considered thick in proportion to the dimensions of the intake. The theoretical curve is thus not applicable close to the boundaries, and the flow in the center should be increased to represent the practical case. This is sufficient to show the importance of the boundary layer in distributing intake flow.

The spanwise distribution of velocity across the duct (Figure 125) is fairly uniform and the approximation to two-dimensional flow seems reasonably close.

Comparison With Zero Tunnel Speed Case

The velocity profile at the intake case for zero forward speed is shown in Figure 126 with the case from Figure 123 superimposed for comparison.

These show that the mass flows are almost identical, indicating that the amount of air swallowed by the intake is independent of forward speed. In the zero speed case the boundary layer is of course quite thin, being developed only over the length of the intake itself.

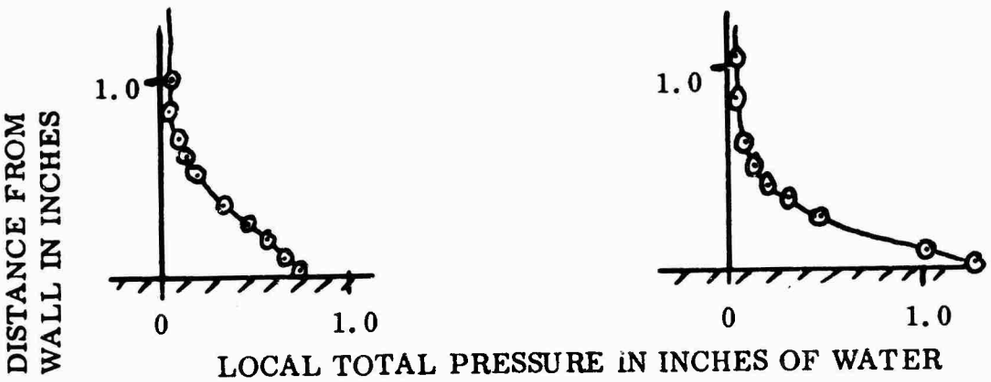

(a) Tunnel Speed Zero.

(b) 90 Ft/Sec. Tunnel Speed.

Figure 124. Total Pressure in Upstream Boundary Layer.

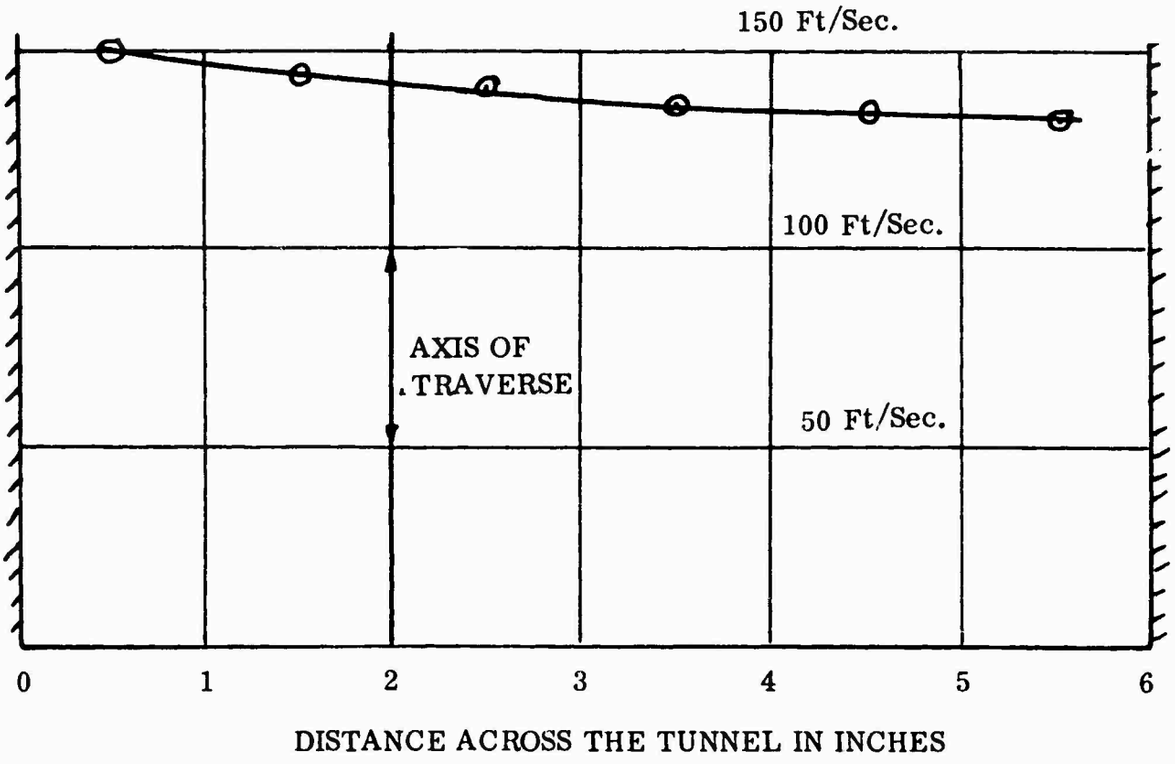

Figure 125. Spanwise Distribution of Velocity at Mouth of Intake.

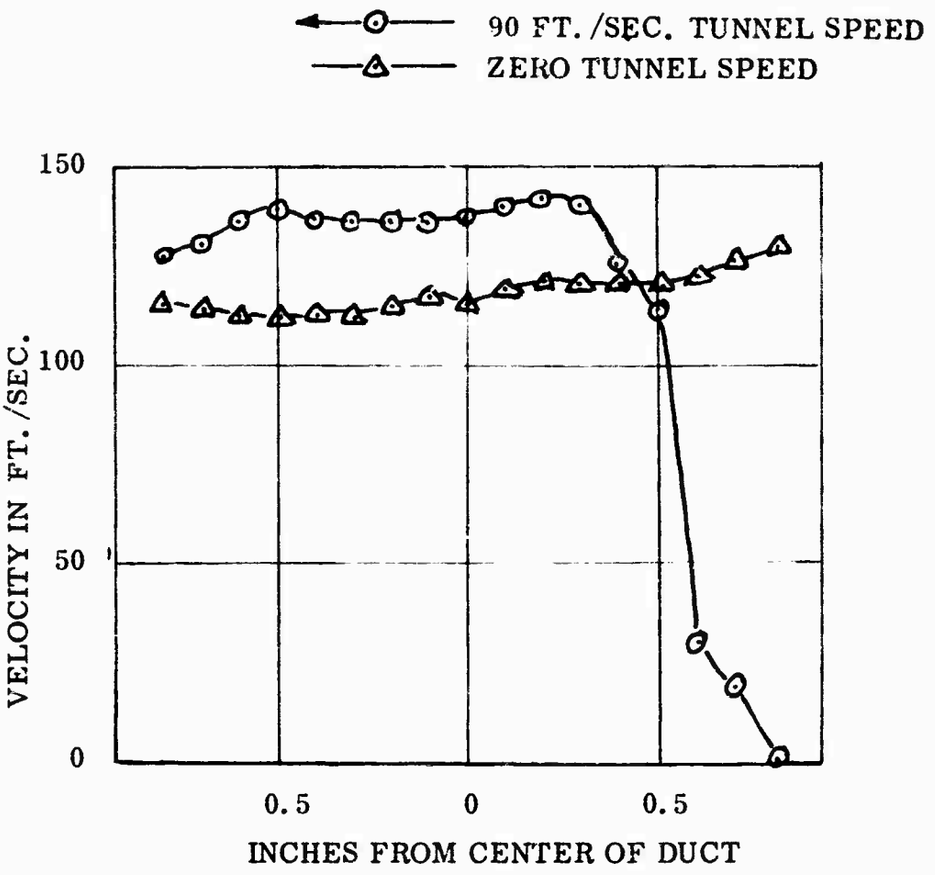

Figure 126. Velocity at Throat of Intake - Tunnel Speed Zero and 90 Feet/Second.

Chapter Eleven

SOME GENERAL PROBLEMS OF A JET DISCHARGING ACROSS A FREE-STREAM FLOW

THRUST LOSS DUE TO MIXING

It was shown in Reference 3 that if a jet of mass flow ($\dot{m}_j$) mixes with an additional quantity of fluid ($n\dot{m}_j$) at a mixing static pressure Δp_1 , the augmentation is

$$\phi = \frac{J_2}{J_a} = \frac{\text{Total momentum flux to ambient}}{\text{Jet momentum flux to the pressure } \Delta p_1}$$

$$= \left[(n+1)^2 \overline{\Delta p_1} + \eta_D (1 + n \cdot u_1/u_0)^2 \right]^{1/2} \qquad (381)$$

where

n is the entrained fluid ratio.

$\overline{\Delta p_1} = \Delta p_1 / \frac{1}{2} \rho u_0^2$

u_0 = primary jet velocity at the pressure Δp_1

η_D = (dynamic head) efficiency of diffusion to ambient

u_1 = velocity of secondary fluid before mixing.

This equation is quite general for incompressible flow; present indications are that compressibility effects are negligible so long as u_1 is subsonic.

When a jet is exhausted across a free-stream flow, the static pressure distribution in the region of the nozzle is quite complex. Generally it is greater than ambient in the forward portion of the jet (Δp_x in Figure 23 for example) so that $\overline{\Delta p_1}$ is positive in Equation (381).

Close to the nozzle, we may take the relative static pressure as the free-stream dynamic head $\frac{1}{2} \rho v_0^2$ on the high pressure side of the jet. On the rear side of the jet the static pressure will be ambient, or somewhat lower. Thus, the mean effective jet static pressure will be between these two extremes and will, in fact, be the arithmetric mean if the jet is thin in relation to its local radius of curvature. Thus, approximately

$$\Delta p_1 = \Delta p_j = \tfrac{1}{2}\left(\tfrac{1}{2}\rho v_0^2\right);$$

$$\therefore \quad \bar{\Delta p_1} = \tfrac{1}{2}\left(\frac{v_0}{u_0}\right)^2$$

and

$$\frac{J_2}{J_0} = \left[\tfrac{1}{2}(n+1)^2\left(\frac{v_0}{u_0}\right)^2 + 1\right]^{1/2}. \tag{382}$$

This equation does not account for the momentum lost by the air which is entrained by the jet, a drag force which is obviously $n\dot{m}v_0$. When this is included

$$\left[\frac{J_2}{J_0}\right]_{NET} = \left[\tfrac{1}{2}(n+1)^2\left(\frac{v_0}{u_0}\right)^2 + 1\right]^{1/2} - n\frac{v_0}{u_0}. \tag{383}$$

Note that as $v_0/u_0 \to 0$,

$$\left[\frac{J_2}{J_0}\right]_{NET} \to 1 - n v_0/u_0 . \tag{384}$$

As $n \to 0$,

$$\left[\frac{J_2}{J_0}\right]_{NET} \to \left[\tfrac{1}{2}\left(\frac{v_0}{u_0}\right)^2 + 1\right]^{1/2}, \tag{385}$$

which describes the effect of the pressure energy in the jet.

Equation (383) is plotted in Figure 127, where we see that, if the entrained air ratio (n) is large enough, the thrust recovery can be negative. The apparent thrust recovery can exceed unity only for very small values of n, and this is due only to the neglect of the pressure thrust term in the analysis.

It is not the primary purpose of this report to discuss jet drag, so that we shall not study the variation of (n) with u_0/v, beyond remarking that we can obviously accomplish this, using the results of the section on jet characteristics.

It seems that this mixing is the primary reason for the loss of propulsive thrust which occurs when a jet flap is deflected through a large angle. For completeness, however, we shall now review the other possible reasons for the "thrust anomaly".

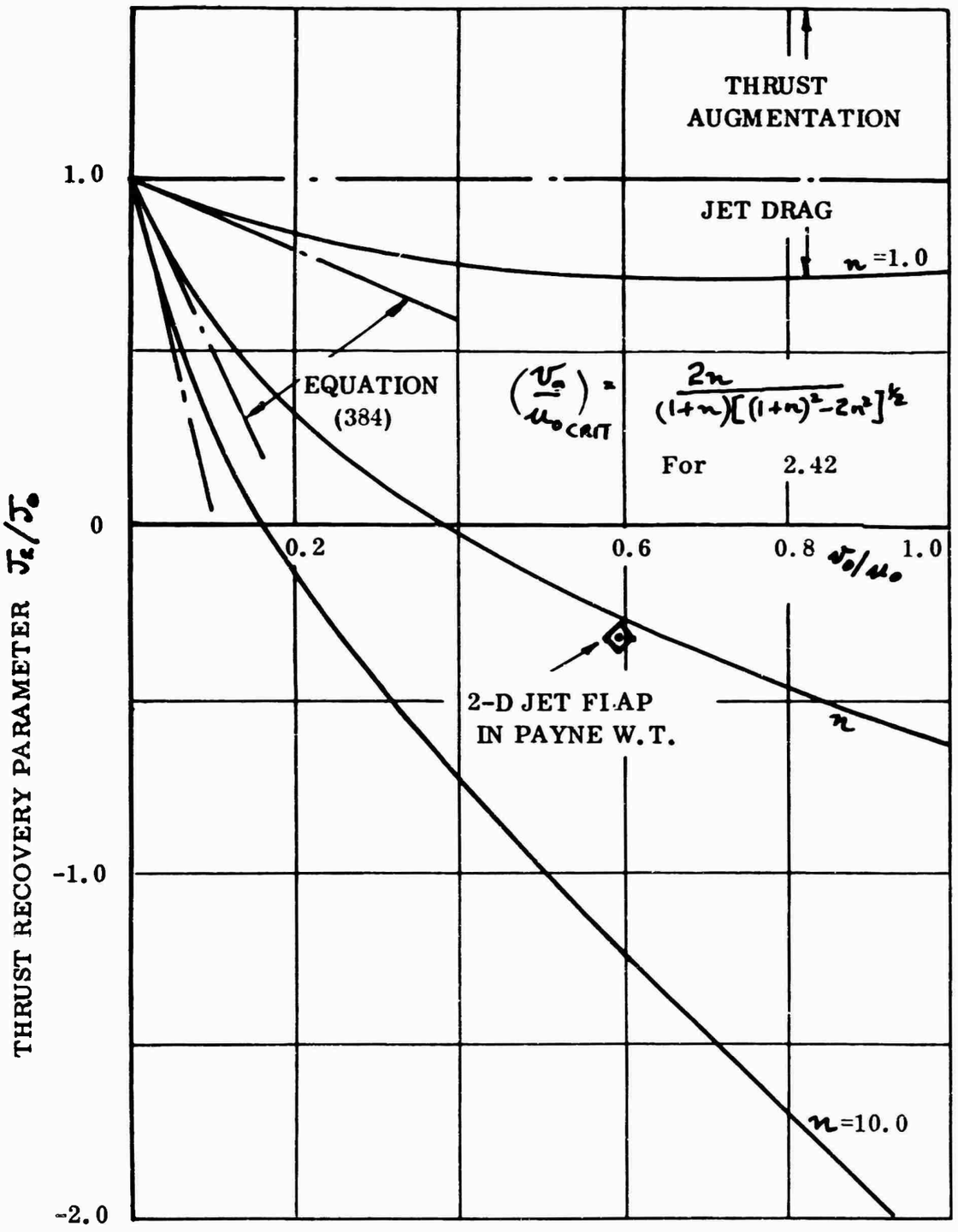

Figure 127. Jet Drag Due to Entrainment in a 90 Degree Jet Flap.

When a jet of mass flow ($\dot{m}_j$) emerges from a body with a uniform velocity u_{j_0} , we anticipate a thrust equal to the product ($\dot{m} u_{j_0}$). This follows from Newton's law that force is equal to the rate of change of momentum; that is,

$$F = \frac{d}{dt}(m_j u_{j_0}) = \frac{dm_j}{dt} u_{j_0} + m_j \frac{du_{j_0}}{dt},$$

the second derivative being zero in steady flow.

More precisely, if u_j is the local velocity in the jet exit plane, and Δp_j the local static pressure measured relative to ambient

$$F = \int_0^{A_j} \Delta p_j \, dA_j + \int_0^{A_j} \rho u_j^2 \, dA_j , \qquad (386)$$

a relationship which can be applied to two- or three-dimensional flow.

SOURCES OF APPARENT JET DRAG COMMON TO ALL JET CONFIGURATIONS

The nozzle static pressure is usually assumed to be equal to ambient and this is usually a safe assumption for static conditions if it is well designed, and of constant section. If vena contracta occurs, however, or the nozzle is either convergent or divergent, then this assumption is invalid.

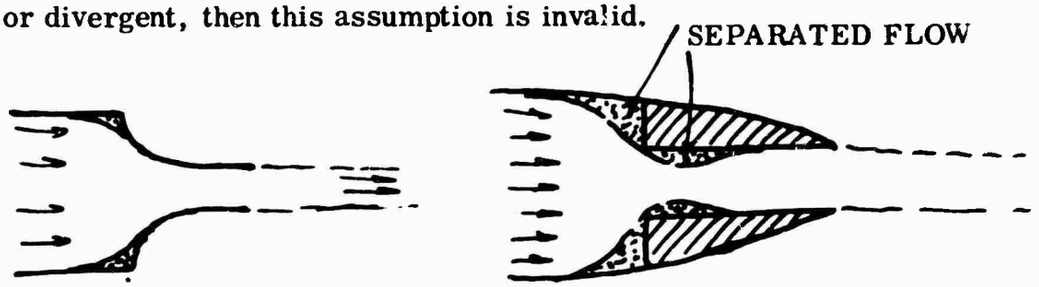

(a) Nozzles for Which the Exit Plane Static Pressure is Essentially Ambient.

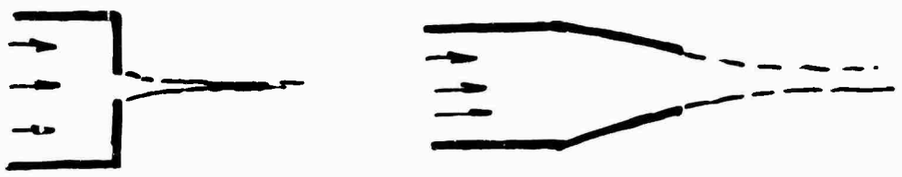

(b) Nozzles for Which the Exit Static Pressure is Greater Than Ambient.

Figure 128. Some Effects of Nozzle Shape on the Discharge Coefficient Under Static Conditions.

This obviously presents difficulties. In some experimental work with GEMs for example, it has been the practice to measure the supply air mass flow. The velocity is then obtained by dividing by the jet area A_j and nozzle force calculated from the expression

$$F_N = \dot{m}_j \left(\frac{\dot{m}_j}{\rho A_j} \right). \tag{387}$$

If appreciable contraction occurs as the jet leaves the nozzle, such a calculation could be as much as 40% in error, of course.

Thus, a first cause of jet drag can be a simple error in estimating the jet force. If the assumed value is F_A, and if the true value is F_T, the apparent drag will be $F_A - F_T$, giving a drag coefficient increment.

$$C_{D_j} = \frac{F_A \left(1 - F_T/F_A \right)}{\frac{1}{2} \rho u_0^2 S}$$

$$= 2 \left(\frac{A_j}{S} \right) \left(\frac{\rho_j}{\rho_0} \right) \left(\frac{u_j}{u_0} \right)^2 \left(1 - F_T/F_A \right). \tag{388}$$

The Effect of Pressure Due to Free-Stream Flow

Major difficulties arise when the jet issues from a body immersed in a free stream flow, since the pressure term in Equation (387) is not now equal to ambient.

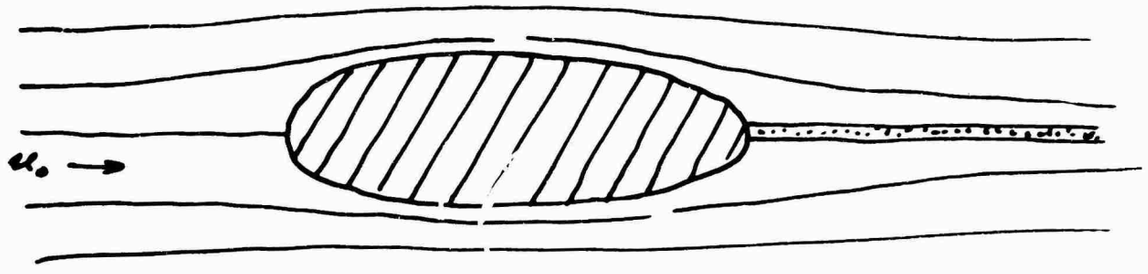

Figure 129. Jet Issuing From a Body in Inviscid Flow.

Consider the idealized case of a jet issuing from the rear of a body in inviscid flow, for example, as shown in Figure 129. If the total head of the jet is known (ΔP_j, say),then its velocity is known from the relationship

$$u_j = \left[\frac{2}{\rho} (\Delta P_j - \Delta p_j) \right]^{1/2}. \tag{389}$$

Now the static pressure at the jet exit for a thin jet will be equal to the free-stream total head, provided that the rear is rounded. That is,

$$\Delta p_j = \tfrac{1}{2} \rho u_0^2$$

$$u_j = \left(\frac{2}{\rho} \Delta P_j - u_0^2 \right)^{1/2}. \tag{390}$$

For a nozzle thickness of (t), the jet mass flow will be

$$\dot{m}_j = \rho C t \left(\frac{2}{\rho} \Delta P_j - u_0^2 \right)^{1/2}. \tag{391}$$

From Equation (387) the jet force will be

$$F = Ct \cdot \tfrac{1}{2} \rho u_0^2 + Ct \rho u_j \left(\frac{2}{\rho} \Delta P_j - u_0^2 \right)^{1/2}. \tag{392}$$

The normal thrust $(\dot{m}_j u_j)_N$ is the force of the jet when exhausting to ambient static pressure. That is,

$$(\dot{m}_j u_j)_N = Ct \rho u_j^2 = 2Ct \Delta P_j ;$$

$$\therefore \quad \frac{F_N}{(\dot{m}_j u_j)_N} = \frac{\tfrac{1}{2} \rho u_0^2}{2 \Delta P_j} + \frac{\tfrac{1}{2} \rho u_0^2}{\Delta P_j} \left(\frac{u_j}{u_0} \right) \left(\frac{\Delta P_j}{\tfrac{1}{2} \rho u_0^2} - 1 \right)^{1/2}. \tag{393}$$

From Equation (390)

$$u_j / u_0 = \left(\Delta P_j / \tfrac{1}{2} \rho u_0^2 - 1 \right)^{1/2} ;$$

$$\therefore \quad \frac{F_N}{(\dot{m}_j u_j)_N} = 1 - \frac{1}{2}\left(\frac{\frac{1}{2}\rho u_0^2}{\Delta p_j}\right). \tag{394}$$

The apparent jet drag is

$$D_j = (\dot{m}_j u_j)_N - F_N = (\dot{m}_j u_j)_N \left[1 - \frac{F_N}{(\dot{m}_j u_j)_N}\right]$$

$$= 2Ct.\Delta p_j \cdot \frac{1}{2} \cdot \frac{\frac{1}{2}\rho u_0^2}{\Delta p_j};$$

$$\therefore C_{D_i} = \frac{D_j}{\frac{1}{2}\rho u_0^2 S} = \frac{Ct}{S}. \tag{395}$$

This very simple result is perhaps what we would have intuitively suspected. By removing a small area (Ct) of the body in order to permit a jet to emerge, we have reduced the forward acting pressure force on the body by $Ct.\frac{1}{2}\rho u_0^2$ and replaced it by an equivalent jet pressure term.

The jet mass flow reduces with increasing u_0 for constant jet total pressure. From Equation (391)

$$\frac{\dot{m}_j}{(\dot{m}_j)_N} = \frac{Ct\rho\left(\frac{2}{\rho}\Delta p_j - u_0^2\right)}{Ct\rho\left(\frac{2}{\rho}\Delta p_j\right)^{1/2}}$$

$$= \left(1 - \frac{\frac{1}{2}\rho u_0^2}{\Delta p_j}\right)^{1/2} \tag{396}$$

$$= \left(1 - \frac{\frac{1}{2}\rho u_0^2}{\frac{1}{2}\rho u_0^2 + \frac{1}{2}\rho u_j^2}\right)^{1/2}$$

$$= \left[1 + \left(\frac{u_0}{u_j}\right)^2\right]^{-1/2}. \tag{397}$$

For the case of known (u_j) rather than constant (Δp_j) we can calculate the apparent jet drag as follows:

From (394)

$$F_N = C_t \cdot \tfrac{1}{2}\rho u_o^2 + C_t \rho u_j^2 \qquad (398)$$

$$(\dot{m}_j u_j)_N = C_t \rho u_j^2 ;$$

$$\therefore \quad \frac{F_N}{(\dot{m}_j u_j)_N} = 1 + \tfrac{1}{2}\left(\frac{u_o}{u_j}\right)^2 ;$$

$$\therefore \quad D_j = -C_t \rho u_j^2 \, \tfrac{1}{2}(u_o/u_j)^2 ;$$

$$\therefore \quad C_{D_j} = -\frac{C_t}{S} , \qquad (399)$$

a result identical to Equation (395) but of opposite sign.

In the case of a body whose rear surface (at the $\mathbb{C}$) is not normal to the free stream flow, the local pressure is $K \cdot \tfrac{1}{2}\rho u_o^2$, where $K < 1.0$ for a local angle of less than 90^o. Equations (395) and (399) are then modified in that they are multiplied by the constant K.

The Effect of "Boundary Layer Pumping"

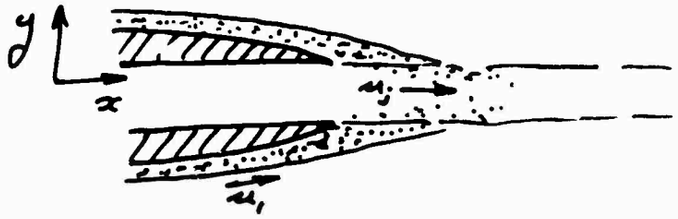

Figure 130. Boundary Layer Entrainment in a Jet.

In a real (viscous) fluid, when a jet issues from the rear of a wing or body, or from anywhere except the leading edge, for that matter, it must entrain a boundary layer which has an average velocity lower than free-stream velocity.

Let us suppose that the boundary layer velocity (u_1) is some arbitrary function of y and that the body is slender enough for all static pressures to be essentially ambient.

The equations governing the force on the symmetrical body are then

$$\text{Force} = \text{free-stream momentum downstream of body}$$

$$+ \text{(jet momentum flux)} - \text{free-stream momentum upstream of body}$$

$$= 2\int_0^\infty \rho u_0^2 dy - 2u_0 \int_0^\delta \rho u_1 dy$$

$$+ 2\int_0^\delta \rho u_1^2 dy + 2\int_0^{\frac{1}{2}t_j} \rho u_j^2 dy - 2\int_0^\infty \rho u_0^2 dy \quad (400)$$

$$= (\dot{m}_j u_j) - \left[2u_0 \int_0^\delta \rho u_1 dy - 2\int_0^\delta \rho u_1^2 dy\right]. \quad (401)$$

The skin friction force must be equal to the change in momentum flux of the boundary layer. That is,

$$F_{SF} = 2u_0 \int_0^\delta \rho u_1 dy - 2\int_0^\delta \rho u_1^2 dy \quad (402)$$

$$\text{Total force} = \dot{m}_j u_j - F_{SF}.$$

Thus, when the mixing zone static pressure is ambient, there is no jet-induced effect on the skin friction drag of a slender body.

Jet-Induced Turbulence

If the rear of the wing or body from which a jet issues is of such a shape that the free-stream air cannot negotiate it without separation, then operation of the jet can result in a larger wake than for the "jet off" condition as indicated in Figure 131. Hence even if the final jet momentum flux is the same as at the nozzle, the total drag will increase, as a direct result of the presence of the jet.

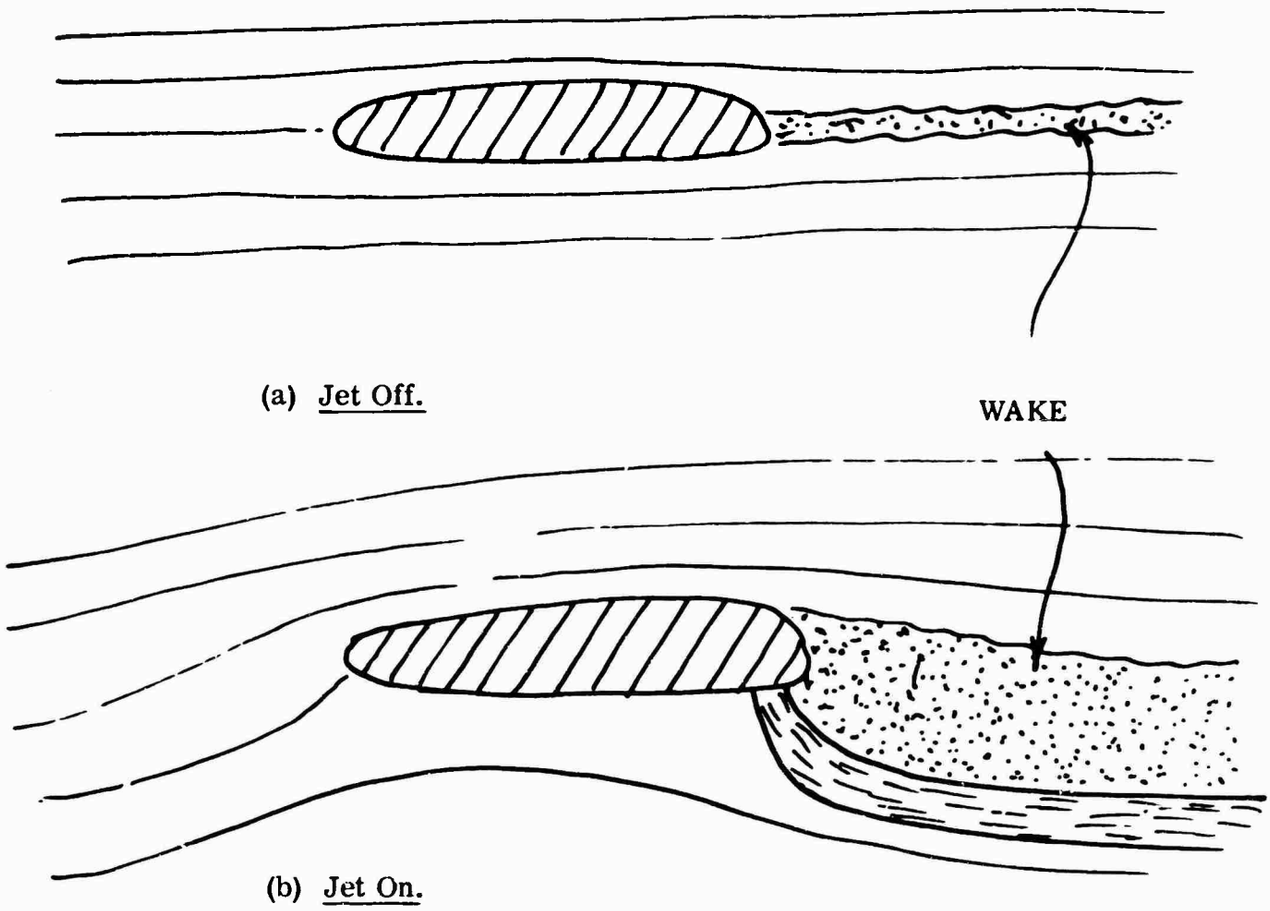

(a) Jet Off.

(b) Jet On.

Figure 131. Jet Influence on a Wake.

By analogy with a flat plate we should expect this drag to be of the form

$$C_{Dj} = K\left(\frac{u_1}{u_0}\right)^2 \cdot \frac{A_j}{S}. \qquad (403)$$

This effect has been observed on an elliptical aerofoil with a 90^0 jet flap, in the two-dimensional tunnel, as reported in the introduction to this report.

Nozzle Diffusion Losses

An oblique jet in a free stream implies that a pressure differential is generated across it. In fact, near the nozzle, the pressure differential across a 90^0 jet can be greater than the free-stream dynamic head.

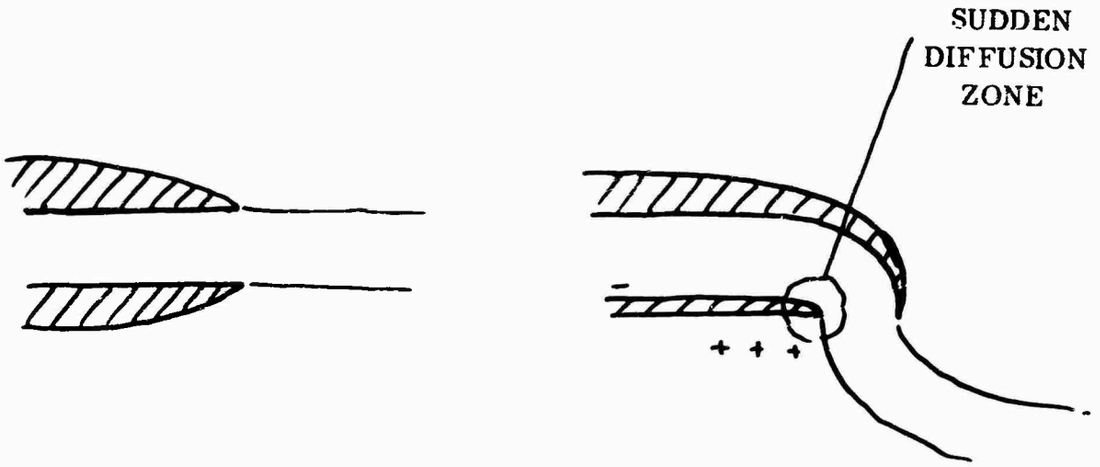

(a) No Diffusion When Jet has no Static Pressure Gradient Across It.

(b) Jet Issuing into a Static Pressure Gradient Undergoes Rapid Diffusion on the High-Pressure Side.

Figure 132. Nozzle Diffusion Losses.

This implies that the jet flow on the high-pressure side of the nozzle suffers a sudden increase in static pressure, causing losses which are analogous to the Borda-Carnot "sudden diffusion" loss discussed earlier. For a known geometry this can obviously be evaluated by the use of Equation (80).

A SIMPLE HYPOTHESIS FOR JET PRESSURE IN A FREE-STREAM FLOW

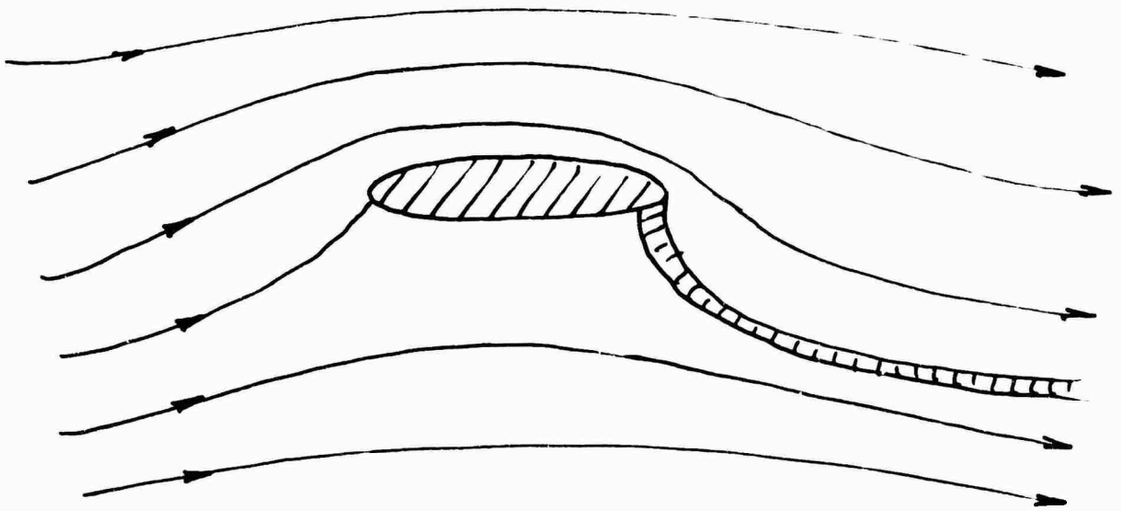

Figure 133. Jet Flap in Inviscid Flow.

The problem of the shape of a jet flap in inviscid flow is theoretically solvable, even though the path of the jet depends upon the external flow field, which in turn depends upon the path of the jet. We could, for example, use a potential tank analog to obtain a solution. However, a closed-form analytic solution would be extremely difficult, if not impossible, to obtain.

When dealing with viscous fluids, we know that the total head in the jet falls rapidly as it moves away from the nozzle, due to entrainment. This does not necessarily imply that the jet sheet will have a greater curvature (giving reduced circulation on the wing) however, because the total jet momentum flux is still conserved at constant static pressure. However, the problem is obviously even more complex than for inviscid flow, and in view of our ignorance on the subject of entrainment coefficients, we may well ask whether attempts to obtain such solutions are justifiable.

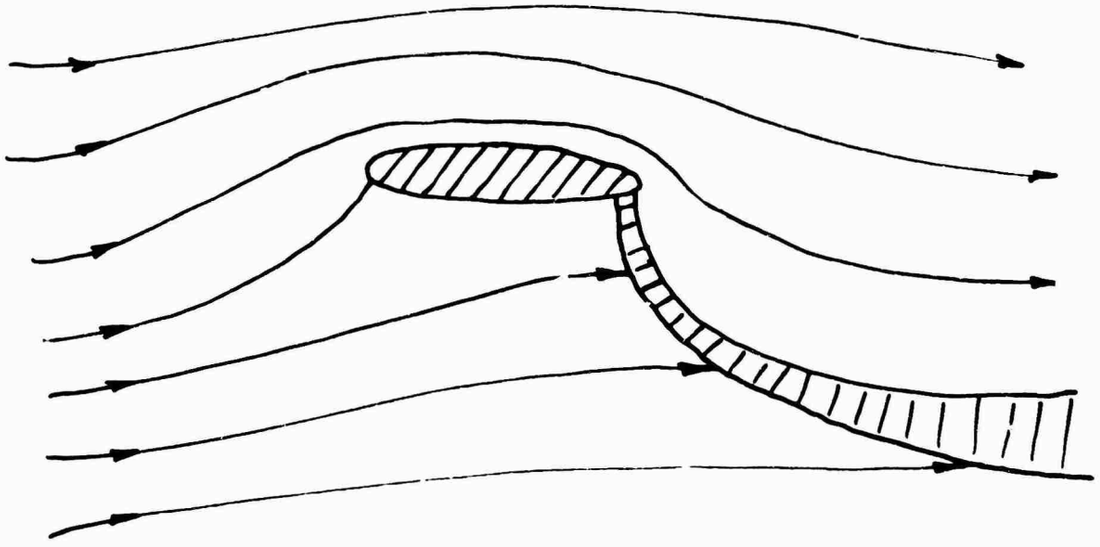

Figure 134. Smoke Tunnel Flow Observations of a Jet Flap.

Smoke tunnel observations of the flow around a jet flap indicate that the free streamlines "enter" the jet, almost without changing their direction (Figure 134). Certainly the flow picture seems quite different from the theoretical picture of Figure 133. This then introduces the possibility of an attractive mathematical simplification analogous to the $M_0^2 \cos^2\Theta$ hypothesis for swept-back wings and the Newtonian theory of hypersonic gas dynamics.

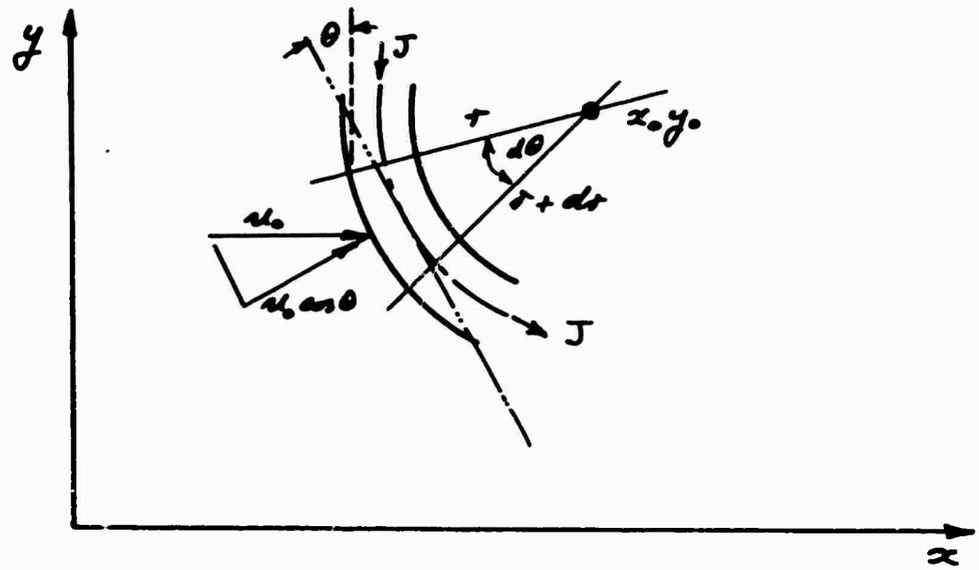

Figure 135. Local Jet Geometry.

From Figure 135 the appropriate assumption is

$$\Delta p = \tfrac{1}{2}\rho (u_0 \cos\theta)^2 = q_0 \cos^2\theta . \tag{404}$$

The change in momentum flux, normal to the initial direction, is evidently θJ , so that the balance of pressure and momentum forces gives

$$J d\theta = \Delta p + C d\theta$$

or

$$\frac{J}{q_0 C} = + \cos^2\theta . \tag{405}$$

In other words, the product ($+\cos^2\theta$) is a constant. Because the center of curvature changes continuously along the curve, this seemingly simple equation is difficult to transform to Cartesian coordinates. However, it can be plotted out graphically.

We note that

$$\tan\theta = -\frac{dx}{dy} . \tag{406}$$

And since

$$\tan\theta = \frac{\sin\theta}{\cos\theta} = \frac{(1-\cos^2\theta)^{1/2}}{\cos\theta},$$

$$\cos^2\theta = \frac{1}{1+\tan^2\theta} = \frac{1}{1+\left(\frac{dx}{dy}\right)^2} . \tag{407}$$

Then from (404) the local pressure is

$$\Delta p = \frac{q_0}{1+\left(\frac{dx}{dy}\right)^2} . \tag{408}$$

Thus for any jet shape, $y = fx$, the horizontal pressure force component is

$$\frac{\Delta p\, dy}{q_0} = \frac{(dy/dx)^2\, dy}{1+(dy/dx)^2} , \tag{409}$$

so that the total pressure force is

$$\int \frac{\Delta p\, dy}{q_0} = \int_0^h \frac{(dx/dy)^2 \cdot dy}{1+(dx/dy)^2} \tag{410}$$

where h is the maximum deflection the y direction.

For an elliptical jet path, for example,

$$\frac{x^2}{a^2} + \frac{y^2}{b^2} = 1 \tag{411}$$

$$x = \frac{a}{b}\left(b^2 - y^2\right)^{1/2} \tag{412}$$

$$\frac{dx}{dy} = -\frac{a}{b}\, y \left(b^2-y^2\right)^{-1/2} ;$$

$$\int \frac{\Delta p\, dy}{q_0} = \int_0^b \frac{dy}{1+\frac{(a/b)^2 y^2}{b^2-y^2}} ,$$

which reduces to

$$\frac{\int \Delta p_y \, dy}{q_0 b} = \frac{\tan^{-1}\left[(a/b)^2 - 1\right]}{\left[(a/b)^2 - 1\right]^{\frac{1}{2}}} \left\{ 1 + \frac{1}{(a/b)^2 - 1} \right\} - \frac{1}{(a/b)^2 - 1} \quad (413)$$

This function is plotted in Figure 136. Note that we have not attempted to determine the static pressure Δp_x behind the jet in this analysis.

SOME EXPERIMENTAL OBSERVATIONS

The behavior of a jet discharging normally into a free-stream air flow was examined using the flush intake in the floor of our two-dimensional tunnel with the air supply from a centrifugal blower discharging into the tunnel flow (Figure 137).

Total and static pressures were measured at three stations:

(1) Jet throat.
(2) Jet outlet to tunnel.
(3) Outlet from tunnel working section.

In addition, the static pressures at the tunnel wall at the working section entry and exit were measured.

The experiment was conducted at three different strengths of jet. Because of the interference with the free-stream flow, the free-stream velocity changed with the jet velocity. This is seen most clearly by considering the volume flow leaving through the tunnel driving fan with the jet at its various values.

Flows in Square Feet Per Second

Tunnel outflow	159	155	104.5	79.3
Jet inflow	0	8	12	20
Tunnel inflow	159	147	92.5	59.3

Velocities in Feet Per Second

Mean free-stream velocity	79.5	73	46.2	29.6

Mean jet velocity	0	41	62	103
Velocity ratio, jet/ free stream	0	0.56	1.34	2.88

All the measurements (except tunnel wall static pressures) were taken with the directional yaw probe described in a previous chapter, in conjunction with inclined manometers. Under set conditions, pressures were steady and repeatable. The data are plotted in Figures 137-143 without any smoothing or selective omission and the quality is such as to indicate a low incidence of random error.

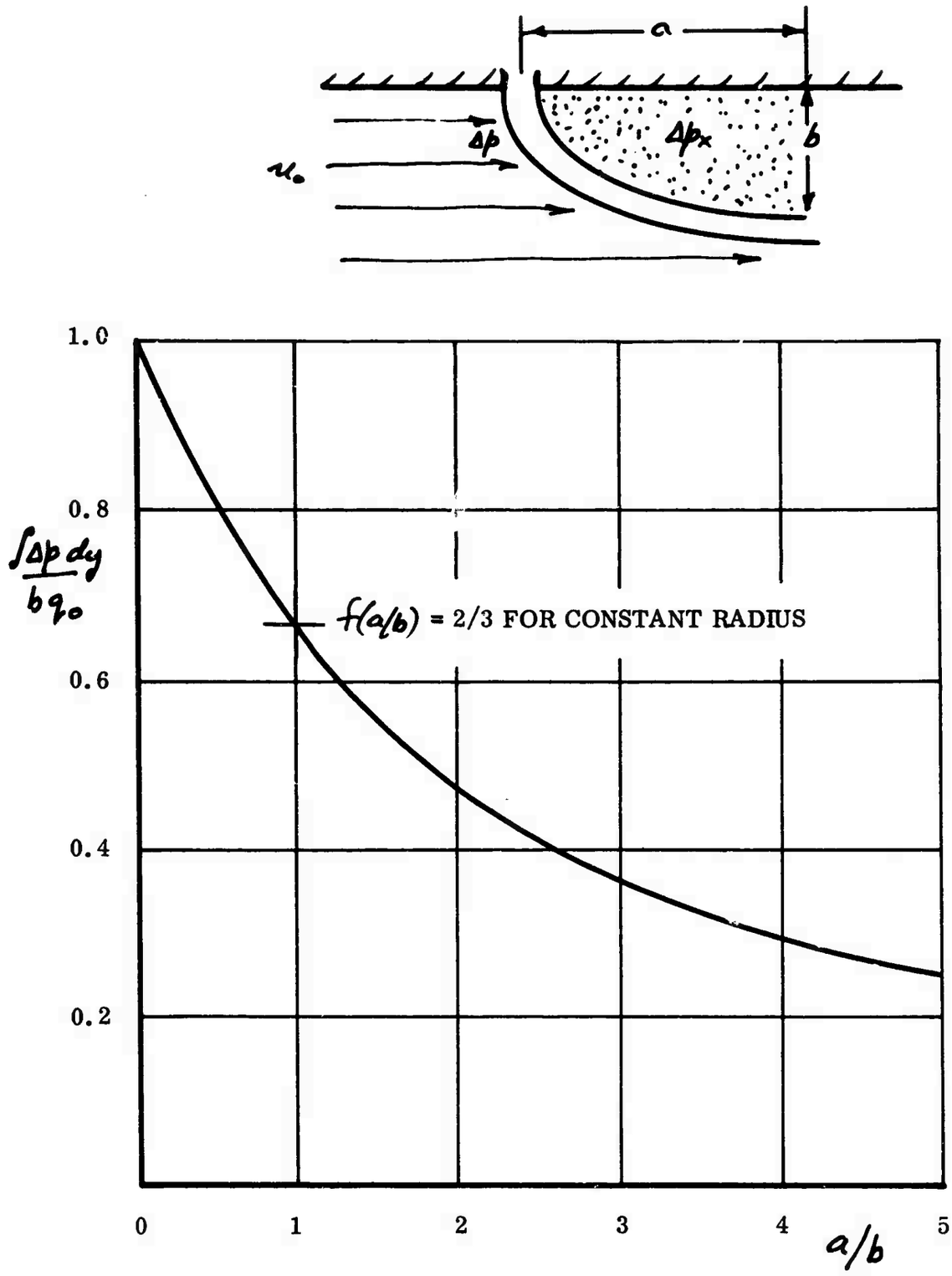

Figure 136. Pressure Integral on the Upstream Side of a Jet Exhausted Normal to a Free-Stream Flow.

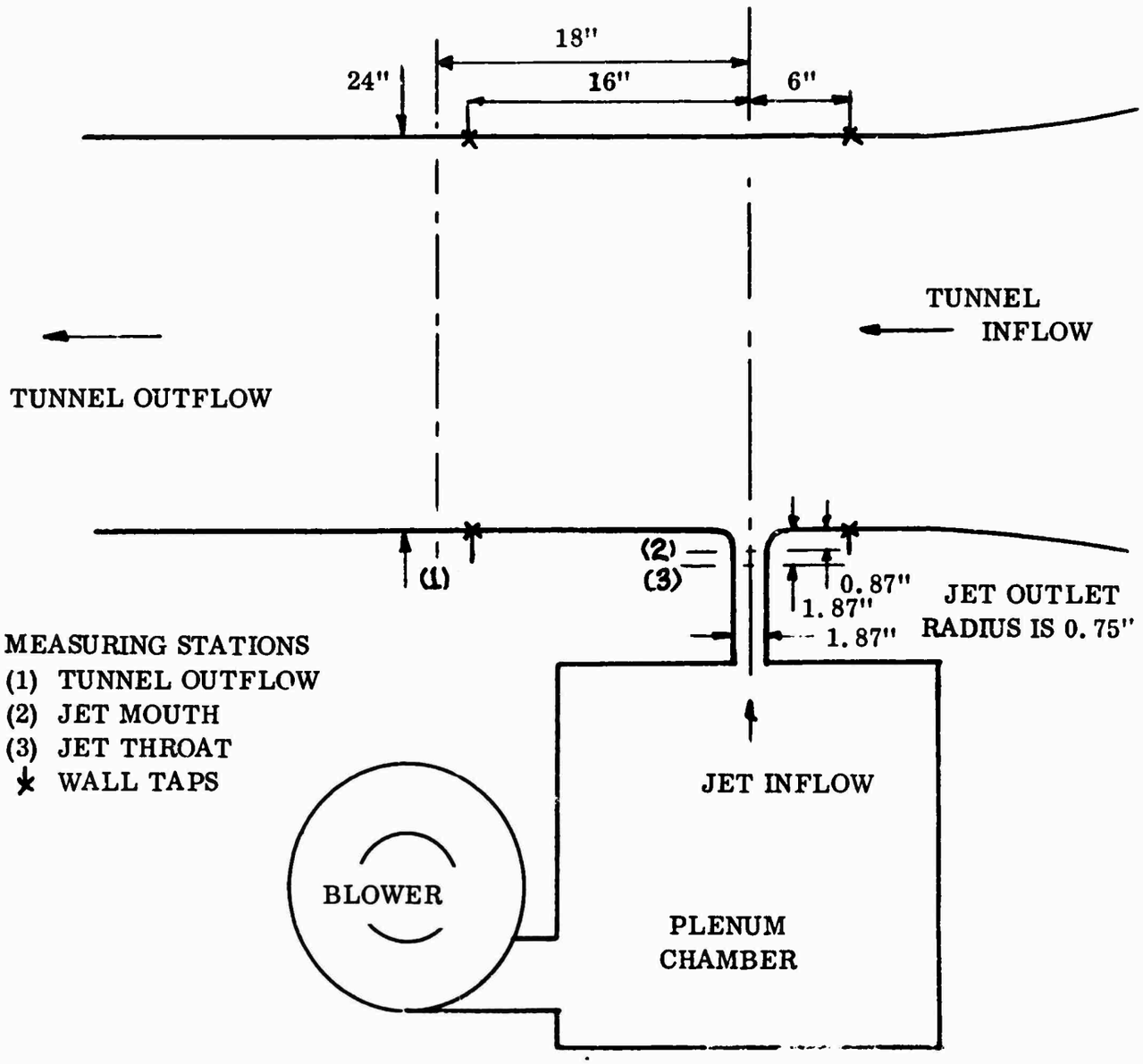

Figure 137. Arrangement of Jet Discharging Through Floor of Wind Tunnel.

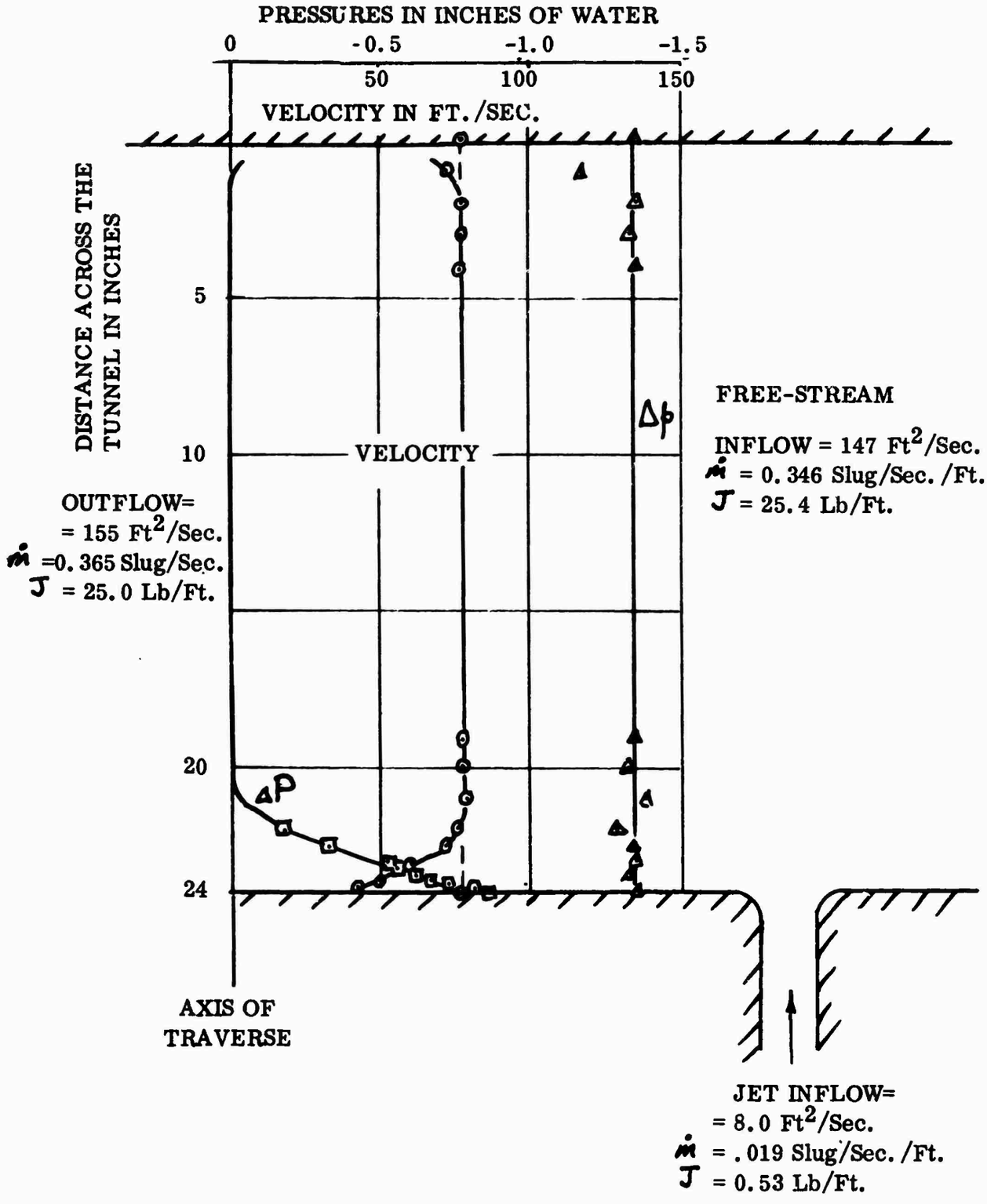

Figure 138. Velocity and Pressure Distribution Downstream From Jet.(Jet/Free-Stream Velocity Ratio 0.56).

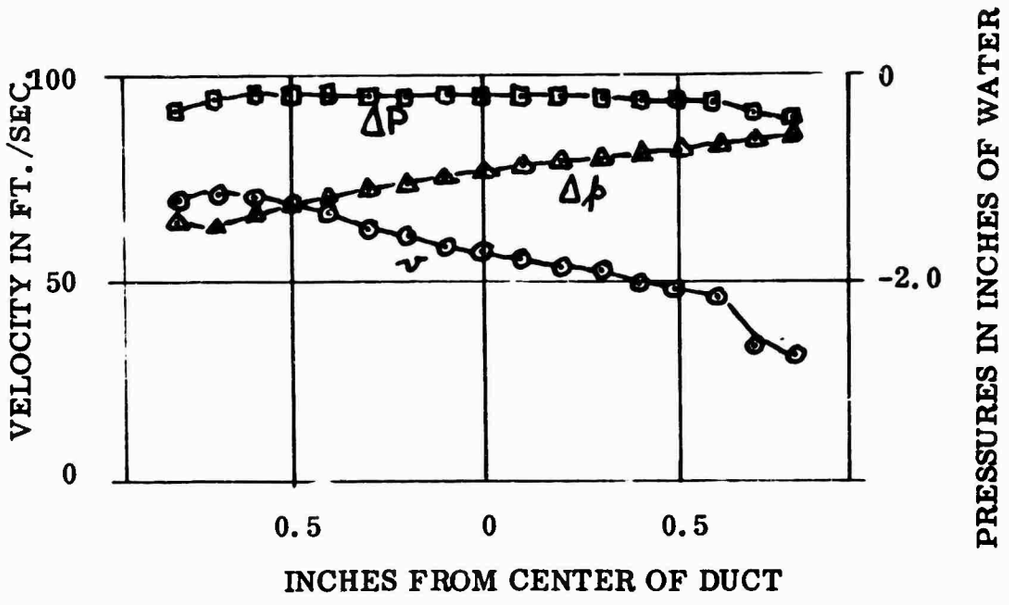

Figure 139(a). Velocity and Pressure Distribution at Mouth of Jet. (Jet/Free-Stream Velocity Ratio 0.56).

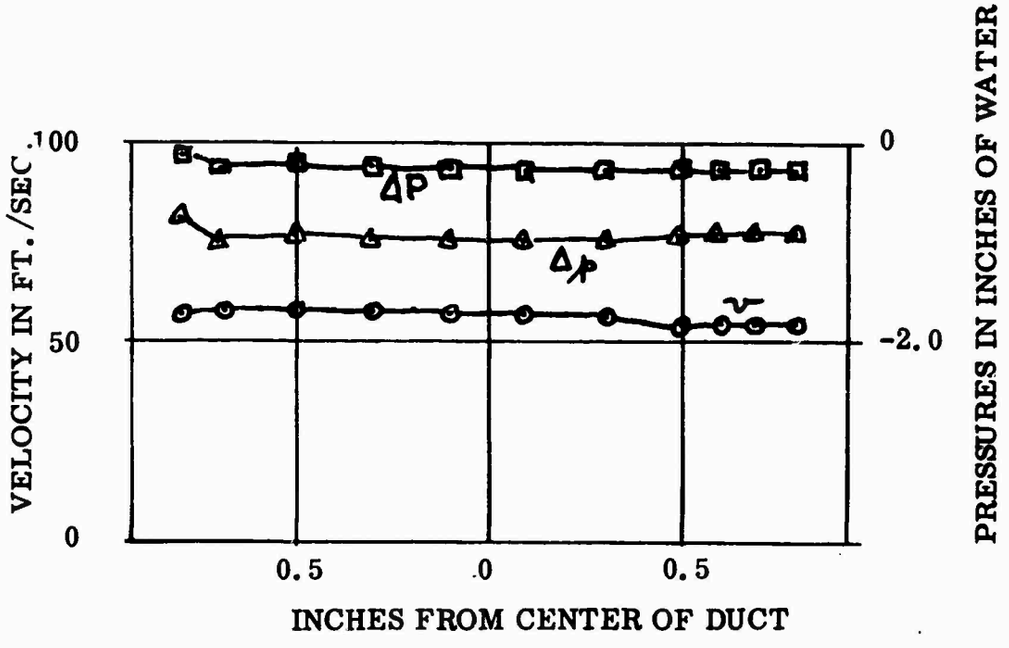

Figure 139(b). Velocity and Pressure Distribution in Jet Throat. (Jet/Free-Stream Velocity Ratio 0.56)

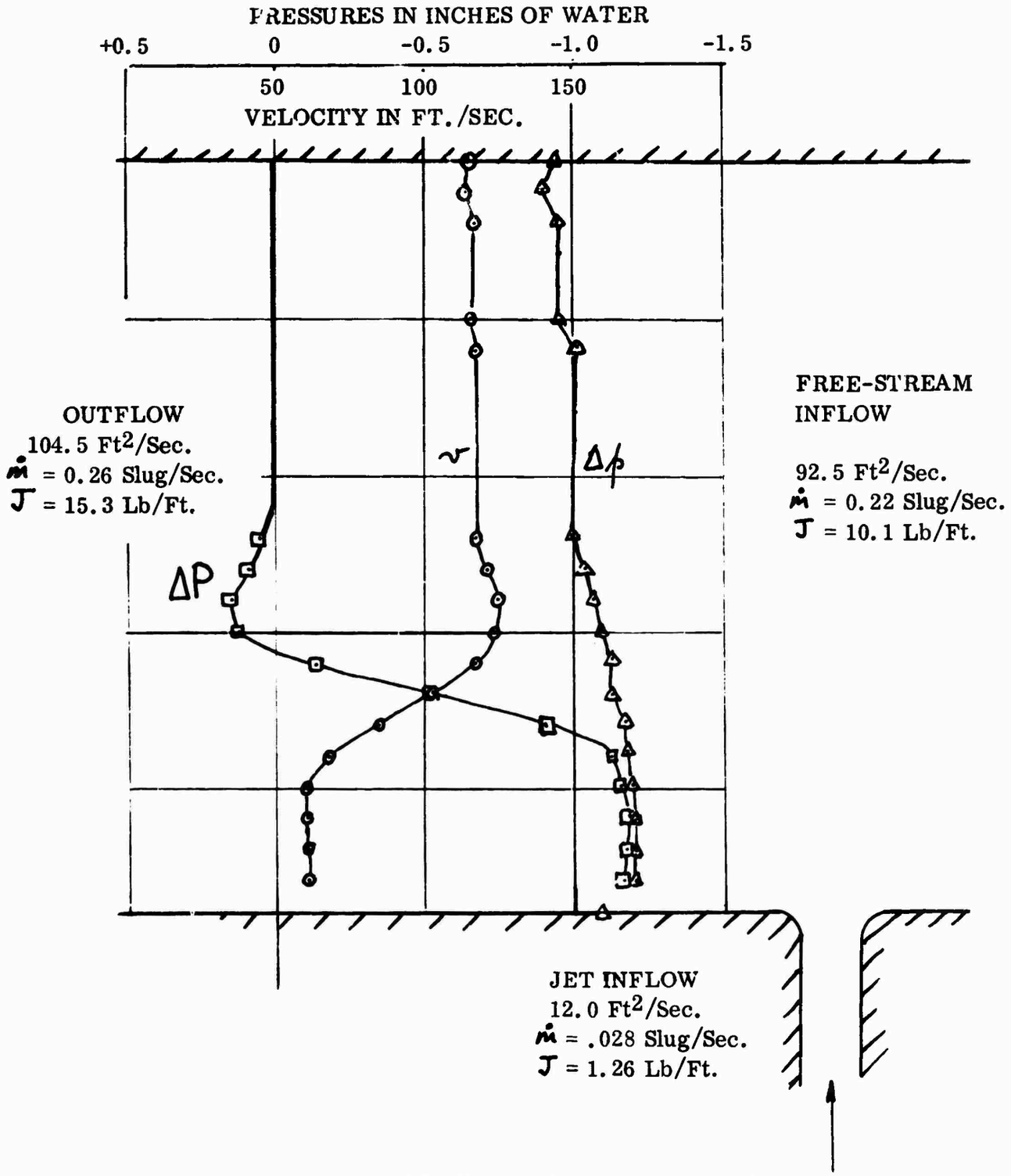

Figure 140. Velocity and Pressure Distribution Downstream From Jet. (Jet/Free-Stream Velocity Ratio 1.34).

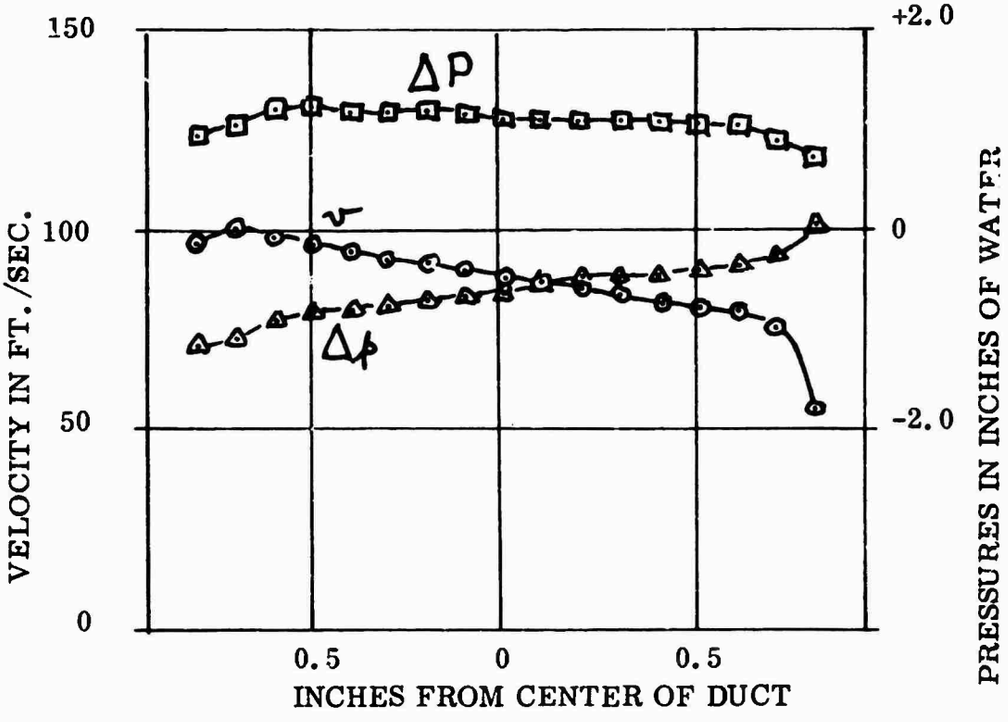

Figure 141(a). Velocity and Pressure Distribution at Mouth of Jet. (Jet/Free-Stream Velocity Ratio 1.34).

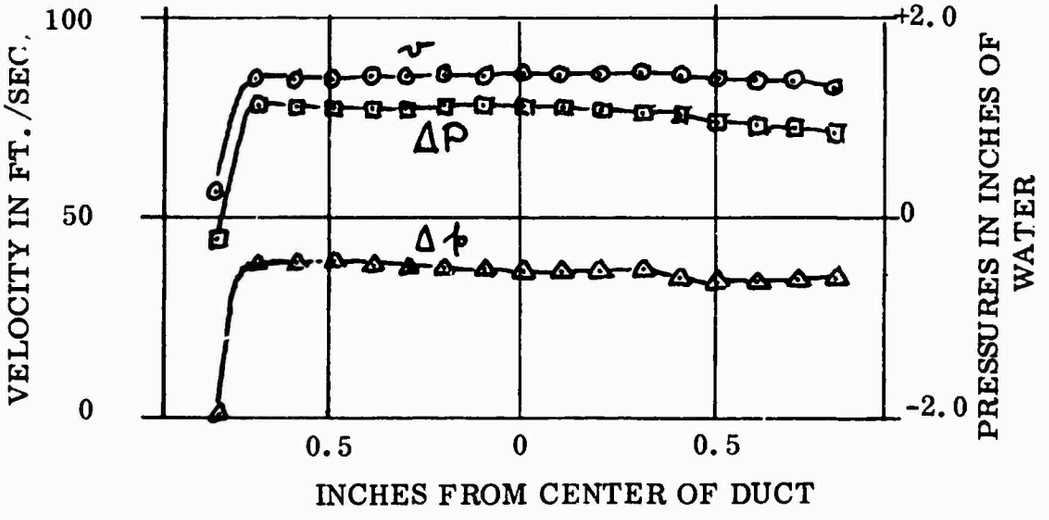

Figure 141(b). Velocity and Pressure Distribution in Jet Duct Throat. (Jet/Free-Stream Velocity Ratio 1.34).

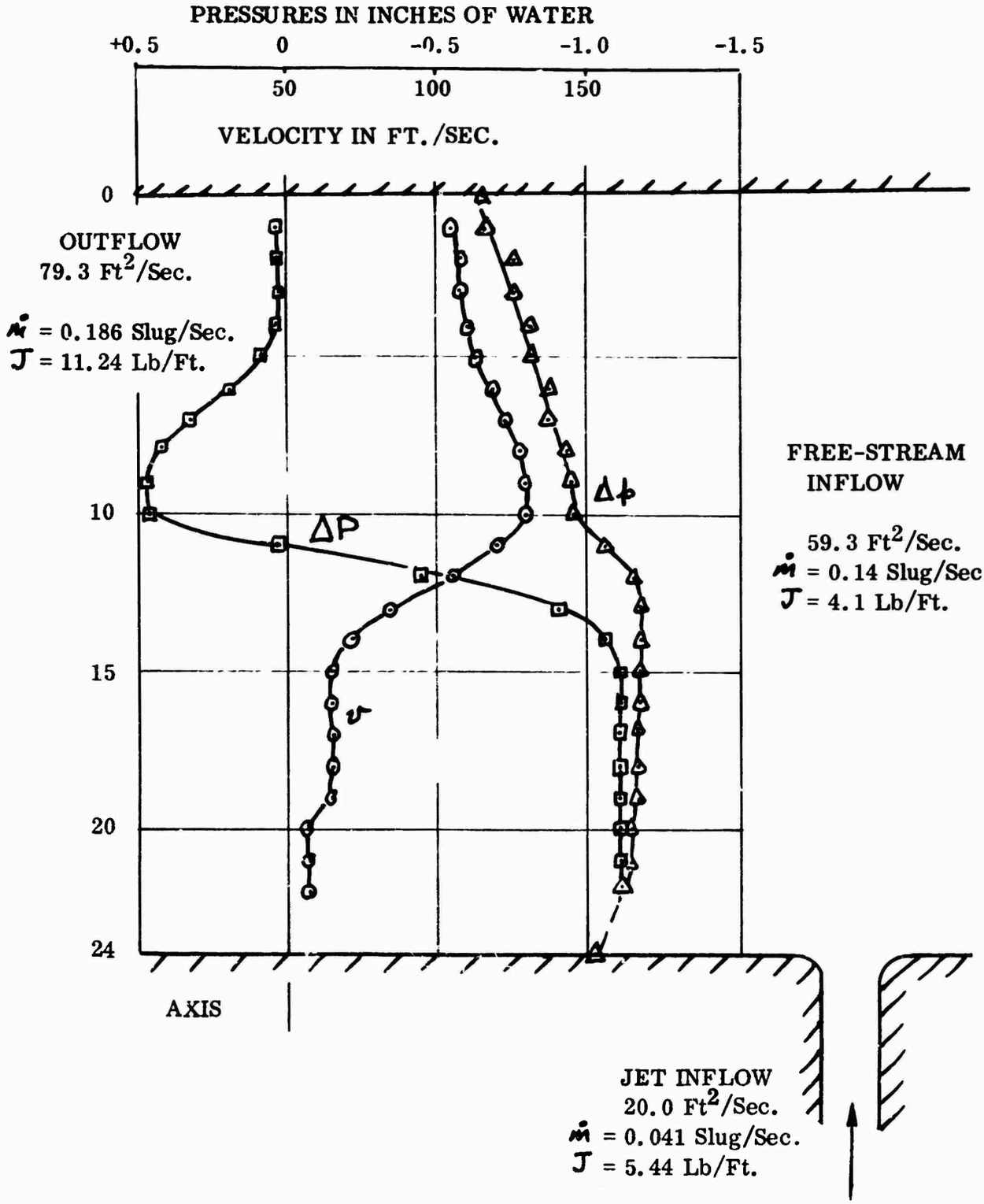

Figure 142. Velocity and Pressure Distribution Downstream From Jet. (Jet/Free-Stream Velocity Ratio 2.88).

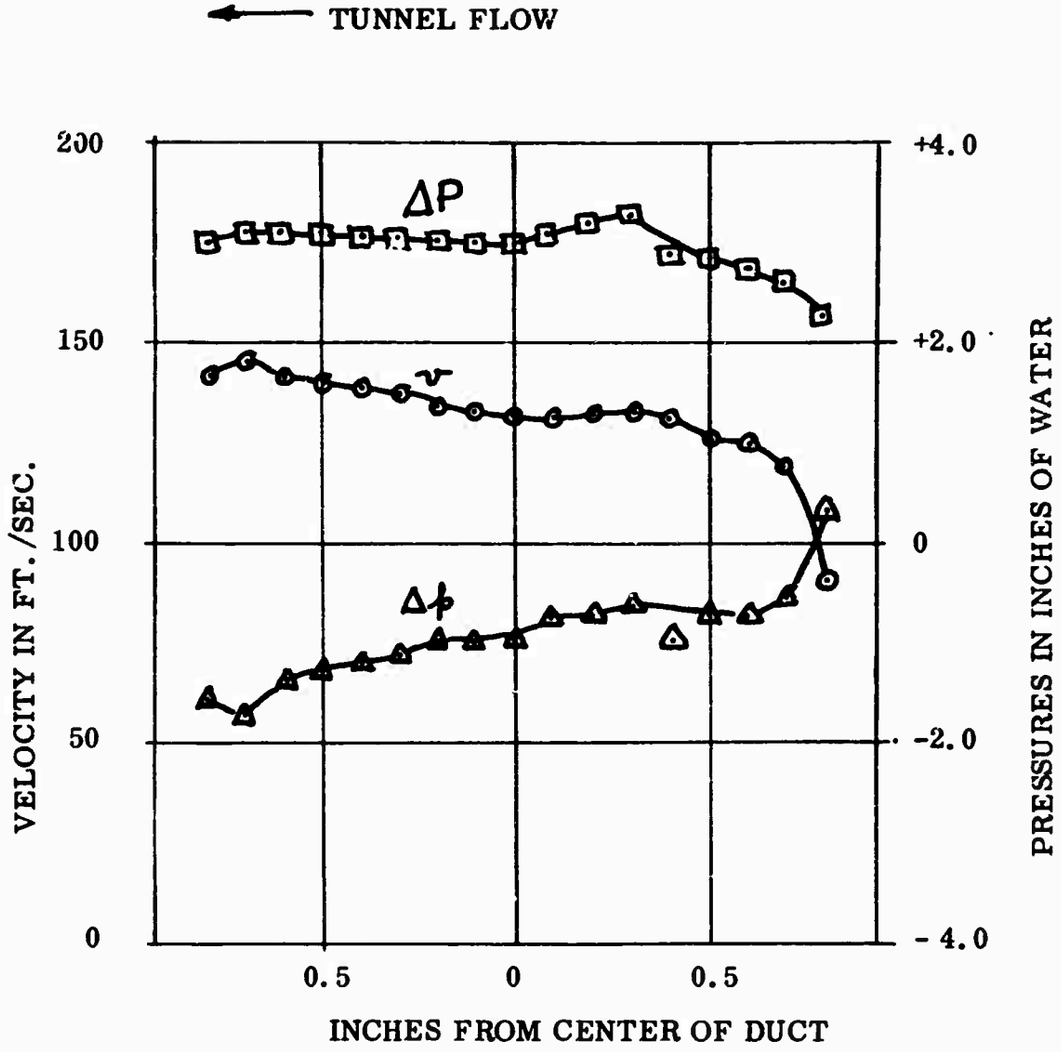

Figure 143(a). Velocity and Pressure Distribution at Jet Mouth. (Jet/Free-Stream Velocity Ratio 2.88).

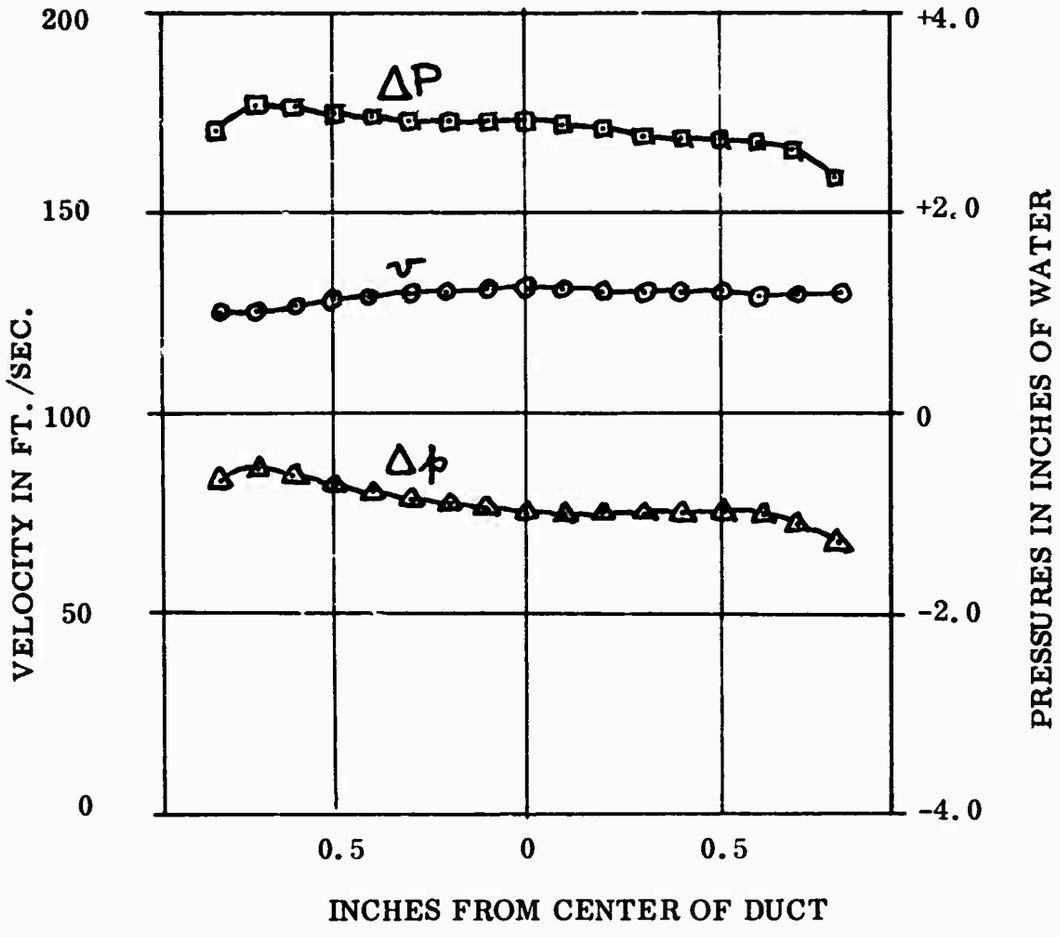

Figure 143(b). Velocity and Pressure Distribution at Jet Throat. (Jet/Free-Stream Velocity Ratio 2.88).

RECOMMENDATIONS FOR FURTHER WORK

The program herein reported is rather diffuse in that, although the basic subject is the equation for curvilinear flow, we have applied it to a number of practical applications. It could not, of course, be rigorously applied to all cases; therefore, most attention has been concentrated on the annular jet problem, since we were most familiar with this and since the annular jet problem possesses the greatest body of previous work, both theoretical and experimental.

As a result, it is believed that no further work is required in this area, except for the tidying up of loose ends. However, considerably more work remains to be done with intake flow and curved-duct flow; such an effort is important because of the substantial reduction in losses which may be obtained.

Annular Jet Theory

The new inviscid theory appears to be completely satisfactory, as far as it goes. In order to make the theory of maximum practical utility, it is recommended that a program be formalized in the following steps:

(a) Solve the inviscid flow annular jet equations for constant total pressure on a digital computer, and both tabulate and plot the results in convenient form. The slide rule computations made for this report are unsatisfactory for general engineering use.

(b) Repeat the above calculations for a range of linear total pressure variations across the jet.

(c) Program the equations for the case of an arbitrary total pressure distribution across the jet, and include both viscous mixing and diffusion pressure loss effects. Such a program, fully checked out and generally available, would constitute a valuable engineering design tool.

(d) Develop an optimum nozzle shape for minimum total pressure loss. The simple experiment reported in Appendix IV of this report shows

that even a very simple "pre-curving" of the flow gives a dramatic reduction in loss, and it is believed that a more sophisticated design would eliminate this loss.

(e) Examine the impact of the new theory on dynamic motions of an annular jet GEM. The work so far done in viscous entrainment of the cushion air indicates strongly that Tulin's concepts of "underfed" and "overfed" jet operation are erroneous and that the predicted damping would be quite different if the airflow were considered as being intimately tied up with the primary vortex.

Intake Flow Theory

The application of curvilinear flow theory to the flow into a skewed intake has been undertaken only for the case of no upstream boundary layer or flow distortion. While it explains all of the observed effects (including the low pressure recoveries) and the phenomenon of lip stall, it would require a separate program as lengthy as the present one, to "tie-up" the subject adequately in the same way as the annular jet theory has been rounded out. In view of the importance of this problem to many hardware applications, it is strongly suggested that this be done.

Curved Duct Flow Theory

For rectangular ducts, the optimum curve shape for minimum diffusion loss must be investigated. Secondary flows due to finite aspect ratio have not been considered at all in this report, and this should obviously be done before a general theory of curved duct losses can be produced. Also, the work should be extended to include circular duct cross sections.

When such a general theory has been developed and adequately checked out by experiment, it would be possible to define optimum duct bend shapes for minimum loss. Needless to say, since ducts are used extensively in almost all aerospace hardware, the definition of low-loss shapes would be of almost universal benefit.

Coanda Flow

The potentialities of Coanda flow around a curved surface are as yet unknown, because the phenomenon has still not been analyzed coherently. On general principles, it is felt that the present work should be extended, both theoretically and experimentally, although there is (at the moment) no obvious hardware application in sight.

Diffusion Theory

The diffusion theory developed during this program appears to be a major breakthrough, even though it is not fully understood. In work not reported herein, for example, this theory has been applied to the inviscid flow around a cylinder and a sphere, and calculated drag coefficients have been obtained in virtually exact agreement with measured values.

There is a great need to find a "unifying theory" which relates this new approach to the established boundary layer theory, to identify its limits of applicability, and to understand its physical basis.

Jet Flap Theory

While significant steps have been made in understanding the jet flap problem and while the "thrust recovery" anomaly has been adequately resolved, there is obviously room for more work in this area. It ought to be possible to obtain the same precision in the theoretical description of the phenomenon as is now possible for the annular jet.

BIBLIOGRAPHY

1. Davidson, I. M., "The Jet-Flap," Journal of the Royal Aeronautical Society, 1956, page 25.

2. Stratford, B. S., "Mixing and the Jet Flap," Aeronautical Quarterly, Vol. VII, May 1956.

3. Payne, Peter R., "Viscous Mixing Phenomena with Particular Reference to Thrust Augmentors," AIAA Paper No. 64-798, October 1964.

4. Viscous Mixing of Two-Dimensional Jets with Particular Reference to Jets in Ground Proximity, USA TRECOM Technical Report 64-11, U. S. Army Transportation Research Command, Fort Eustis, Virginia, April 1964.

5. Schlichting, H., "Application of Boundary Layer Theory in Turbomachinery," Transactions of A. S. M. E., Journal of Basic Engineering, Series D, Vol. 81, No. 4, December 1959.

6. Lieblein, S., "Loss and Stall Analysis of Compressor Cascades," Transactions of A. S. M. E., Journal of Basic Engineering, Series D, Vol. 81, No. 3, September 1959.

7. Senoo, Yasutoshi, "Considerations on the Lifting Fan-Duct Systems of Ground Effect Machines," Proceedings of the National Meeting on Hydrofoils and Air Cushion Vehicles, I. A. S., Washington, D. C., September 1962.

8. Goldschmied, Fabio R., "An Approach to Turbulent Incompressible Separation and the Determination of Skin-Friction under Adverse Pressure Gradients," AIAA Paper No. 64-465, July 1964.

9. Chaplin, Harvey R., "Theory of the Annular Nozzle in Proximity to the Ground," David Taylor Model Basin, Aero Report 923, Washington, D. C., July 1957.

10. Cross, F. G., "Outstanding Problems of Air Cushion Vehicles," paper presented to Dansk Ingeniorforening, Copenhagen, Denmark, November 1961.

11. Stanton-Jones, R., "Some Design Problems of Hovercraft," IAS Paper No. 61-45, January 1961.

12. Pinnes, Robert W., "The Propulsion Aspects of Ground Effect Machines," Bureau of Naval Weapons Report No. RRSY-60-1, January 1960.

13. Payne, Peter R., "Annular Jet Theory, Part I - Jets with a Constant Total Head Distribution," Norman K. Walker Associates, Inc., Report No. 17, Contract No. NObs-90127, May 1964.

14. Strand, T., "Inviscid-Incompressible-Flow Theory of Static Peripheral Jets in Proximity to the Ground," Journal of the Aerospace Sciences, Vol. 28, No. 1, January 1961.

15. Schlichting, H., "Boundary Layer Theory," McGraw-Hill, New York, 1960.

16. Kuhn, Richard E., and Carter, Arthur W., "Research Related to Ground Effect Machines," Princeton Symposium on Ground Effect Phenomena, October 1959.

17. Hughes, D. L., "Air Cushion Craft Research at the University College of Swansea," University of Wales, 1964.

18. Gabbay, E. J., "On the Coefficients of Contraction for Nozzles and Valve Openings," Doctorate Thesis in Theoretical Fluid Mechanics, University of London, 1960.

19. Preliminary Studies of the Application of Peripheral Fans to Ground Effect Machines, USA TRECOM Technical Report 64-10, U. S. Army Transportation Research Command, Fort Eustis, Virginia, April 1964.

20. Chaplin, Harvey R., "Effects of Jet Mixing on the Annular Jet," David Taylor Model Basin Report No. 1375, February 1959.

21. Yen, Ben-Chie, "Patterns of Flow Under a Two-Dimensional GEM," Iowa Institute of Hydraulics Research, ONR Contract No. 1509(03), January 1962.

22. Albertson, M. L., Dai, Y. B., Jensen, R. A., and Rouse, Hunter, "Diffusion of Submerged Jets," Transactions of the American Society of Civil Engineers, Vol. 115, 1950.

23. Rawlings, William L., and Seiveno, Donald H., "Program for Reduction of Hydro-Skimmer Power Requirements," Aeronutronic Publication No. U-1458, Contract No. NObs 84364, November 1961.

24. Experimental Investigation of the Viscous Effects on Balanced Jets in Ground Proximity, USA TRECOM Technical Report 63-61, U. S. Army Transportation Research Command, Fort Eustis, Virginia, October 1963.

25. Bailey, A. B., "Use of the Coanda Effect for the Deflection of Jet Sheets Over Smoothly Curved Surfaces," UTIA Technical Note No. 49, University of Toronto, August 1961.

26. Wallis, R. A., "Axial Flow Fans," Academic Press, N. Y., 1961.

27. Eames, M. C., "Fundamentals of the Stability of Peripheral Jet Vehicles; Effect of Jet Thickness," Pneumo-Dynamics Report No. 6633-5, 1963.

DISTRIBUTION

US Army Materiel Command	7
US Army Mobility Command	4
US Army Aviation Materiel Command	5
US Strike Command	1
Chief of R&D, DA	3
US Army Transportation Research Command	69
USATRECOM Liaison Officer, US Army R&D Group (Europe)	1
US Army Engineer R&D Laboratories	4
US Army Human Engineering Laboratories	1
Army Research Office-Durham	2
US Army Research Support Group	1
US Army Medical R&D Command	1
US Army Engineer Waterways Experiment Station	1
US Army Combat Developments Command Transportation Agency	1
US Army War College	1
US Army Command and General Staff College	1
US Army Transportation School	1
US Army Tank-Automotive Center	2
US Army Arctic Test Center	1
TC Liaison Officer, US Army Airborne, Electronics and Special Warfare Board	1
US Army General Equipment Test Activity	1
Chief of Naval Operations	1
Bureau of Ships, D/N	1
Bureau of Naval Weapons	2
Bureau of Supplies and Accounts, D/N	1
US Naval Supply R&D Facility	1
US Naval Postgraduate School	1
David Taylor Model Basin	1
Marine Corps Landing Force Development Center	1
Marine Corps Educational Center	1
Marine Corps Liaison Officer, US Army Transportation School	1
Ames Research Center, NASA	2
NASA-LRC, Langley Station	2
Lewis Research Center, NASA	2
NASA Representative, Scientific & Technical Information Facility	2
Human Resources Research Office	2
US Army Standardization Group, Canada	2
Canadian Liaison Officer, US Army Transportation School	3
British Army Staff, British Embassy, Washington	4
US Army Standardization Group, U. K.	1
Defense Documentation Center	20
US Government Printing Office	1

APPENDIX I

SCALE EFFECT IN ANNULAR JET FLOW

Scale effects can be studied experimentally without any need for hypotheses to explain them. Sufficient information is now available to indicate whether there is any very large variation of the cushion pressure ratio $\Delta p_c / \Delta P_j$ with Reynolds number, and it seems that no such variation can be detected.

Little attention seems to have been devoted to this subject in the literature. In Reference 16, Kuhn and Carter suggest that "there are no first order scale effects...", on the basis of tests with 4, 8, and 42-inch-diameter models. However, it is doubtful whether the differences in Reynolds numbers between these models were large enough for a scale effect trend to become larger than the experimental scatter, particularly since additional variables are introduced by the use of three-dimensional models.

The comparison most free of extraneous variables is the two-dimensional flow case, and some recent English work[17] now enables us to cover the range $Re = 2 \times 10^3$ with two-dimensional rigs.

The results of Reference 17 are compared with the measurements of Rawlings and Seiven in Figure 144, and a very large scale effect is at first sight seen to be present. Although it is not explicitly stated in Reference 17, however, it can be inferred that the jet total head is measured upstream of the actual nozzle. Thus, even if the flow into the nozzle were perfect, we should still expect some loss from skin friction.

Let us use exponential theory to obtain a rough idea of this loss. The mass flow will be

$$\dot{m}_j = Ct(2\rho\Delta P_j)^{\frac{1}{2}} \cdot \frac{1 - e^{-t/R}}{t/R}, \qquad (414)$$

so that the duct velocity is

$$v_D = \frac{\dot{m}_j}{etC} = \left(\frac{2}{\rho}\Delta P_j\right)^{\frac{1}{2}} \cdot \frac{1 - e^{-t/R}}{t/R}. \qquad (415)$$

The skin friction force

$$F_s = \Delta(\Delta P_j)\,Ct = C_f \cdot \tfrac{1}{2}\rho v_D^2 \cdot S_{wet} \cdot \qquad (416)$$

Assuming ℓ_D = mean length of one nozzle wall,

$$S_{wet} = 2\ell_D C$$

$$\therefore \quad \Delta(\Delta P_j) = C_f \cdot \tfrac{1}{2}\rho v_D^2 \cdot 2\ell_D/t \qquad (417)$$

$$\frac{\Delta p_c}{\Delta P_j} = \left(1 - e^{-2t/R}\right)\left(1 - C_f \cdot \frac{\tfrac{1}{2}\rho v_D^2}{\Delta P_j} \cdot \frac{2\ell_D}{t}\right)$$

$$= \left(1 - e^{-2t/R}\right)\left[1 - \frac{2\ell_D}{t} \cdot C_f \cdot \frac{\left(1 - e^{-t/R}\right)^2}{(t/R)^2}\right]. \qquad (418)$$

This has been evaluated for $\theta = 30^\circ$ and $\ell_D/t = 6.0$, figures which are believed to be about right for the Hughes rig. As shown in Figure 145, skin friction gives the same order of apparent $\Delta p_c/\Delta P_j$ variation with R_e as was actually observed.

It is concluded that the apparent scale effect is illusory, and that there is no appreciable variation in the range $2000 < R_e < 200{,}000$. This is satisfactorily in accordance with mixing theory[3], which indicates that scale has no effect on the turbulent or laminar mixing processes. It also emphasizes the need for measuring ΔP_j at the nozzle exit when appreciable skin friction loss is to be expected in the nozzle.

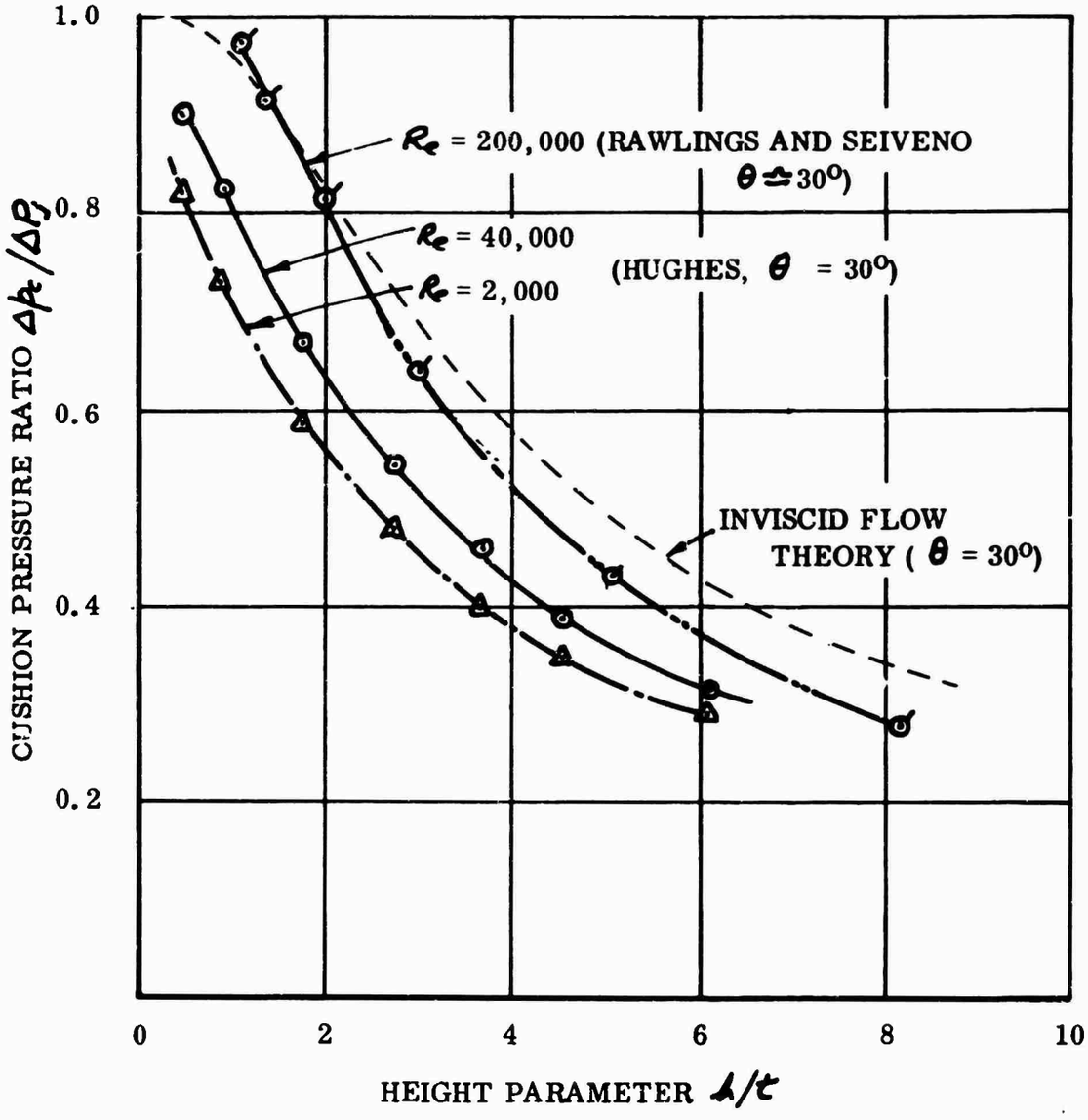

Figure 144. Apparent Effect of Reynolds Number on the Cushion Pressure Ratio.

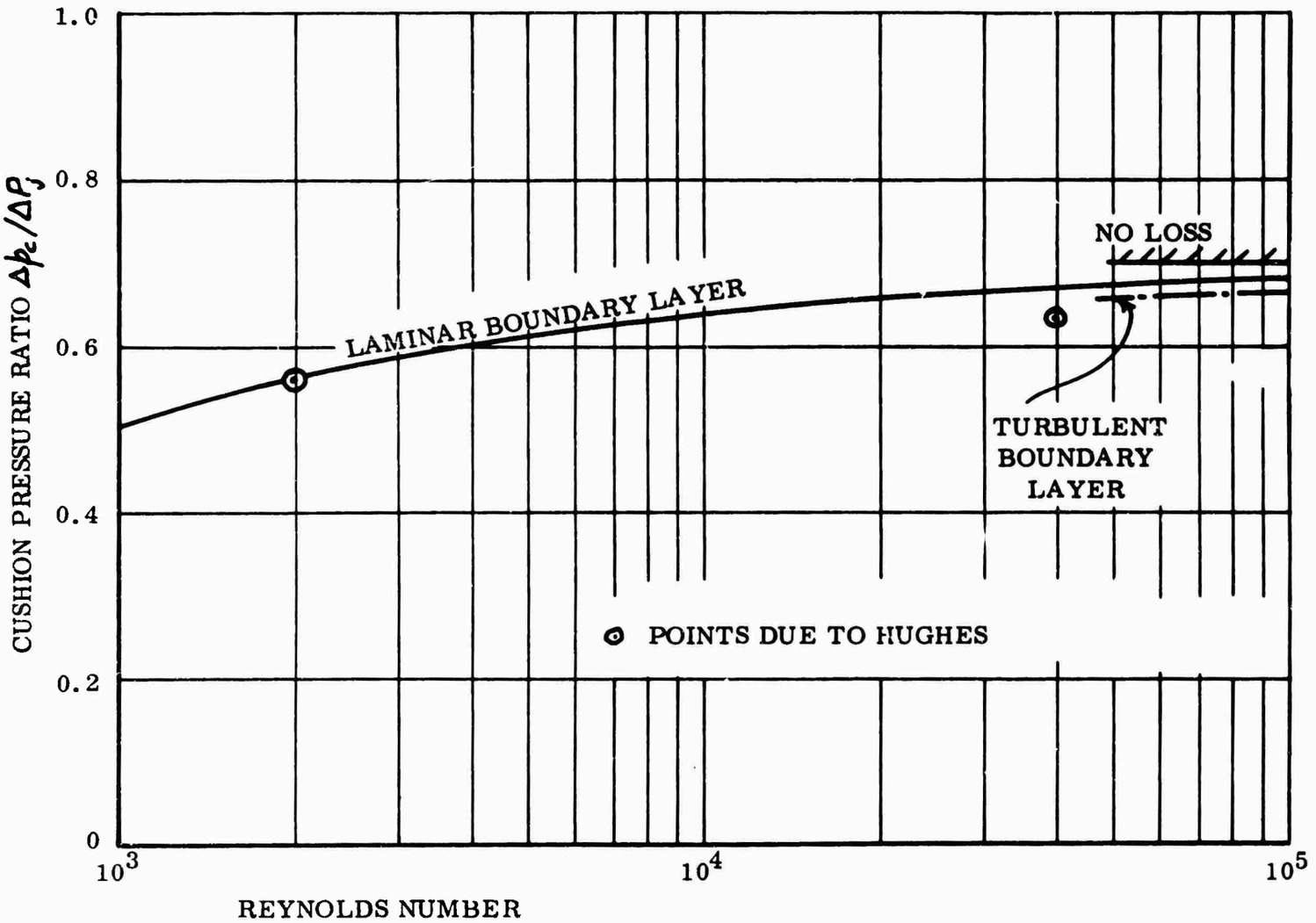

Figure 145. Effect of Nozzle Skin Friction Loss on Apparent Cushion Pressure Ratio.

APPENDIX II

ESTIMATION OF DRAG FROM TOTAL HEAD SURVEYS

From Chapter XXIV of Reference 15, the drag of a body is given by the momentum integral

$$D = \rho \int_{-\infty}^{+\infty} u (v_\infty - u)\, dy \tag{419}$$

where u is the velocity measured well downstream of the body, and v_∞ is the free-stream velocity.

In a wind tunnel which draws air from ambient,

$$\begin{aligned} v_\infty &= \left(-\frac{2}{\rho}\Delta p_\infty\right)^{1/2} \\ u &= \left[\frac{2}{\rho}(p_y - p_y)\right]^{1/2} \\ &\doteq \left[\frac{2}{\rho}(\Delta p_y - \Delta p_\infty)\right]^{1/2}. \end{aligned} \tag{420}$$

Substituting into Equation (419),

$$\begin{aligned} D &= b\rho \int_{-\infty}^{+\infty} \frac{2}{\rho}(\Delta p_y - \Delta p_\infty)^{1/2}\left[\Delta p_\infty^{1/2} - (\Delta p_y - \Delta p_\infty)^{1/2}\right] dy \\ &= b\Delta p_\infty \int_{-\infty}^{+\infty} \left[-1 - \frac{\Delta p_y}{\Delta p_\infty} + \left(1 - \frac{\Delta p_y}{\Delta p_\infty}\right)^{1/2}\right] dy. \end{aligned} \tag{421}$$

In most experiments $\Delta p_y \ll \Delta p_\infty$, if the rake is sufficiently far downstream;

$$\therefore \quad \left(1 - \frac{\Delta p_y}{\Delta p_\infty}\right)^{1/2} \doteq 1 - \frac{1}{2}\cdot\frac{\Delta p_y}{\Delta p_\infty}$$

$$\therefore \quad D = 2b\Delta p_\infty \int_{-\infty}^{+\infty} \left[-1 - \frac{\Delta p_y}{\Delta p_\infty} + 1 - \frac{1}{2}\frac{\Delta p_y}{\Delta p_\infty}\right] dy,$$

or

$$D = -b\int_{-\infty}^{+\infty} \Delta p_y\, dy. \tag{422}$$

This is the equation generally used in reduction of tunnel data.

APPENDIX III

A NOTE ON THE THEORY OF A FREE VORTEX

The classical theory of a vortex in inviscid flow, based on the irrotational properties of an infinitely small fluid element, is very rigorous; see, for example, Chapter VII of Lamb.* The basic results can be demonstrated much more simply for two-dimensional flow, however, although at the expense of losing some of the rigor and elegance of the classical analyses of Helmholtz and Lord Kelvin.

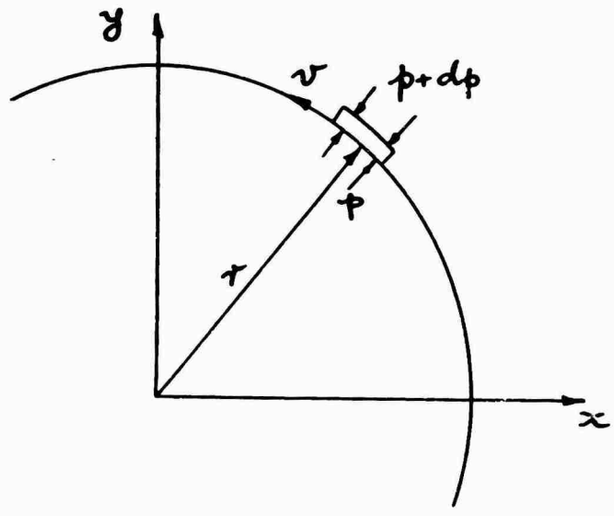

Figure 146. Geometry of a Two-Dimensional Vortex.

For a balance between centrifugal and pressure forces on the element shown in Figure 146,

$$r\,d\theta \cdot dp = r\,d\theta \cdot dr \cdot \rho v^2/r \qquad (423)$$

(pressure force) = (centrifugal force).

---

* Sir Horace Lamb, "Hydrodynamics," Sixth Edition, Dover Publications, New York, 1932.

$$\frac{dp}{dr} = \rho v^2/r \qquad (424)$$

But for conservation of total head,

$$p + \tfrac{1}{2}\rho v^2 = P. \qquad (425)$$

From Equation (425),

$$\frac{dp}{dr} = \frac{dP}{dr} - \rho v \cdot \frac{dv}{dr} \qquad (426)$$

If P is constant throughout the fluid, $dP/dr = 0$. Thus, substituting Equation (426) for dp/dr in Equation (424),

$$\frac{dv}{dr} + \frac{v}{r} = 0 . \qquad (427)$$

$$\therefore \quad vr = \text{constant}. \qquad (428)$$

This is the classic relationship which is used in potential flow theory. However, there is another way of expressing Equations (424) and (425):

From Equation (425),

$$\rho v^2 = 2(P - p). \qquad (429)$$

Substituting for ρv^2 in Equation (424),

$$\frac{dp}{dr} = \frac{2}{r}(P - p).$$

That is,

$$\frac{dp}{dr} + \frac{2}{r} \cdot p = \frac{2}{r} \cdot P. \qquad (430)$$

This is identical with Equation (87) in the main body of the report. Thus, the general techniques developed are also applicable to the treatment of vortex fields, including the effects of viscosity.

Integrating Equation (430),

$$p = \frac{2}{r^2} \left[\int r P_r \, dr + k \right]. \qquad (431)$$

In most problems, inviscid flow theory will apply at large values of r, where $dv/dr \rightarrow 0$. Equation (431) then takes the form

$$p_a = P_0 + \frac{2k}{r^2}$$

where p_a is the ambient static pressure and P_0 the total pressure in the vortex at large values of the radius.

Equation (431) may then be written as

$$p = \frac{2}{r^2} \int r P_r \, dr - (P_0 - p_a). \qquad (432)$$

Equation (432) can be used to study such problems as vortex flow in a real (viscous) fluid.

APPENDIX IV

DIFFUSION LOSS MEASUREMENTS IN A PRE-CURVED NOZZLE

It was shown in the main body of the report that a diffusion loss occurs in the nozzle of an annular jet and that it is somewhat larger than predicted by theory. The theory is based upon the assumption that an initially straight flow curves suddenly to a radius (R), and, of course, there is no means of assuming that this is so in a straight nozzle.

With this in mind, we built a circular section fairing for the annular jet rig nozzle, as shown in Figure 147, in order to ensure that the air behaved as assumed in the theory. The total pressure was then measured by means of Kiel probe traverses, with and without this fairing in place.

The results plotted in Figure 147 show a marked reduction in loss when the fairing is fitted, the integrated loss now being almost exactly equal to the theoretical prediction. The experimental points do not lie along the theoretical curve, however, because the process of diffusion necessarily distorts the ζ axis, and this is not taken into account in the theory.

It seems clear that if the fairing had been carefully blended into the nozzle to give a distributed total pressure rise (instead of being merely tangential to the nozzle surface), the total head loss would have been negligible.

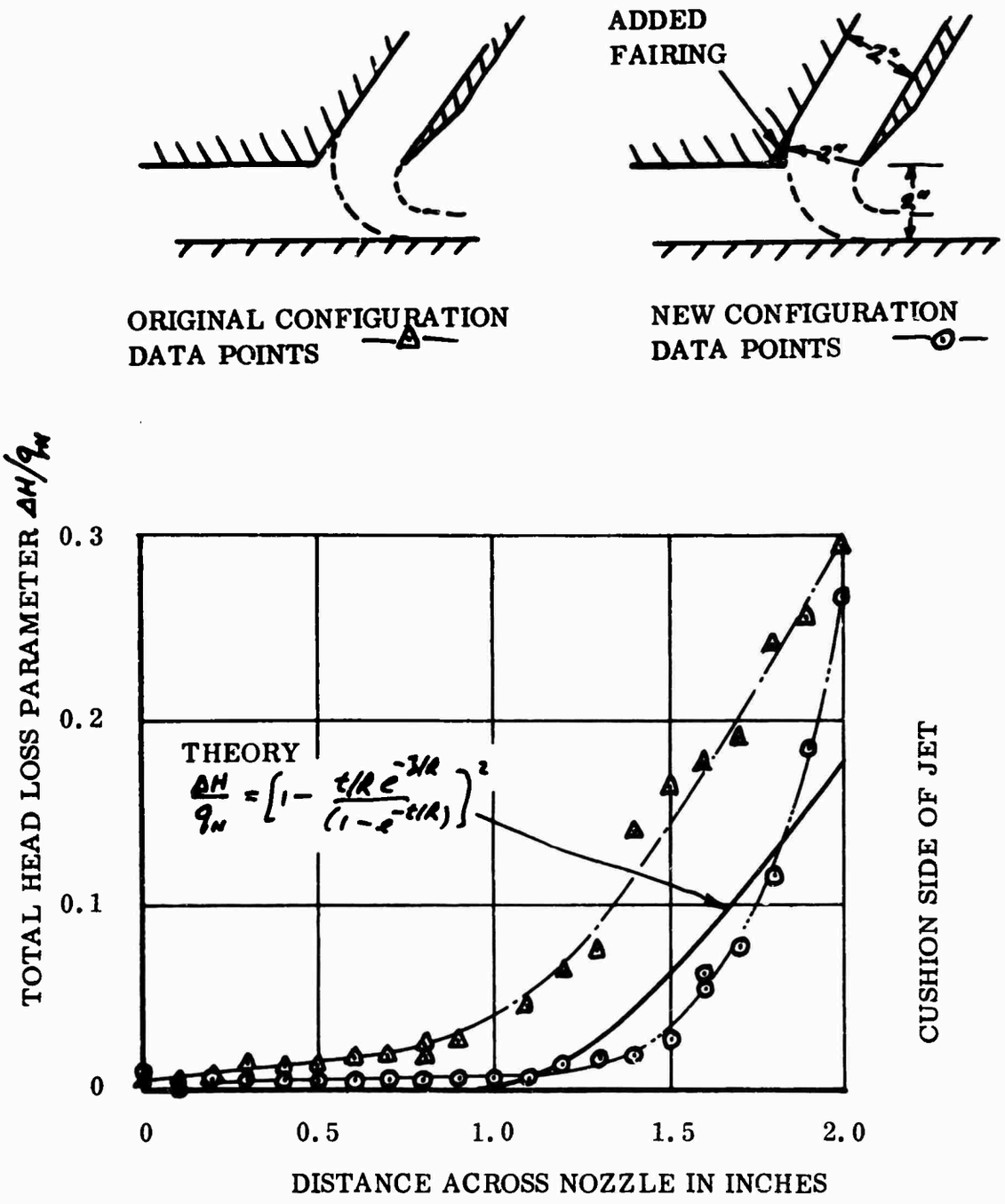

Figure 147. Total Pressure Loss at the Exit Plane of an Annular Jet Nozzle.